Muscle Fibre and Motor Unit Action Potentials

A biophysical basis for

clinical electromyography.

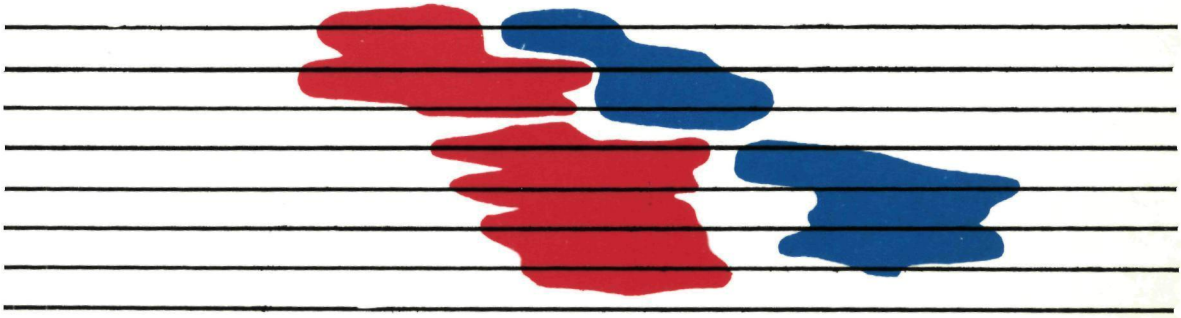

T.H.J.M. Gootzen

Muscle Fibre and Motor Unit Action Potentials

A biophysical basis for clinical electromyography.

Een wetenschappelijke proeve op het gebied van
de geneeskunde en tandheelkunde,
in het bijzonder de geneeskunde.

PROEFSCHRIFT

ter verkrijging van de graad van doctor
aan de Katholieke Universiteit te Nijmegen,
volgens het besluit van het college van decanen
in het openbaar te verdedigen op maandag 14 mei 1990,
des namiddags te 3.30 uur,

door

Theodorus Hubertus Johannes Maria Gootzen

geboren op 22 september 1962 te Horst.

Promotores: Prof.Dr. A. van Oosterom
Prof.Dr. S.L.H. Notermans
Co-promotor: Dr.Ir. D.F. Stegeman

This investigation was carried out at the Department of Medical Physics and Biophysics and the Department of Clinical Neurophysiology (Institute of Neurology) of the University of Nijmegen.
It was part of the research programmes "Bioelectricity" and "Disorders of the Neuromuscular System".

Financial support by Hoek Loos Medical Equipment for the publication of this thesis is gratefully acknowledged.

CIP-GEGEVENS KONINKLIJE BIBLIOTHEEK, 'S GRAVENHAGE

Gootzen, Theodorus Hubertus Johannes Maria

Muscle Fibre and Motor Unit Action Potentials : a biophysical basis for clinical electromyography / Theodorus Hubertus Johannes Maria Gootzen. - [S.l. : s.n.]. - Ill.
Proefschrift Nijmegen. - Met lit. opg.
ISBN 90-9003335-1
SISO 606.1 UDC 612.08:616.8-072(043.3)
Trefw.: klinische neurofysiologie.

Contents

"To all scientists: Whatever you loose, your teeth or your abilty to run, don't loose your curiousity because that's what keeps you alife"

Danny Kaye

Chapter I

General Introduction

Electromyography

Although the reading of a thesis is in general not associated with muscular effort, the holding of this thesis and turning over its pages cannot be achieved without countless firings of many motoneurons and subsequent contractions of muscle fibres. And although the electric activity is unnoticed when voluntary contractions of skeletal muscle are performed, it has been known since 1791 that muscle contractions and electric activity are closely related. In that year Galvani showed that current pulses applied to a nerve trunk could be used to make frog-muscles contract. In spite of the fame of the discoverer of muscle electricity, the history of modern electromyography (EMG) is rather short. As the starting point of the wide use of intramuscular electromyography, the year 1929 can be chosen when Adrian and Bronk [2] developed the concentric needle electrode and succeeded in obtaining clear intramuscular recordings of myo-electric activity. The concept of the motor unit, consisting of an α-motoneuron, its axon towards the muscle, the axon branches inside the muscle connected to the muscle fibres and the muscle fibres themselves, was established at about the same time [113]. The real breakthrough of clinical EMG came in the mid-fifties when Buchthal, Guld, Rosenfalck and many others [17,18,35] started measuring and analysing EMG signals on a larger scale. Even more important is that they pointed out the potential clinical significance of these signals. They were especially interested in what may be called the electric signature of a motor unit: the motor unit action potential (MUAP). From that moment on the diagnosis of neuromuscular disorders has learned to make use of MUAP registrations.

Volume conductor modelling

Parallel to the development of the EMG as a clinical method, many biophysical researchers have been studying the electrophysiology of the neuromuscular system. The work of Hodgkin and Huxley [71] is the most famous example and one of the pillars on which electrophysiological modelling is constructed. In this large

field we want to concentrate especially on the physical models of extracellularly recorded electrophysiological phenomena in the muscle. This approach starts from the physical principles described in classical electrodynamics and develops the mathematical tools that are necessary to formulate the derived principles.

Electrophysiological modelling of extracellular fields originates from the work by Lorente de Nó published in 1947 [83], who succeeded in calculating the potential field around the axon of an active giant squid nerve cell. Although many fundamental insights were gained in those years, these calculations, which were performed by hand, were so cumbersome (Lorente de Nó could afford a "calculating staff" of thirty persons) that it was only after the arrival of the computer as number cruncher in the late sixties, that a considerable break through could be achieved. The basis for this type of modelling, the volume conduction theory, also made substantial progress at that time. The theory of volume conduction is the part of electrodynamics which describes potential fields and current lines in three dimensional electric current conducting objects. In the application of this theory to the electrophysiology of the nerve fibre and cardiac strands the contributions of Plonsey and Clark [24,94] are still highlights. In 1969 Poul Rosenfalck was the first to adapt the newly obtained possibilities to the modelling of striated muscle single fibre action potentials (SFAPs) [103]. By doing so he initiated the next two decades of SFAP and MUAP modelling with an ever increasing accuracy and complexity (e.g. [6,42,48,62,87,107]). The insight which has been gained in this research is being used more and more in a dialogue with clinical research to achieve a better understanding of electromyographic measurements.

SFAP and MUAP modelling

The modelling of intramuscular EMG signals is performed at two levels. At the first level the action potentials from single muscle fibres are the subject of study. After Rosenfalck a steady development of SFAP models has been reported in literature [6,42,49,86,107]. The second level is formed by the models in which the spatio-temporal structure of the whole motor unit is involved. This kind of modelling started about ten years later than the SFAP modelling [62,129,87].

During the last decade these two levels of modelling have developed more or less independently. Most attention has been paid to the SFAP level. Ten years ago the first motor unit models that were published used the state of the art models of that period to obtain the SFAPs which have to be added to form the MUAP. From then on the MUAP models have almost uniquely been concentrating on finding proper descriptions for the morphological structure of the motor unit and the changes in this structure under various pathological conditions [89,90]. That part of the motor unit modelling in this thesis which is concerned with describing the motor unit morphology is a continuation of this research.

In spite of the vast amount of information gathered on the motor unit parameters there remained a substantial discrepancy between recorded and simulated MUAPs [64]. This discrepancy has been attributed to inaccurate descriptions of the motor unit structure [87] and to the great variation in the contribution to the MUAP from the muscle fibres lying closest to the recording electrode [64]. The fact that a very simple SFAP model, describing a bi, tri or multipolar current source density distribution, moving uniformly along an infinitesimally thin

fibre embedded in a homogeneous, infinite medium, usually formed the basis of the MUAP models was rarely discussed. An important reason for this was that the combination of a complex SFAP model with an accurate MUAP model was not possible at all on the computers available or could only be performed with unacceptably long calculation times. A major goal of the research reported in this thesis is to find out which aspects of SFAP modelling that were omitted from MUAP modelling in the past need to be incorporated in a MUAP model.

Analysis of the clinical EMG

For clinical routine many straightforward EMG characterization procedures have been developed, e.g. [11,75,131]. Empirical MUAP parameters such as amplitude, duration, number of phases and spectral content play an important role in intramuscular and surface EMG diagnosis [119]. Although some of the methods developed succeeded very well in obtaining a proper diagnosis of certain neuromuscular pathologies, these methods made no contribution to a better insight into the EMG generation, owing to their empiric character. Recently, sophisticated pattern recognition methods [36,79,85] have become available which make it easy to obtain individual MUAPs at force levels at which only an overall description of the interference pattern could previously be made. With the use of these methods, information is obtained on the temporal firing behaviour of the motoneuron [79,85]. This type of information is very useful when studying e.g. motor control or muscle fatigue [31]. In spite of these achievements new insights in the MUAP waveshape cannot be obtained from these methods either.

As the preceding paragraphs suggest, the application of MUAP models in electrophysiologic, diagnostic methods for the assessment of neuromuscular disorders is feasible. Bearing in mind the difficulties surrounding MUAP modelling which were mentioned in the previous section, this is a challenging task. It should bring EMG quantification to a level where results are more directly associated with results from histochemical and (sub)microscopical techniques, which have developed into powerful methods for the diagnosis of neuromuscular disorders.

Unanswered basic questions

In the effort that has to be made to model MUAPs with realistic properties in order to achieve the goals described above, the incorporation of the results of the continuing research during the last decade in the field of SFAP modelling will play an important role. The research on the SFAP models provided answers to questions about a proper description of the muscle tissue conductivities, the influence of the recording electrode etc. These were questions that had not been answered yet at the moment when MUAP models started to use the "classical" SFAP model.

In this thesis, four important items will be added to the classical SFAP modelling which is extensively reviewed in Andreassen and Rosenfalck 1981 [6]. These items are :

1) Can muscle tissue be described as a purely resistive medium or do the capacitive properties of the muscle fibre membranes have to be incorporated into the volume conductor description in SFAP and MUAP models?

This item has been the subject of many studies during the last decades. Plonsey and Heppner estimated [94] that both the dielectric constant and the magnetic permeability of muscle tissue can be neglected. More recent studies, however, in which the muscle tissue conductivities were measured by the four electrode technique [22] indicate that the muscle tissue conductivity is frequency dependent. Gielen et al. [48,49] and Albers et al. [3,4] describe a volume conductor model in which these frequency dependencies are included. This was achieved by a microscopic electrical network description including a capacitive element in the muscle fibre membrane impedance. Their model was developed to investigate the relationship between recorded SFAPs from an animal preparation in which the distance between the active muscle fibre and the recording wire electrode was known and simulated SFAPs in which this distance information has been incorporated. Including the frequency dependent conductivities, however, appeared not to be the proper means to eliminate most of the discrepancies still present [5].

A later study by Roth et al. [107] revealed that the muscle tissue conductivity depends on the spatial frequency (and thus also on the inter-electrode distance in the four-point measurements) and that the temporal frequency dependence is coupled via the conduction velocity to this spatial frequency dependence. They also estimate that the temporal frequency dependence caused by the presence of a capacitive term in the muscle fibre membrane impedance can be neglected. In this thesis an attempt is made to confirm this by a homogenised, macroscopic description of the muscle tissue.

2) Is there a substantial influence on SFAPs and MUAPs from the initiation of the action potential at the motoneuron endplate(s) and the extinction of the action potential at the fibre endings at the muscle tendon?

The observation has often been made that, close to the end-plate and close to the fibre end, SFAPs are different from SFAPs recorded between these two locations [73]. The first study concerning the modelling of these phenomena, however, is of a rather recent date [65,66]. In this thesis, a method is described by which these start and stop phenomena can be efficiently incorporated in the SFAP calculation.

3) What is the influence of the finiteness of the muscle and limb dimensions on SFAPs and MUAPs or can the consideration of the volume conduction as an infinite conducting medium be preserved?

Once the characteristics of the muscle fibre as a spatio-temporal current source and those of the medium directly surrounding the active muscle fibre have been derived, attention has to be paid to the overall environment of the muscle fibre: the entire muscle and its surroundings. The most usual approach in dealing with this environment is formulating a cylinder symmetrical potential field problem. Application of the proper boundary conditions in the solution of Laplace's equation then results in the potential field. Examples of this method can be found for both muscle and nerve simulations [42,121]. The numerical facilities available in te past for the modelling of the inhomogeneous surroundings of active muscle fibres, however, are not suitable for simulations of many aspects of recorded EMG signals. In most of the models, the application of the boundary conditions entails the problem that very ill-conditioned matrix equations have to be solved or that

numerical computer overflow or underflow occur during the calculations, especially when the active fibre is located eccentrically in a limb model. In this thesis, new mathematical tools are described for avoiding these numerical problems in calculating potential fields in cylindrical bounded volume conductors.

After studying the influence of the muscle fibre environment an MUAP model can be built. In this thesis we shall use a description of the motor unit geometry similar to those that have been used before but with the inclusion of the adaptations to the SFAP modelling mentioned above. Especially the influence of the two finite aspects : the muscle fibre length and the muscle dimension, will be illustrated by simulating skin surface SFAPs and MUAPs.

4) Can an analytical description be formulated which describes the influence of the presence of a needle electrode shaft on EMG recordings?

The influence of the recording electrode on the recorded potentials is an important subject in our study. Some reports can be found in which an attempt was made to incorporate this influence. One example is a study in which, for the SFAP calculation in an MUAP model, the potential was averaged over a rectangular surface whose size is comparable to the tip surface of a concentric needle electrode [62]. Another method for incorporating the influence of the concentric needle electrode has been presented in which the muscle fibres crossing the insertion channel are pushed to one side by the bevelled electrode tip, and in which the action potentials from muscle fibres lying on the back of the electrode shaft are registered by the shaft only [88]. Although both methods contain appealing aspects, neither of them describes the electrochemical interaction that will take place between the metal electrode shaft and the surrounding tissue. This effect is well known to electrochemists [61] but its consequences for EMG recordings are not yet fully understood. In this thesis, the influence of the presence of the electrode shaft and its interactions with the surrounding tissue shall be treated as a perturbation of the potential field in the homogeneous situation. As we have discussed above, the SFAP recordings must first be fully understood before MUAP recordings can be completely understood. In this thesis, therefore, a model is developed that describes the influence of a standard single fibre electrode on the recording of an SFAP on a short distance. The most important results and implications of this analysis will be discussed.

Experimental techniques : Scanning EMG and multi-electrode EMG.

The importance of a volume conductor model can only be established by experimental verification. In order to obtain experimental results which can be compared with the predictions of the volume conductor models described in the previous section, sophisticated EMG techniques have to be used. In the investigations concerning the finite dimensions of the volume conductor, a combination of an EMG decomposition technique [85] applied to simultaneous intramuscular and skin surface EMG recordings has been used.

Besides verifying various aspects of SFAP and MUAP modelling, gathering information on the motor unit structure is another experimental aspect which should be a main goal in diagnostic applications. In spite of all the efforts in this direction many questions about the motor unit in human skeletal muscle under

normal and pathological conditions remain unanswered. In the description of the motor unit geometry above, the values of several parameters must be based on data concerning animal muscles.

An electrophysiological method by which a clear view of the morphological structure of the end plate region can be obtained is the scanning EMG method. It was first described by Stålberg et al. [117]. In this technique a concentric EMG needle electrode is pulled through the territory of a motor unit. The recording of data and the motion of the pulling stepper motor are controlled by the action potential recorded from one single muscle fibre belonging to the same motor unit. After Stålberg et al. had developed the method, its main application was found to be in comparing the summation of all recorded signals with a macro EMG recording. After that, the interest in this technique remained limited, partially because of the complexity of the measurements. For the basic questions in this thesis, the scanning EMG technique was re-evaluated.

Apart from gathering information on motor unit structure, we also used scanning EMG to study whether this method could be used to gain insight into the volume conduction of MUAPs and into the influence of the standard concentric needle electrode on the MUAP recording. Besides this, we performed scanning EMG on a group of healthy test subjects and two patient groups with clearly diagnosed neuropathic and myopathic disorders, as a pilot study for the clinical usefulness of the method.

The results of the model describing the influence of the needle electrode will be compared with multiple SFAP recordings obtained with a multi-electrode. Such electrodes, which have been used in the past for MUAP recordings [17] and SFAP recordings [115], contain a linear array of 8 to 14 leading-off surfaces along the needle shaft. The electrode used in our research is typically devised for multiple SFAP recordings. The next section introduces the way in which recordings obtained with this electrode can be used in an application of the volume conductor model described in Chapter 5 and Chapter 6.

The inverse problem

As we mentioned before, there are many useful methods available for obtaining and classifying MUAPs in clinical measurements. These methods cannot in general produce information about functional parameters underlying the generation of SFAPs and MUAPs (the inverse problem). To obtain this kind of information an inverse procedure is necessary. Recorded SFAPs and MUAPs have to be compared with the simulation results obtained from a valid, forward model. When this model is appropriate, useful parameters describing the functional state of muscle fibres in a motor unit can be obtained and can be used in methods for diagnosing pathologies earlier and more accurately than is possible with the present MUAP analysis. Successful applications of such inverse procedures have been reported in other parts of the bio-electric research field [92,110,123,127].

As the first step towards the inverse approach, a parameter estimation on recorded SFAPs is presented in this thesis. From multiple SFAP recordings, obtained both by scanning EMG and by multi-electrode single fibre EMG, some parameters describing the recording geometry and electrical properties of the muscle fibre and the muscle tissue are estimated. The model in which the influence of the

single fibre electrode is included is used as the underlying forward model for this inverse problem.

Survey of the present study

In Chapter II, which follows this General Introduction, the frequency dependence of the muscle tissue conductivities and the spatio-temporal source description of the finite length muscle fibre are evaluated. In Chapter III, a numerical method is presented which enables the solution of potential field problems with cylinder symmetrical boundary conditions, without suffering from ill conditioning of the matrix equations implied by the boundary conditions, or from numerical machine overflow or underflow during the calculations. The results obtained in Chapters II and III are applied to both SFAP and MUAP modelling in Chapter IV, where the influence of the finite volume conductor on the simulated potentials is documented. Some of the main conclusions based on the simulations will be evaluated by comparing them with recorded surface MUAPs. Chapters V and VI contain the description of and the results obtained with the model describing SFAPs recorded by a single fibre electrode. The model includes an electrical double layer formed by electrochemical interaction between the metal electrode shaft and the surrounding tissue. In Chapter V the mathematical formulation of the model is derived. The evaluation of the model results and some practical consequences which follow from these results are presented in Chapter VI. In Chapter VII the scanning EMG technique is reviewed. Results of the clinical application of the scanning EMG and of the volume conductor effects studied with it, will be shown. Chapter VIII describes the inverse procedure on multiple SFAP recordings, based on the model developed in Chapter V. In Chapter IX the main results and conclusions are summarised and discussed.

Chapter II

A general approach to modelling extracellular action potentials of finite length muscle fibres. [1]

Abstract
A new algorithm for single muscle fibre action potential simulations is presented. The temporal and spatial properties of the muscle fibre activity pattern and of the volume conduction weighting function are treated separately. In this way the aspects of finite muscle fibre length and capacitive tissue properties are easily incorporated in the model. Simulation results stress the importance of considering muscle fibres of finite length, whereas the effects resulting from the capacitive muscle tissue properties appear to be negligible.

II.1 Introduction

The history of modelling extracellular single fibre action potential fields (SFAP) of the peripheral neuromuscular system started in 1947 with the well known work of Lorente de No [83]. In the late sixties, when computers brought better computational facilities, new interest arose in the modelling of the electrophysiology of nerve and muscle [24,103]. In the two decades that have passed since then a number of papers on this subject have been published (e.g. [6,28,38,86,96]).

About ten years ago the first motor unit action potential (MUAP) simulations were presented in literature [14,62,63]. Each of these publications stressed its own restricted aspects of MUAP simulation. Together they led to the present state of the art in MUAP simulation in which the volume conductor description can be characterised as being homogeneous, anisotropic and resistive.

In the field of SFAP modelling new aspects such as (i) finite fibre length [65,66],

[1] T.H.J.M. GOOTZEN, D.F. STEGEMAN and A. VAN OOSTEROM. *Submitted to IEEE Trnas. Biomed. Eng.*

(ii) capacitive muscle tissue properties [49,107], (iii) inhomogeneous modelling of muscle tissue, both in discrete numerical methods [3,48] and in analytical expressions [42,55,105] and (iv) current redistribution [98,106] have been studied in the past few years.

No attempt is known to the authors in which these aspects are included in a compact MUAP simulation model. The main reason for this is the enormous increase in computational complexity which most of the new aspects brought with them. To overcome this problem we have developed a new algorithm for SFAP calculations in which the aspects mentioned in the previous paragraph can easily be included, without losing the efficient structure of the algorithm. This last condition is necessary when the SFAP simulation model is used as the basis of a MUAP simulation model. The resulting MUAP simulation model in its turn should be an appropriate basis for the development of a procedure for estimating structural and functional parameters of a motor unit from intramuscular and surface electromyographical recordings.

This chapter reports on the inclusion of two of the aspects mentioned above, namely the finite muscle fibre length and the capacitive muscle tissue properties, in the SFAP modelling. It will be demonstrated how the conventional method for calculating SFAPs, i.e. through a convolution of a source function and a volume conduction weighting function, can be converted into a method which does not require the uniform propagation of an action potential along a muscle fibre of infinite length (section II.2.1). This is achieved by treating the spatial and temporal properties of the activity of a muscle fibre separately. For this goal the muscle fibre activity is stored in a matrix (section II.2.2), which allows a description of the excitation of the SFAP at the motoneuron endplate and the extinction of the SFAP at the muscle fibre ending.

The treatment of the volume conduction weighting function as a spatial and time dependent function will enable us to include the capacitive muscle tissue properties in an elegant method, in which the volume conduction weighting function is also represented in a matrix form. (section II.2.3). In section II.3.2 a description of the muscle tissue conductivities is derived in which the influence of the muscle fibre membrane capacitance in incorporated in a method deviating from methods reported in literature bu Roth and co-workers [106,107]. Our model, which intentionally does not contain this current redistribution, will be used to show the isolated influence of the frequency dependence of the muscle fibre membrane capacitance.

The parameters chosen for the construction of the two matrices, representing the source and the weighting function, are described in section II.2.4. Section II.3 shows some representative results, which will be discussed in section II.4.

II.2 Methods

II.2.1 Analytical description of the SFAP

The most straightforward method for calculating the potential at observation point (r, z) resulting from a source distribution along a fibre is the integration of the current source density distribution I weighted by the volume conductor weighting

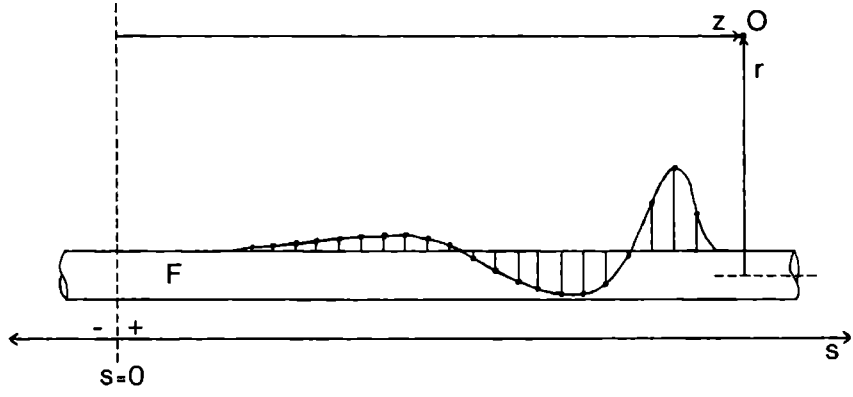

Figure II.1 : Muscle fibre with distributed electric activity. O = observation point with r = radial distance and z = axial distance from origin, F = active muscle fibre with s = location in axial direction.

function W. In the line source approximation [103], the fibre is assumed to have diameter zero and, therefore, an integration has to be carried out along this source line only.

$$\phi(r,z) = \int_{-L}^{L} I(s)W(r,z,s)ds \tag{II.1}$$

In eq. II.1, r and z represent the radial and axial coordinate respectively of the observation point, s the location of the sources along a muscle fibre (fig. II.1) of length $2L$, I the current source density distribution and W the volume conductor weighting function. Most commonly, the assumption $L = \infty$ is made for the integration boundaries and one action potential (from which the current source function is derived) is assumed to be propagating at a constant velocity.

The assumption of infinite fibre length usually seems reasonable for recordings from peripheral nerves, but for the majority of musclular recordings it is questionable. The activity pattern of an active muscle fibre of finite length shows three discontinuities. First, at the endplate, the action potentials are initiated. From this location, two separate action potentials start propagating in two opposite directions. The propagation of the two action potentials stops at the two endings of the muscle fibre and the action potentials extinct in some way. The total electric activity of a muscle fibre under these conditions will be described in section II.2.4.

Eq. II.1 describes the observed potential for one time instant when propagating action potentials are present. The time dependence can be described by replacing $I(s)$ by $I(s,t)$

$$\phi(r,z,t) = \int_{-L}^{L} I(s,t)W(r,z,s)ds \quad . \tag{II.2}$$

Electrophysiologic phenomena are usually observed as a function of time at a fixed observation point. Eq. II.2 can be easily adapted to this situation by no longer considering r and z as variables

$$\phi(t) \mid_{r,z} = \int_{-L}^{L} I(s,t)W(s)ds \quad . \tag{II.3}$$

The integration of the muscle fibre source strength I multiplied by the observation distance dependent weighting function W is carried out over the entire length of the muscle fibre for each time instant t.

There have been reports in literature suggesting the necessity of incorporating a general, non-quasistatic, nature of the volume conductor. In muscle tissue this time dependence is thought to be caused by the capacitive effects in the muscle fibre membranes. In these cases, the volume conductor weighting function will also be time dependent. It describes in which way the observation of the potential at time t is influenced by the activity of the muscle fibre at earlier time instants (causality). Introducing the time dependence in eq. II.3 leads to

$$\phi(t) \mid_{r,z} = \int_{-L}^{L} \int_{0}^{\infty} I(s,\tau)W(s,t-\tau)d\tau ds \quad . \tag{II.4}$$

This double integral is the compact formulation of SFAP genesis which will be the basis of the subsequent analysis.

If no time dependent effects are present the volume conductor is called quasi-static. The temporal dependence of the volume conductor weighting function then reduces to a Dirac δ-function

$$W(s,t-\tau) = W(s)\delta(t-\tau) \quad . \tag{II.5}$$

The convolution in the temporal domain over τ can be replaced by a multiplication in the temporal frequency domain. Eq. II.4 then changes into

$$\phi(t) \mid_{r,z} = \int_{-L}^{L} \mathcal{F}^{-1}\left[\mathcal{I}(s,\nu)\mathcal{W}(s,\nu)\right] ds \quad , \tag{II.6}$$

$$= \mathcal{F}^{-1}\left[\int_{-L}^{L} \mathcal{I}(s,\nu)\mathcal{W}(s,\nu)ds\right] \quad , \tag{II.7}$$

where $\mathcal{I}$ and $\mathcal{W}$ represent the Fourier transformed functions, ν the temporal frequency and $\mathcal{F}^{-1}$ the inverse Fourier transform. From eq. II.5 it can be concluded that in a quasi-static situation

$$\mathcal{W}(s,\nu) = W(s) \quad . \tag{II.8}$$

II.2.2 Algebraic equivalences of the SFAP calculation

Algebraic expressions, corresponding to their analytical counterparts as described in the previous subsection, need to be formulated in order to be able to perform the SFAP calculations. From these expressions a numerical implementation can be derived. We start from eq. II.3 in which the functions ϕ, W and I can be replaced by two vectors and a matrix. The resulting system of linear equations is

$$\phi = Iw \quad , \tag{II.9}$$

where element i, j of the matrix I is defined by

$$I_{i,j} = I(s_i, t_j) \quad , \tag{II.10}$$

and element i of the vector w by

$$w_i = W(s_i) \quad . \tag{II.11}$$

The resulting elements of the vector ϕ are calculated according to

$$\phi_j = \sum_i I_{i,j} w_i \quad . \tag{II.12}$$

Eq. II.4 can be transformed into the following algebraic expression, in which the vector w from eq. II.9 is replaced by a matrix W with the time index j as second dimension

$$\phi_j = \sum_{i=1}^{N} \sum_{k=1}^{j} I_{i,k} W_{j-k,i} \quad . \tag{II.13}$$

The frequency domain analogy, equivalent to eq. II.6 reads

$$\phi_j = \left[\sum_{i=1}^{N} \mathcal{F}^{-1} \left[\mathcal{I}(s_i, \nu) \mathcal{W}(s_i, \nu) \right] \right]_j \tag{II.14}$$

$$= \left[\mathcal{F}^{-1} \left[\sum_{i=1}^{N} \mathcal{I}(s_i, \nu) \mathcal{W}(s_i, \nu) \right] \right]_j \quad . \tag{II.15}$$

The compact formulation of expression II.15 provides a powerful basis for the numerical implementation of the SFAP calculations.

II.2.3 The volume conduction weighting function

Mathematical formulation

Appropriate volume conductor weighting functions can be derived for many different volume conductor configurations, e.g. [6,103,121], including boundaries and inhomogeneities in the volume conductor.

The most widely used and simplest configuration is the one in which the muscle fibre is assumed to be placed in an infinite, *isotropic* medium. The potential measured at a distance R from a point-shaped source i then equals [72]

$$\phi = \frac{1}{4\pi\sigma}\frac{i}{R} \quad , \tag{II.16}$$

where σ is the conductivity of the medium.

The line-source model for *anisotropic* tissue described e.g. by Rosenfalck [103] is an extension of eq. II.1 to infinite, anisotropic media. The extracellular potential from a muscle fibre in a homogeneous tissue with cylinder symmetrical, anisotropic conductivity can be expressed as

$$\phi_e(r,z) = \frac{1}{4\pi\sigma_r}\int_{-L}^{L}\frac{2\pi a I_m(s)}{\sqrt{r^2\frac{\sigma_z}{\sigma_r}+(z-s)^2}} \tag{II.17}$$

where a is the diameter of the fibre and $2L$ its length, σ_r and σ_z are the conductivities in radial and axial direction and $I_m(s)$ is the membrane current source density distribution along the muscle fibre.

In this homogeneous situation, σ_r can be brought within the integral

$$\phi_e(r,z) = \int_{-L}^{L}\frac{\frac{a}{2}I_m(s)}{\sqrt{r^2\sigma_z\sigma_r+(z-s)^2{\sigma_r}^2}} \tag{II.18}$$

Eq. II.18 corresponds to eq. II.1 with

$$I(s) = 2\pi a I_m(s) \tag{II.19}$$

and

$$W(s)\mid_{r,z} \quad \frac{1}{4\pi\sqrt{r^2\sigma_z\sigma_r+(z-s)^2{\sigma_r}^2}} \tag{II.20}$$

Note that, in this approach, the fibre diameter is present in the source function I and absent in the volume conductor weighting function W (line source approximation).

SFAP calculations are often performed in the spatial frequency domain. The volume conductor weighting function is then expressed in the spatial frequency k, in combination with the use of modified Bessel functions, and reads for an infinite volume conductor

$$W(k) = \frac{1}{2\pi\sigma_r}K_0\left(k\rho\sqrt{\frac{\sigma_z}{\sigma_r}}\right) \quad . \tag{II.21}$$

The frequency dependent volume conductor

The capacitive effects caused by the muscle fibre membranes can be effectively incorporated by assuming the tissue parameters σ_r and σ_z to be frequency dependent, complex conductivities $\sigma_r(\nu)$ and $\sigma_z(\nu)$. The weighting function from eq. II.20 expressed in the frequency domain now depends on the spatial parameters, r and s, and on the frequency ν as

$$\mathcal{W}(s,\nu)\,|_{r,z} \quad \frac{1}{4\pi\sqrt{r^2\sigma_z(\nu)\sigma_r(\nu)+(z-s)^2\sigma_r(\nu)^2}} \tag{II.22}$$

Note that $\mathcal{W}(s,\nu)$ has the form required for eq. II.6.

In purely resistive tissue, $W(s,t)$, the corresponding time-domain analogy of $\mathcal{W}(s,\nu)$, is a δ-function in time of which the strength is determined by r, $z-s$, σ_r and σ_z (eq. II.20). In capacitive tissue, this function includes a non-zero part in the direction of the past time representing the influence of the source strength at an elapsed time instant.

The properties of $\sigma_r(\nu)$ and $\sigma_z(\nu)$ can be determined or estimated in three ways. The first method is by measurements, using the four point electrode technique [108,109]. Gielen [48,49] e.g. carried out several measurements on rat skeletal muscle. Data on human skeletal muscle are very scarce in literature [45].

The second method uses a geometrical representations of muscle tissue, which can be translated in equivalent electrical networks [3,48]. From this network direct calculations of SFAPs can be carried out [4].

For reasons to be discussed in section II.4.3, we introduce here a third method which also uses an electrical analogon but assumes the elements of the network to be homogeneously distributed.

Similar to the second method a simple tissue model is constructed (fig. II.2). From the cross-section of a piece of muscle tissue a "unit cell" is selected. This unit cell is approximated by a rectangular piece of tissue which contains two membrane layers, separating extracellular and intracellular tissue. For the modelling of σ_r we assume that there is only current flowing in a direction perpendicular to the membrane layers. From this model, we construct an equivalent network consisting of five resistors and two capacitors. The values of these components are calculated from σ_i and σ_e, the intra- and extra-cellular conductivities, and G_m and C_m, the conductivity and capacitance per unit area of membrane. A macroscopic frequency dependent conductivity $\sigma_r(\nu)$ can be calculated from the total impedance of this network Z_{eq} , according to

$$Z_{eq} = \frac{d}{A\sigma_r(\nu)} \quad , \tag{II.23}$$

where d, the height of the piece of muscle tissue, equals $d_1 + d_2$ (see table II.1) and A, the area of the top surface, equals $d_1(d_1 + d_2)$.

From the same unit cell $\sigma_z(\nu)$ is calculated. Under the first order approximation that all current flows parallel to the membrane layers and no current passes the membranes, σ_z is mainly determined by the fraction p of the cross section of the unit cell (=front surface) occupied by intracellular tissue [49]

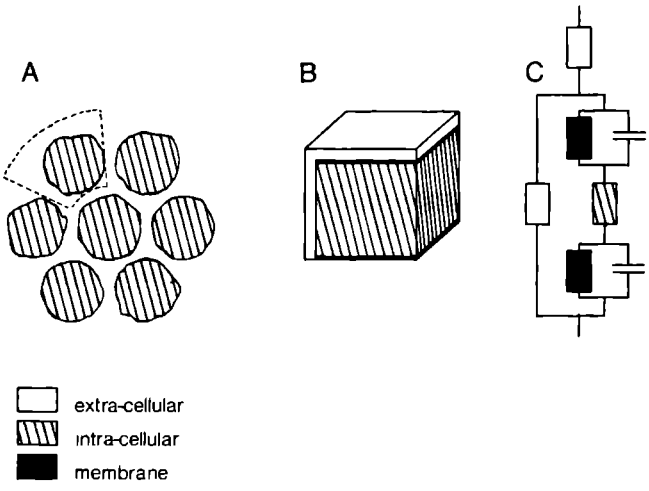

Figure II.2 : Simple network model for calculating radial and axial conductivity of muscle tissue. A) cross section of a piece of muscle tissue, dotted line indicates unit cell, B) transformed unit cell, C) equivalent electrical network.

$$\sigma_z = (1-p)\sigma_e + p\sigma_i \quad , \; 0 < p < 1 \quad . \tag{II.24}$$

Note that σ_z calculated in this way is frequency independent. The parameter values listed in table II.1 are taken from [49].

Table II.1 Tissue parameters

parameter	value	unit	
σ_i	0.55	$(\Omega\mathrm{m})^{-1}$	intracellular conductivity
σ_e	2.4	$(\Omega\mathrm{m})^{-1}$	extracellular conductivity
G_m	1	$\Omega^{-1}\mathrm{m}^{-2}$	membrane conductivity
C_m	0.01	Fm^{-2}	membrane capacitance
d_1	50	μm	muscle fibre diameter
d_2	1.35	μm	distance between fibres

The conductivities defined in this way only describe the frequency dependence caused by the fact that current floating through the muscle fibre membranes encounters capacitive elements. Another important aspect, also introducing a frequency dependence, is the current redistribution between the intracellular and the extracellular space [106,107]. This aspect is intentionally omitted from our model, in an attempt to isolate the first frequency dependence described above. The consequences shall be discussed in section II.4. The parameter values listed in table II.1 are taken from [49].

II.2.4 The muscle fibre activity pattern

The muscle fibre source function

For the construction of the matrix I we need to specify the muscle fibre source function. Here we start from the analytic expression for the intracellular action potential, introduced by Rosenfalck [103]

$$V_i(z) = Az^3e^{-\lambda z} - B \quad z \geq 0. \tag{II.25}$$

The original numbers given by Rosenfalck for the parameters A,B and λ are respectively 96 mV.mm^{-3}, -90 mV and 1 mm^{-1}. By using the transformation $z = vt$, with $v = 4$ m.s^{-1}, the waveform is transformed to the temporal domain. The value of 4 m.s^{-1} for the conduction velocity is the one Rosenfalck used to fit his spatial representation of the intracellular action potential to measured intracellular action potentials in the temporal domain. After the transformation, the values of the three parameters equal 6.144 10^9 V.s^{-3}, 0.09 V and 4.0 10^3 s^{-1}.

The intracellular action potential according to eq. II.25 corresponds reasonably well to the intracellular action potentials as measured by Wallinga-de Jonge et al. [128] in the soleus muscle in the rat and by Ludin [81] in human muscle fibres.

The physical quantity which actually describes the muscle fibre activity is the transmembrane current source density, which is proportional to the second derivative of eq. II.25 [103], (fig. II.3)

$$I_m(z) = \frac{\sigma_i a}{2} \frac{d^2V_i(z)}{dz^2} \tag{II.26}$$

$$\frac{d^2V_i(z)}{dz^2} \propto A\lambda z(6 - 6\lambda z + \lambda^2 z^2)e^{-\lambda z}$$

The triphasic waveform of V_i'' (" denotes the second temporal derivative) was calculated over a total duration of 2.5 ms with a time resolution dt of 0.05 ms. This sampled version of the V_i'' waveform is used for constructing the matrix I. For reasons to be discussed in Chapter VI and VIII a modified version of this source waveform will be used in these two chapters.

Finite muscle fibre length

As mentioned before in section II.2.1, the geometry found in skeletal muscle is that of muscle fibres which are innervated by the motoneuron endplate, which is located somewhere half-way the length of the muscle fibre. After excitation by the endplate, two action potentials start propagating uniformly, in opposite directions, towards the two fibre endings. The two action potentials will extinct at the two endings. The current source density distribution (CSDD) for every location between the endplate and the fibre endings as a function of time is characterised by the V_i" waveform shown in fig. II.3. Different CSDD have to be present at the endplate and at the fibre endings, in order to maintain a total current

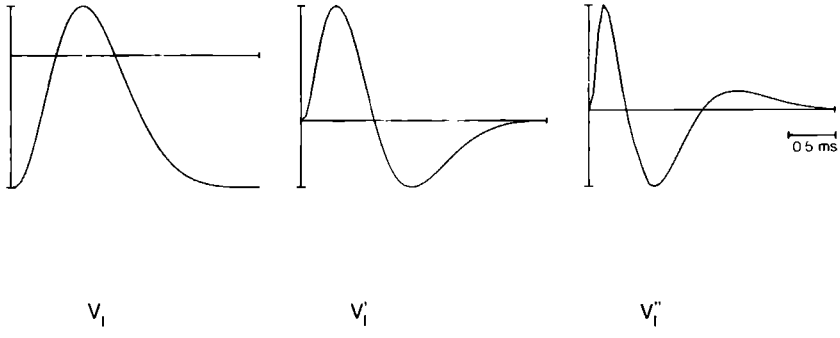

Figure II.3 : Intracellular action potential (V_i) with first (V_i') and second (V_i'') derivative.

source density (CSD) of zero, regarded over the entire muscle fibre length and at every time instant. These CSDDs have to compensate for that part of the action potential CSDD which is not yet propagating along the muscle fibre or is no longer propagating respectively.

We assume that these changes in the CSDDs occur over a very small part of the muscle fibre only. In the discretised version of the complete CSD pattern, which is stored in the I matrix (see eq. II.2 and II.10, these locations are the middle row of the matrix and the two outer rows only. In order to obtain the necessary CSD compensation the middle row of the matrix has to be filled with a CSDD which equals the time-integration of V_i'', multiplied with a factor -2. The two outer rows are filled with a CSDD which equals the time-integration of V_i''. The shape of this CSDD is equal to the V_i' waveform from fig. II.3. The total number of rows needed for the description of a complete CSD pattern, of which an example is shown in fig. II.4, depends on the muscle fibre length, the muscle fibre diameter and the chosen spatial resolution.

The assumptions underlying this approach shall be extensively discussed in section II.4.2.

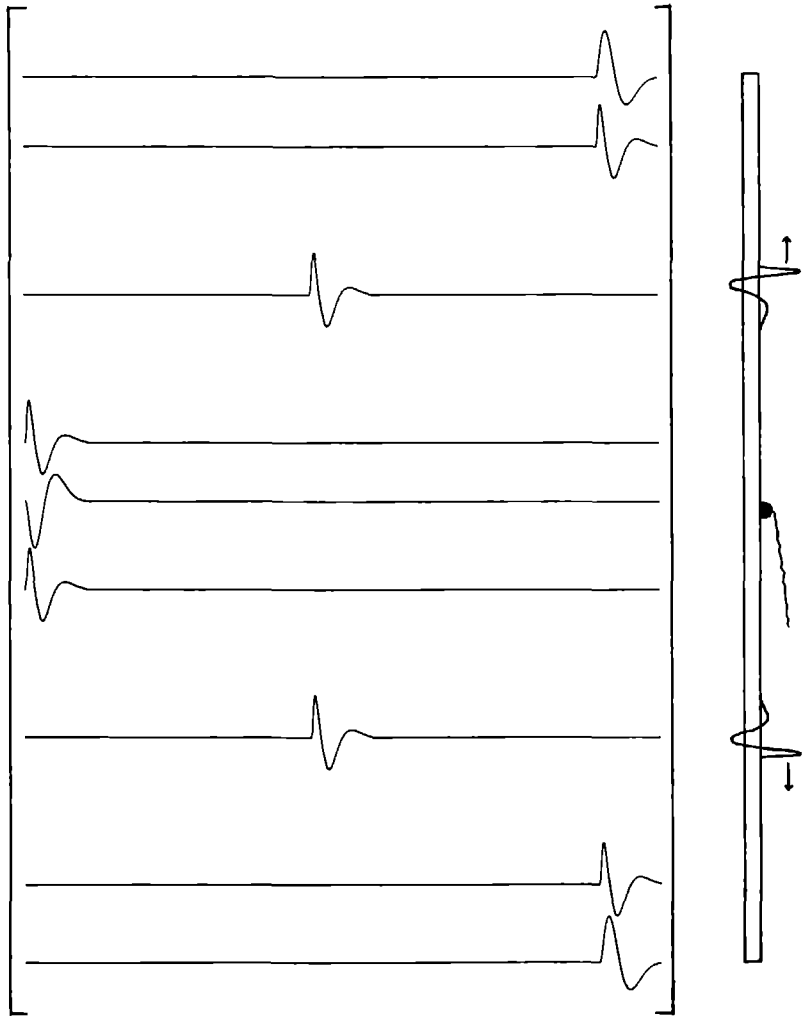

Figure II.4 : Matrix I represented by plotting its rows as continuous functions with two action potentials propagating in opposite directions and with biphasic waveforms for start and stop effects. At the right side of the matrix a schematic drawing of the muscle fibre is presented. The situation with the two action potentials indicated on the muscle fibre corresponds to a column of the matrix I somewhere in the middle of the matrix.

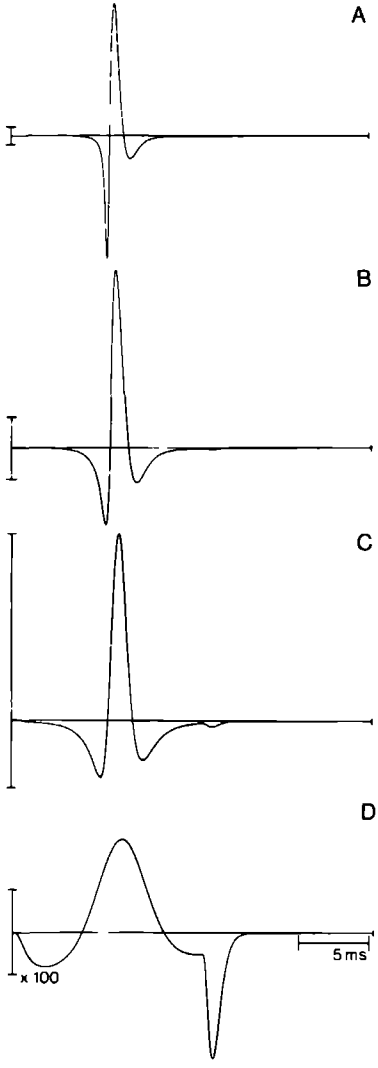

Figure II.5 : SFAP simulations at different radial distances with σ_r = 0.05 (for ν =0) and σ_z = 0.5. A) 0.1 mm, B) 0.5 mm, C) 1.0 mm, D) 5.0 mm. 1 scale division = 100 μV.

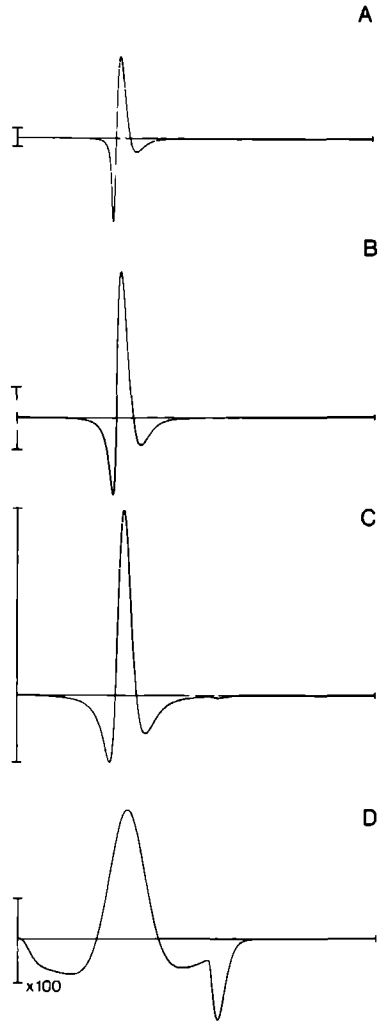

Figure II.6 : SFAP simulations at the same radial distances as in fig. II.6 but with a changed anisotropy ratio : σ_r = 0.1 (for ν = 0) and σ_z = 0.5.

II.3 Results

SFAP waveforms, simulated as a recording of a point shaped electrode relative to a reference electrode at infinity, are shown in fig. II.5 and II.6 for radial distances of 0.1, 0.5, 1.0 and 5.0 mm and an axial distance of 25 mm from the centre of the endplate zone. The fibre length was 100 mm, so the observation was half-way the motor end plate and the fibre ending. Fig. II.5 shows the four SFAPs at different radial observation distances to the muscle fibre for the conductivities $\sigma_r|_{\nu=0} = 0.05$ and $\sigma_z = 0.5$ and fig. II.6 for $\sigma_r|_{\nu=0} = 0.1$ and $\sigma_z = 0.5$. In both figures one scale division corresponds to 100 μV. Note that the SFAPs are plotted with negative potentials upwards, according to the neurophysiological tradition. This tradition will be upholded until Chapter IV, but in Chapter V it shall be broken with.

The intra- and extracellular conductivities listed in table II.1 have been adapted to obtain these effective radial and axial conductivities. These changes are well within physiological range [45]. The influence of changes in the anisotropy ratio on the SFAP amplitude and on the radial decline of the SFAP amplitude can be seen clearly.

An extra positive dip, most clearly seen in fig. II.5D and II.6D, appears in the tail of the SFAP. This dip is caused by the extinction of the action potential at the end of the muscle fibre. At the starting moment of the action potential a different notch, much smaller in amplitude, can be found at the beginning of the first positive peak.

Fig. II.7 and II.8 show SFAP waveforms simulated around the endplate location and around the muscle fibre-tendon transition respectively. The amplitudes for fig. II.7 are 40 μV full scale for the upper row, 500 μV for the middle row and 2.5 mV for the lower row. In fig. II.8 the full scale amplitudes are 30 μV, 500 μV and 1.5 mV respectively. The length of the muscle fibre is 100 mm. Since the amplitudes of waveform 9 in fig. II.7 and of waveform 7 in fig. II.8 are equal (athough not plotted on the same scale), it can be concluded that in close observation the amplitude of the biphasic waveform 7 in fig. II.7 at the end-plate is much greater than the amplitude of the biphasic waveform 9 in fig. II.8 at the fibre ending.

In fig. II.9 the four SFAPs from fig. II.5 are shown, together with the difference between the SFAPs modelled with and without capacitive effects included in the model. As can be seen clearly, the influence of the capacitive effects is maximal during the fast slopes of the action potential, but the effect as such is small.

II.4 Discussion

II.4.1 General

We presented an algorithm for calculating single muscle fibre action potentials as the first part of a study whose aim it is to make an inventory of all the essential aspects of single muscle fibre and motor unit action potential simulation. Two important modifications with respect to the SFAP calculations presented in earlier models described for MUAP simulations are the incorporation of finite muscle fibre length and the frequency dependent description of the muscle tissue conductivity in the volume conductor weighting function. The matrix representation, presented in

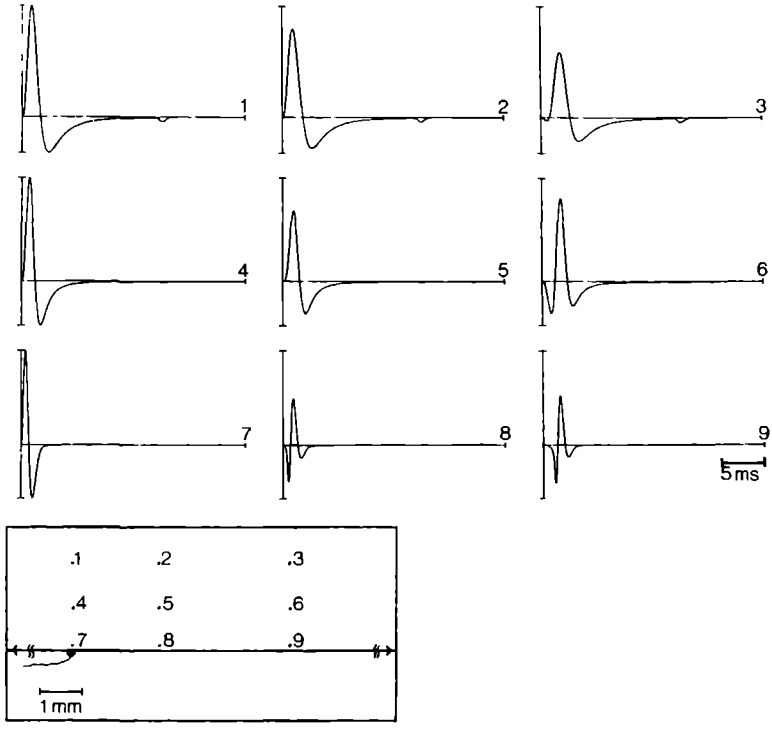

Figure II.7 : Different SFAP waveforms due to start effects near endplate region for $r = 0.1$, 1.0 and 2.0 mm $z = 0.0$, 2.0 and 5.0 mm. Other parameters as in table II.1. SFAPs in the same row (e.g. 1, 2 and 3) are plotted with the same scaling. The full scale amplitudes for the upper, middle and lower row are 40 μV, 500 μV and 2.5 mV respectively.

the theoretical part of this chapter, resulted in a simple numerical implementation of the model.

Certain basic SFAP simulations have been presented of which some aspects shall be discussed below.

II.4.2 Finite fibre length

The SFAP simulations fig. II.5 and II.6 seem to be in good accordance with other simulation results reported in literature and also show a reasonable agreement with measured single fibre potentials [33]. The biphasic start and stop effects, described in section II.2.4 are clearly present in fig. II.7 and II.8, and appear to be similar to the measurements reported by Gydikov et al. [65] and Katz and Miledi [73].

The assumptions made to describe the start and stop effects are, although

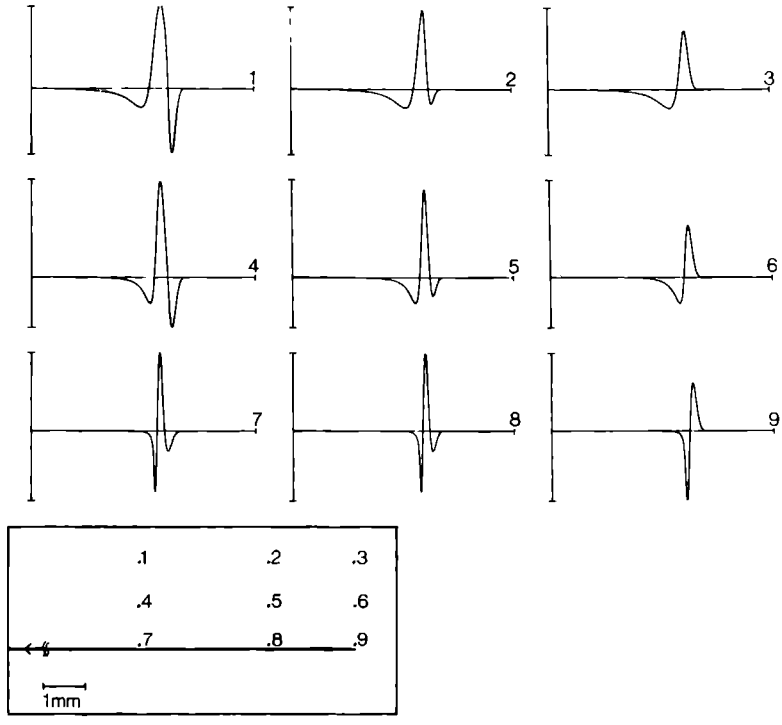

Figure II.8 : Different SFAP waveforms due to stop effects near fibre-tendon transition ($z = L$) for r = 0.1, 1.0 and 2.0 mm $z = L$, L-2.0 and L-5.0 mm. The full scale amplitudes are 30 μV, 500 μV and 1.5 mV for the upper, middle and lower row respectively.

simple of nature, in agreement with evidence provided earlier by Plonsey [97] and by Dimitrova [30] about the stop effect for action potentials at the muscle fibre-tendon transition and measurements by Katz and Miledi [73] in the endplate region. According to Plonsey [97], the transmembrane current source density at the fibre-to-tendon transition point is such that the total transmembrane current source density over the active part of the fibre is zero. Also Gydikov et al. [65] and Gydikov and Trayanova [66] showed in their measurements and calculations that near the endplate and near the fibre-tendon transitions biphasic waveforms arise, which correspond to the first derivative (V_t') of the intracellular action potential V_t from eq. II.25.

The advantage of our description is that, unlike e.g. the model described by Ganapathy et al. [42], no intracellular potentials or membrane kinetics have to be evaluated. Our model is able to generate an effective description direct at the level of the source functions (the current source density distributions) which have to be used in the volume conductor models. The storage of a complete current source

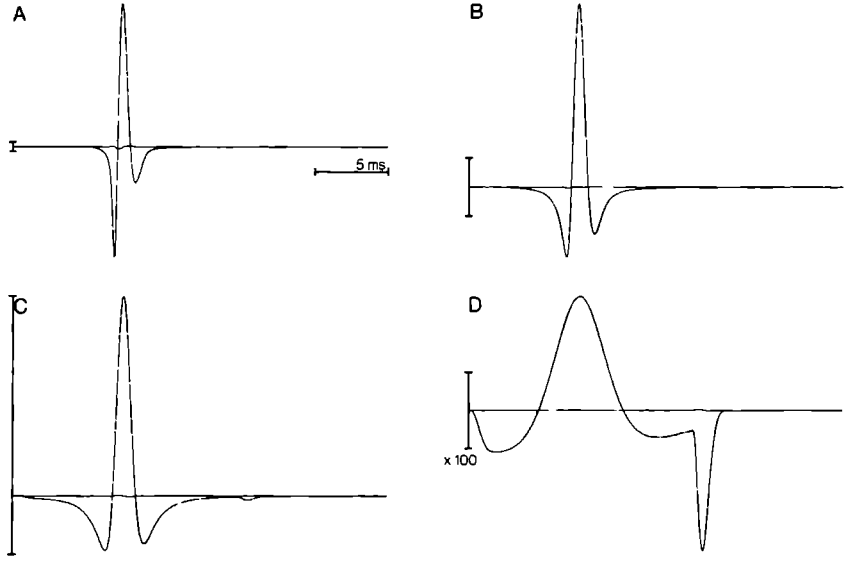

Figure II.9 : SFAP simulation, corresponding to fig. II.5, with capacitive effects (larger waveforms) and difference between simulation with and without capacitive effects (smaller waveforms). Note that no baselines but only the small waveforms presenting the difference are plotted. 1 scale division = 100 μV.

density pattern of an active muscle fibre allows an easier and faster adaptation to changing geometrical parameters than conventional descriptions.

Although other models for the extinction of the action potential can be proposed [10], the simple solution chosen in our algorithm is able to explain extracellular potentials near the endplate and the tendon resulting from more detailed modelling of the action potential stop, carried out by Kleinpenning et al. [74]. The physical interpretation of the start and stop effects is that non-moving dipoles occur at the motoneuron terminal and at the muscle fibre-tendon transition. Near the motoneuron terminal two dipoles are present, with the dipole vectors standing in opposite directions. This accounts for the fact that in fig. II.5 the extra phase in the SFAP due to the start effect is small whereas a clear extra positive dip can be seen from the stop effect, even near the endplate, at great distance from the muscle fibre-tendon transition (fig. II.7).

In the simulations shown so far, the volume conductor has been assumed to be of infinite size. A strong influence can be expected on the amplitude of this dip from volume conductors of finite extend, because of the dipolar character of the start and stop effects [122].

Fig. II.10A and II.10C, and fig. II.10B and II.10D, show simulated SFAP's, at corresponding longitudinal locations of z = 1 mm and z = 25 mm respectively. In fig. II.10C and II.10D, however, a medium with a finite radial dimension is as-

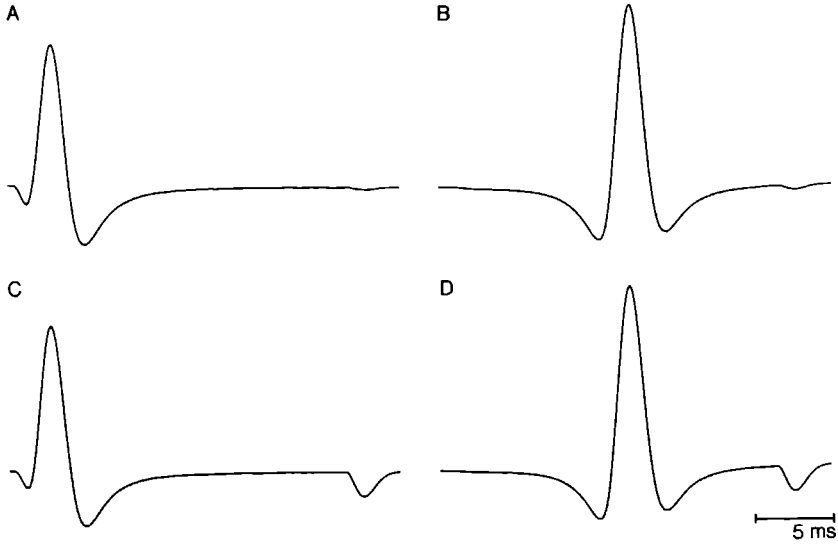

Figure II.10 : Effects of finite muscle dimensions on SFAP simulations. Radial distance $r = 2$ mm for all simulations. A) SFAP simulated at $z = 1$ mm, infinite muscle tissue, B) SFAP simulated at $z = 25$ mm, infinite muscle tissue, C) same location as A, finite radial dimension muscle tissue, D) same location as B, finite radial dimension muscle tissue.

sumed. The stop effect is considerably enhanced, whereas the start-effect remains unvisible in fig. II.10B and II.10D. From these results in a simple finite volume conductor, we concluded that further investigations have to be carried out on the influence of the finite muscle and limb dimensions [51,55].

II.4.3 Frequency dependence

The treatment of the frequency dependence of the conductivities appears to be numerically elegant. The capacitive effects, however, seem to be small. Other simulation studies reporting larger effects due to the inclusion of frequency dependent muscle tissue properties [3,48], used methods for describing the tissue properties in which temporal frequency dependence was in some way intermingled with its spatial frequency dependence, as was shown by measurements [49] as well as by theoretical study [107]. Roth and Gielen [107] showed that this extra frequency dependence is caused by the current redistribution between the extracellular and intracellular medium. For an action potential, uniformly propagating with velocity v, the temporal frequency dependence can be translated into a spatial frequency dependence ($k = \frac{\omega}{v}$, the k-domain is the Fourier transform of the z-domain which represents the axial direction of the muscle fibre). The frequency dependence can

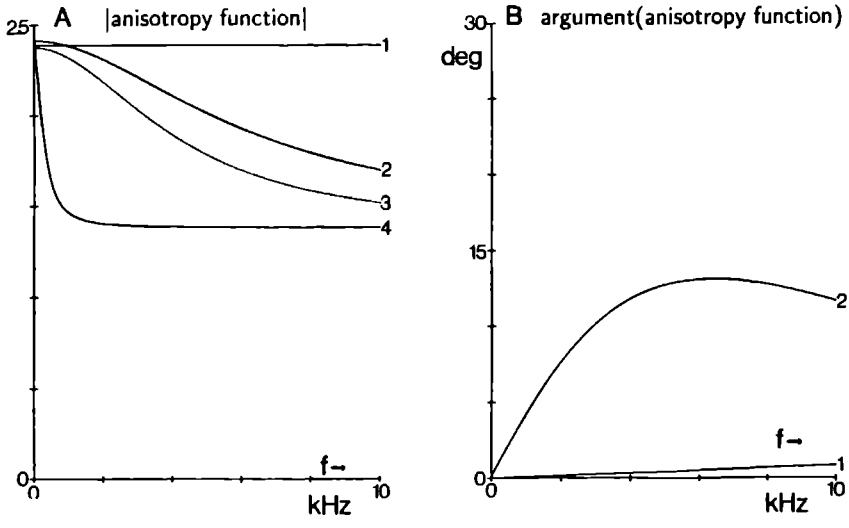

Figure II.11 : Mode and argument of the anisotropy function $\eta(k)$ for different models. (1) Model from section II.3.2, (2) Model from Roth et al. [107], (3) Adapted version of 2 with $C_m = 0$ and $G_m = 200$, (4) Adapted version of 2 with $C_m = 0$ and G_m at default value (see Table II.1). A) Mode of the anisotropy function, B) Argument of the anisotropy function.

be described by

$$\eta(k) = \sqrt{\frac{\sigma_z(k)}{\sigma_r(k)}} \quad , \tag{II.27}$$

in which $\eta(k)$ can be called the frequency dependent anisotropy function. In fig. II.11 the mode and the argument of this anisotropy function are plotted for several models.

The anisotropy function is plotted as a function of the temporal frequency ν ($\nu = \frac{\omega}{2\pi} = \frac{kv}{2\pi}$). The curves indicated with 1 represent the model described in section II.2.3. From these curves it becomes clear why in our model the frequency dependence is so small. The curves indicated with 2 correspond to the model described by Roth et al. [107]. In fig. II.12A SFAPs are plotted for the frequency dependent model of Roth et al. (solid curves) and our model (dotted curves, 1 scale division = 200 μV). Although, in fig. II.11, the difference between the two models does not seem to be negligible, in the SFAPs in fig. II.12A the differences can hardly be seen, both for small and great observation distances.

In fig. II.9, we showed that in our model the influence of removing the capacitive term in the membrane impedance did not cause noticeable changes. When in the Roth model the membrane capacitance is removed the anisotropy function changes from model 2 in fig. II.11 to model 4. This relevant change in the behaviour of the anisotropy function will cause considerable changes in the SFAP amplitudes. The cause of these changes is, however, not the transition from a partially capacitive to a purely resistive description of the muscle tissue conduc-

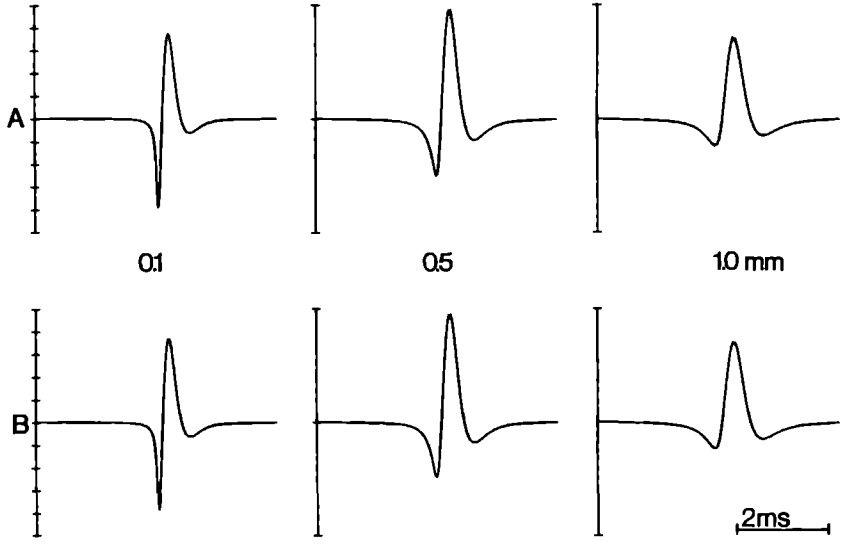

Figure II.12 : SFAPs for observations distances 0.1, 0.5 and 1.0 mm calculated with the different anisotropy functions shown in fig. II.13. A) solid curves: model from Roth et al. (model 2), dotted curves: model from section II.3.2 (model 1), B) solid curves: model from Roth et al. (model 2), dotted curves: adapted version of model 2 : $C_m = 0$ and $G_m = 200$ (model 3). 1 scale division = 200 μV.

tivities but the fact that no longer a proper current redistribution can take place since the remaining membrane resistance is very high. Reducing this membrane resistance by increasing G_m from 1 to 200 $\Omega^{-1}\mathrm{m}^{-2}$ results in an anisotropy function represented by model 3 in fig. II.11. In fig. II.12B SFAPs are plotted for the capacitive version (model 2) of the Roth model (solid curves) and the resistive version with adapted G_m (model 3) of the Roth model (dotted curves). Now, the differences are so small that the dotted curves can hardly be distinguished from the solid curves.

This analysis of the Roth model, and the findings of our own model, indicate undoubtedly that, effectively, there is no need for a capacitive component in the characterisation of muscle tissue conductivities (fig. II.12B) and no practical need for the implementation of the current redistribution (fig. II.12A). Although in a physiological situation, the membrane capacitance appears to be the only way along which current redistribution can take place, the frequency dependence of this capacitance as such does not play an important role. In models describing current redistribution a proper frequency dependence can be obtained with a purely resistive description.

We decided not to incorporate capacitive effects, nor the current redistribution in future SFAP and MUAP simulations, thereby replacing the matrix W by the

vector w, and calculating the SFAPs according to eq. II.12 instead of according to eq. II.15. Although the above results are not based on detailed information on human muscle tissue properties, the assumptions made in the Roth model and in our own model would have to be changed far beyond a physiological range to make the influence of the capacitive effects so strong that the above mentioned decision would have to be overruled.

II.4.4 Conclusions

We conclude from our results that action potential start and stop effects can be adequately described by the model algorithm presented in this paper. We also conclude that the frequency dependence of the capacitive components in the muscle fibre membrane impedance can be neglected. The effects caused by the current redistribution between the intracellular and the extracellular space are found to be small. We concluded that there is no need to incorporate a bi-domain description in the SFAP model described in this chapter. We shall incorporate the effects of the finite dimensions of the (inhomogeneous, anisotropic) volume conductor on the volume conductor weighting function in Chapter IV ([55]). This allows the possibility of accurately simulating surface electromyographic signals.

Chapter III

On numerical problems in analytical calculations of extracellular fields in bounded cylindrical volume conductors. [1]

Abstract
A method is presented for dealing with numerical problems in calculations of potential fields using expansions in modified Bessel functions. With this method, problems in mathematical physics with cylindrical symmetry, e.g. volume conductor problems, can be solved with high accuracy.

III.1 Introduction

In various fields of physical research, a common problem is the calculation of potential fields under cylinder symmetrical conditions. Examples of such calculations can be found in electrostatics, heat transfer and the deformation of solids. These potential problems can be solved by applying Laplace's equation expressed in cylindrical coordinates. The solutions of Laplace's equation can be expressed in (modified) Bessel functions. When these functions are being calculated on digital computers numerical difficulties arise very easily. The inherent difficulty with Bessel functions is their very great or very small magnitude for regularly occurring arguments. In the numerical evaluations, as a result, we are faced with the fact of machine overflows and underflows [27,105], especially for higher orders of n.

In this chapter, we shall describe a recipe by which the numerical problems occurring in such calculations can be circumvented. It consists of two modifications with respect to the usual way of solving Laplace's equation. The first alteration is a slightly different implementation of the boundary conditions, and the second is the use of a numerical expression of the logarithms of the Bessel functions. These

[1] T.H.J.M. Gootzen, D.F. Stegeman and A. Heringa, *Journal of Applied Physics* 66:4504-4508, 1989.

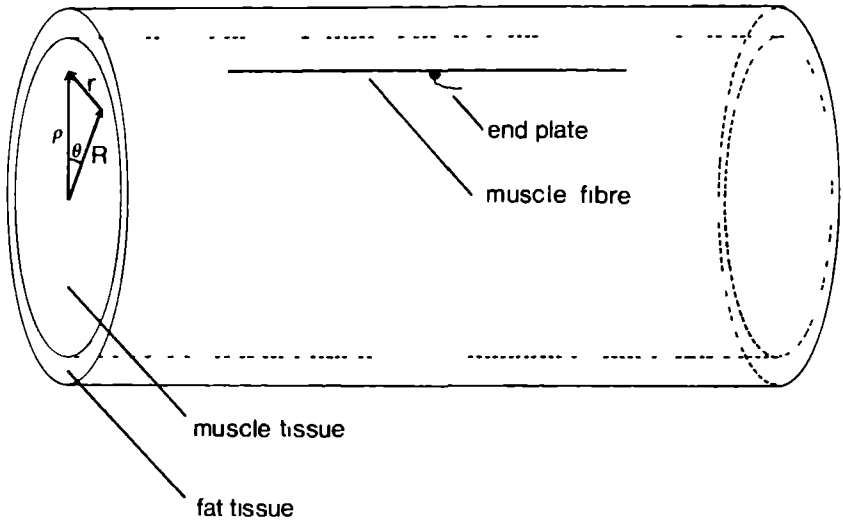

Figure III.1 Volume conductor geometry with eccentrically located muscle fibre

alterations enable us to calculate the potential fields in all kinds of inhomogeneous cylinder symmetrical potential fields, whereby Bessel functions of orders up to 40 can be incorporated in the series expansions

The proposed method will be illustrated by describing its application to a problem from the field of volume conductor theory In volume conductor problems, analytical solutions of potential problems in cylinder symmetrical configurations are most commonly expressed in the spatial frequency domain of the longitudinal direction coordinate, also when the source is placed off-axis In this domain, the modified Bessel functions of the first $I_n(x)$ and of the second $K_n(x)$ kind constitute the solution to Laplace's equation [72,95] Here we shall calculate the potential field of an active muscle fibre, lying eccentrically in a cylinder symmetrical volume conductor

In the solution of the analytical expressions, resulting from the various boundary conditions a Gaussian elimination procedure is generally used The second problem is that the coefficient matrix may become ill conditioned even before the machine range is exceeded It then becomes necessary to condition the matrix equation

III.2 Method

Consider a volume conductor with two concentric boundaries Fig III 1 shows that there are two compartments of tissue One may think e g of a limb consisting of muscle tissue in the inner compartment and of fat tissue in a layer around it The

outer layer is surrounded by air (i.e. a compartment with conductivity zero). The general solution of Laplace's equation in cylindrical coordinates, and expressed in the spatial frequency k for this volume conductor configuration reads [24]

$$\Phi_1(r,k) = \frac{d}{\sigma_{1_r}} K_0(r\sqrt{\frac{\sigma_{1_z}}{\sigma_{1_r}}} \mid k \mid) G(k) \quad + \quad \sum_{n=-\infty}^{\infty} e^{-in\Theta}[A_n(k) I_n(\rho\sqrt{\frac{\sigma_{1_z}}{\sigma_{1_r}}} k)] \quad \text{(III.1)}$$

$$\Phi_2(r,k) = \frac{d}{\sigma_{2_r}} K_0(r\sqrt{\frac{\sigma_{2_z}}{\sigma_{2_r}}} \mid k \mid) G(k) \quad + \quad \sum_{n=-\infty}^{\infty} e^{-in\Theta}[C_n(k) I_n(\rho\sqrt{\frac{\sigma_{2_z}}{\sigma_{2_r}}} k) + D_n(k) K_n(\rho\sqrt{\frac{\sigma_{2_z}}{\sigma_{2_r}}} \mid k \mid)] \quad , \quad \text{(III.2)}$$

where Φ_1 represents the potential field in the inner compartment (the muscle tissue) and Φ_2 the potential field in the surrounding layer (the fat tissue), $G(k)$ represents the current source density distribution along the active fibre, σ_{1_r} and σ_{1_z} represent the conductivities of the muscle tissue in radial and axial direction, σ_{2_r} and σ_{2_z} are the conductivities of the fat tissue in radial and axial direction and d is the diameter of the active fibre. The parameters R, ρ, r and Θ are indicated in fig. III.1 and represent the radial distance between the central axis and the line on which the observation point is located, the radial distance between the central axis and the line on which the muscle fibre is located, the radial distance between the observation line and the source line and the angle between the radial directions of the source line and the observation line respectively.

In case of an eccentrically located fibre, the first, homogeneous term of $\Phi_1(r,k)$ and $\Phi_2(r,k)$ is expanded [60] for $\rho > R$ as

$$K_0(r\sqrt{\frac{\sigma_{1_z}}{\sigma_{1_r}}} \mid k \mid) = \sum_{n=-\infty}^{\infty} e^{-in\Theta} I_n(R\sqrt{\frac{\sigma_{1_z}}{\sigma_{1_r}}} k) K_n(\rho\sqrt{\frac{\sigma_{1_z}}{\sigma_{1_r}}} \mid k \mid) \quad , \quad \text{(III.3)}$$

$$K_0(r\sqrt{\frac{\sigma_{2_z}}{\sigma_{2_r}}} \mid k \mid) = \sum_{n=-\infty}^{\infty} e^{-in\Theta} I_n(R\sqrt{\frac{\sigma_{2_z}}{\sigma_{2_r}}} k) K_n(\rho\sqrt{\frac{\sigma_{2_z}}{\sigma_{2_r}}} \mid k \mid) \quad . \quad \text{(III.4)}$$

In order to determine the coefficients $A_n(k)$, $C_n(k)$ and $D_n(k)$ the following boundary conditions have to be applied to $\Phi_1(r,k)$ and $\Phi_2(r,k)$

$$\Phi_1|_{\rho=a} = \Phi_2|_{\rho=a} \quad , \quad \text{(III.5)}$$

$$\sigma_{1_r} \frac{\partial \Phi_1}{\partial \rho}\bigg|_{\rho=a} = \sigma_{2_r} \frac{\partial \Phi_2}{\partial \rho}\bigg|_{\rho=a} \quad , \quad \text{(III.6)}$$

$$\sigma_{2_r} \frac{\partial \Phi_2}{\partial \rho}\bigg|_{\rho=b} = 0 \quad . \quad \text{(III.7)}$$

Substitution of eq. III.3 in eq. III.1 and of eq. III.4 in eq. III.2, followed by substitution of eq. III.1 and eq. III.2 in eq. III.5, III.6 and III.7 results in a set of three equations in three unknown variables $A_n(k)$, $C_n(k)$ and $D_n(k)$ for every value of n and k.

$$\begin{pmatrix} I_n(a_1k) & -I_n(a_2k) & -K_n(a_2k) \\ \sqrt{\sigma_{1_r}\sigma_{1_z}}\mathcal{I}_n(a_1k) & -\sqrt{\sigma_{2_r}\sigma_{2_z}}\mathcal{I}_n(a_2k) & -\sqrt{\sigma_{2_r}\sigma_{2_z}}\mathcal{K}_n(a_2k) \\ 0 & \sqrt{\sigma_{2_r}\sigma_{2_z}}\mathcal{I}_n(b_2k) & \sqrt{\sigma_{2_r}\sigma_{2_z}}\mathcal{K}_n(b_2k) \end{pmatrix} \begin{pmatrix} A_n(k) \\ C_n(k) \\ D_n(k) \end{pmatrix}$$

$$= G(k)d \begin{pmatrix} \dfrac{I_n(R_2k)K_n(a_2k)}{\sigma_{2_r}} - \dfrac{I_n(R_1k)K_n(a_1k)}{\sigma_{1_r}} \\ I_n(R_2k)\mathcal{K}_n(a_2k)\sqrt{\frac{\sigma_{2_z}}{\sigma_{2_r}}} - I_n(R_1k)\mathcal{K}_n(a_1k)\sqrt{\frac{\sigma_{1_z}}{\sigma_{1_r}}} \\ -I_n(R_2k)\mathcal{K}_n(b_2k)\sqrt{\frac{\sigma_{2_z}}{\sigma_{2_r}}} \end{pmatrix} . \qquad \text{(III.8)}$$

The following notations are used

$$x_1 = \sqrt{\frac{\sigma_{1_z}}{\sigma_{1_r}}}x \ , \ x_2 = \sqrt{\frac{\sigma_{2_z}}{\sigma_{2_r}}}x \ , \qquad \text{(III.9)}$$

and

$$\mathcal{I}_n(x) \equiv \frac{\partial I_n(x)}{\partial x} = \frac{I_{n-1}(x) + I_{n+1}(x)}{2}, \qquad \text{(III.10)}$$

$$\mathcal{K}_n(x) \equiv \frac{\partial K_n(x)}{\partial x} = -\frac{K_{n-1}(x) + K_{n+1}(x)}{2}. \qquad \text{(III.11)}$$

In principle, the coefficients A, C and D can now be calculated. However, in solving the linear set of equations in eq. III.8 the two numerical difficulties mentioned in the introduction arise. For increasing values of n and for small or great values of k, the matrix becomes very ill conditioned, due to the behaviour of the I and K Bessel functions, even for combinations of k and n whose contributions to the solution appear not to be negligible. When the parameters in table III.1 are used the contribution for e.g. $k = 2000\ m^{-1}$ and $n = 30$ requires the solution of the following matrix equation:

Table III.1

parameter	value	unit	parameter	value	unit
a	18	mm	σ_{1_r}	0.1	$(\Omega m)^{-1}$
b	20	mm	σ_{1_z}	0.5	$(\Omega m)^{-1}$
R	15	mm	σ_{2_r}	0.05	$(\Omega m)^{-1}$
ρ	17	mm	σ_{2_z}	0.05	$(\Omega m)^{-1}$
Δz	0.185	mm	Δt	0.05	ms

$$\begin{pmatrix} 0.28472E-4 & -0.13749E+9 & 0.13345E-11 \\ 0.29957E-4 & -0.10583E+10 & -0.10144E-10 \\ 0.0E0 & 0.40524E+12 & -0.15633E-12 \end{pmatrix} \begin{pmatrix} A_{30} \\ C_{30} \\ D_{30} \end{pmatrix} = \begin{pmatrix} 0.56223E-4 \\ 0.17027E-5 \\ 0.10814E-5 \end{pmatrix}. \qquad \text{(III.12)}$$

This linear system is solved by the DECOMP algorithm [39]. This algorithm initially calculates the condition of the matrix in order to decide whether or not the set of equations can be solved. When the condition of the matrix exceeds the limiting value based on the machine accuracy, it refuses to solve the linear system

since the solutions would not be reliable. For the VAX 11/785 we have used, this limiting value is $0.3 \times 10^{+8}$. The condition of the matrix shown in eq. III.12 is $0.361 \times 10^{+23}$ and therefore the equation can not be solved.

It appears to be necessary to condition the linear system. This can be achieved by rewriting eq. III.8, based on the following considerations. It will be shown later that expressions like

$$\frac{I_\ell(x_1)}{I_m(x_2)}, \frac{K_\ell(x_1)}{K_m(x_2)} \text{ and } I_\ell(x_1) * K_m(x_2) \tag{III.13}$$

are all well dimensioned as long as the value of $\mid \ell - m \mid$ is not too great. The fraction $\frac{x_1}{x_2}$ should preferably be in a region around 1 for higher orders l and m. When it goes beyond the range 0.1 to 10. problems in calculating the individual terms of the matrix equation will not arise rapidly but the condition of the matrix will tend to increase again.

From eq. III.1 and III.2, it can be concluded that the combinations of the coefficients A, C and D with the corresponding I or K Bessel function

$$\begin{array}{c} A_n(k)I_n(\rho_1 k) \\ C_n(k)I_n(\rho_2 k) \\ D_n(k)K_n(\rho_2 k), \end{array} \tag{III.14}$$

will be restricted to physically acceptable values, i.e. within a limited range, since they constitute contributions which are added to the potential field in a homogeneous situation. Since the I and K functions will not yield stable solutions for all arguments or orders, the coefficients A, C and D counteract this instability. In doing so, they may become instable themselves. It therefore is appropriate to calculate the expressions as they occur in eq. III.14 instead of calculating the coefficients A, C and D separately.

Combinations as in eq. III.13 already appear in the right hand vector of eq. III.8. Such combinations can be introduced in the matrix and the left hand vector of eq. III.8 respectively, by rewriting it into

$$\begin{pmatrix} \frac{I_n(a_1 k)}{I_n(\rho_1 k)} & -\frac{I_n(a_2 k)}{I_n(\rho_2 k)} & -\frac{K_n(a_2 k)}{K_n(\rho_2 k)} \\ \sqrt{\sigma_{1_r}\sigma_{1_z}}\frac{I_n'(a_1 k)}{I_n(\rho_1 k)} & -\sqrt{\sigma_{2_r}\sigma_{2_z}}\frac{I_n'(a_2 k)}{I_n(\rho_2 k)} & -\sqrt{\sigma_{2_r}\sigma_{2_z}}\frac{K_n'(a_2 k)}{K_n(\rho_2 k)} \\ 0 & \sqrt{\sigma_{2_r}\sigma_{2_z}}\frac{I_n'(b_2 k)}{I_n(\rho_2 k)} & \sqrt{\sigma_{2_r}\sigma_{2_z}}\frac{K_n'(b_2 k)}{K_n(\rho_2 k)} \end{pmatrix} \begin{pmatrix} A_n(k)I_n(\rho_1 k) \\ C_n(k)I_n(\rho_2 k) \\ D_n(k)K_n(\rho_2 k) \end{pmatrix}. \tag{III.15}$$

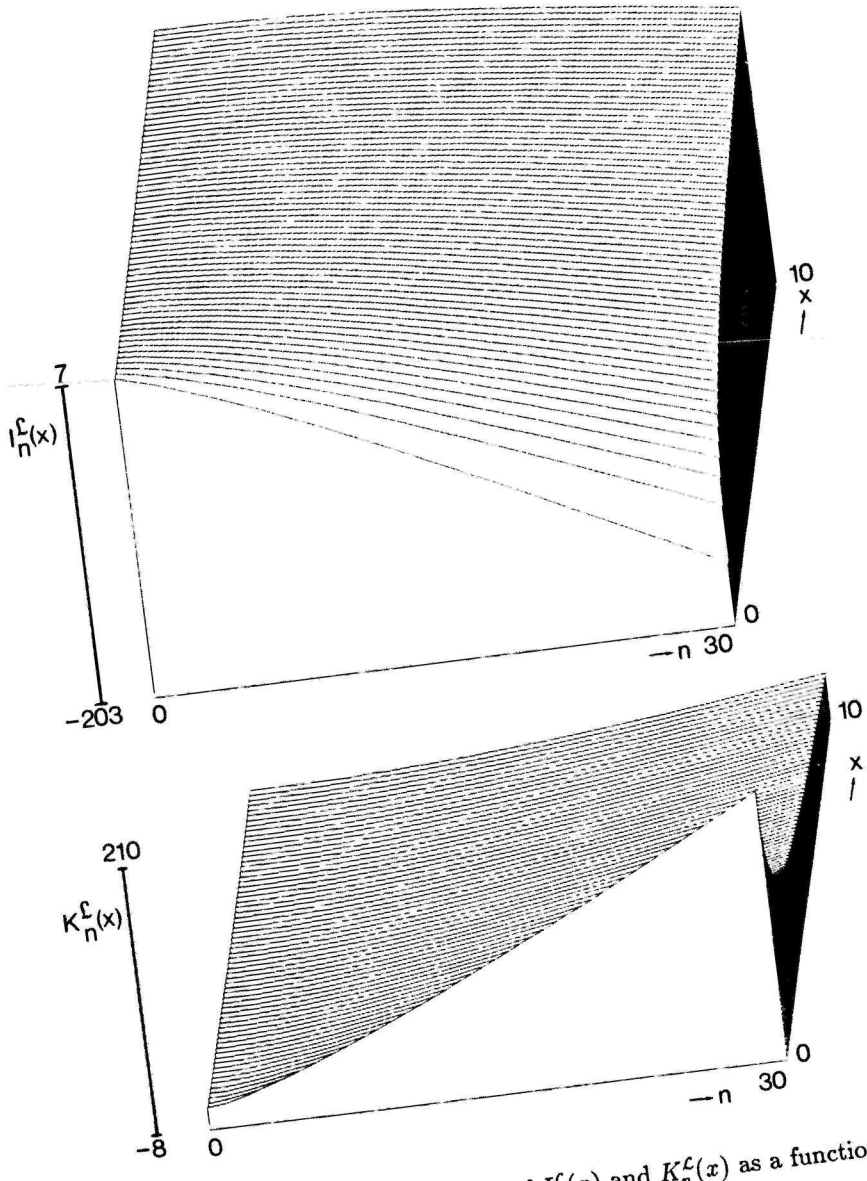

Figure III.2 : Three-dimensional plot of $I_n^{\mathcal{L}}(x)$ and $K_n^{\mathcal{L}}(x)$ as a function of x and n.

The manipulations described above, cure the ill conditioning of the matrix. We have, however, to solve the problem of calculating the values of the Bessel functions themselves. To achieve this, we have introduced a modification in the scientific subroutines used for calculating the modified Bessel functions. The main alteration with respect to standard routines for calculating modified Bessel functions is that the numerical expansions for the zero and first order terms [1] are calculated logarithmically. The recursive relations that are subsequently used for calculating the higher order terms are comparable to those in standard scientific subroutines [102]. The logarithmical Bessel functions are notated as

$$\begin{aligned} I_n^{\mathcal{L}}(x) &\equiv \log(I_n(x)) \quad \text{and} \\ K_n^{\mathcal{L}}(x) &\equiv \log(K_n(x)). \end{aligned} \tag{III.16}$$

Fig. III.2 shows a 3-D impression of $I_n^{\mathcal{L}}(x)$ and $K_n^{\mathcal{L}}(x)$ for arguments $0 < x \leq 10$ and n-values 0 to 30. It illustrates that $I_n^{\mathcal{L}}$ and $K_n^{\mathcal{L}}$ never show up with a numerically non acceptable value and that the range 0.1 to 10 for the arguments of the Bessel functions will not cause numerical problems in the logarithmic version of the calculations. The calculation of the elements of eq. III.13 now is e.g.

$$\frac{I_n(x_1)}{I_m(x_2)} = \exp\left(I_n^{\mathcal{L}}(x_1) - I_m^{\mathcal{L}}(x_2)\right), \tag{III.17}$$

and

$$I_n(x_1)K_m(x_2) = \exp\left(I_n^{\mathcal{L}}(x_1) + K_m^{\mathcal{L}}(x_2)\right) . \tag{III.18}$$

All numerical obstacles have been removed and all elements of expression III.15 can be calculated.

Application of the described method now yields the following linear system for $n = 30$ and $k = 2000\ m^{-1}$

$$\begin{pmatrix} 0.65082E+1 & -0.17537E+1 & 0.94333E-2 \\ 0.68475E+1 & -0.13498E+2 & -0.71704E-1 \\ 0.0E0 & 0.51687E+4 & -0.11058E-2 \end{pmatrix} \begin{pmatrix} A_{30}I_{30} \\ C_{30}I_{30} \\ D_{30}I_{30} \end{pmatrix} = \begin{pmatrix} 0.56223E-4 \\ 0.17027E-5 \\ 0.10814E-5 \end{pmatrix}. \tag{III.19}$$

The condition decreases now to $0.655 \times 10^{+5}$, a value which is well within the reliable range for solving the equations. The resulting coefficients from expression III.15 can be used in eq. III.1 and III.2.

Fig. III.3 shows the potential $\phi(z)$ along the entire length of the observation line, calculated from $\Phi_1(r, k)$ according to equations (8) and (15) with the parameters as listed in table III.1.

As can be seen from eq. III.1, this potential is the summation of a homogeneous term and a correction term, necessary for incorporating the finite volume conductor. The homogeneous and correction part of $\phi(z)$ are shown separately in fig. III.4 and III.5. The amplitude of the correction part, caused by the existence of volume conductor boundaries, is 18 % of the amplitude of the homogeneous part and is therefore certainly not negligible.

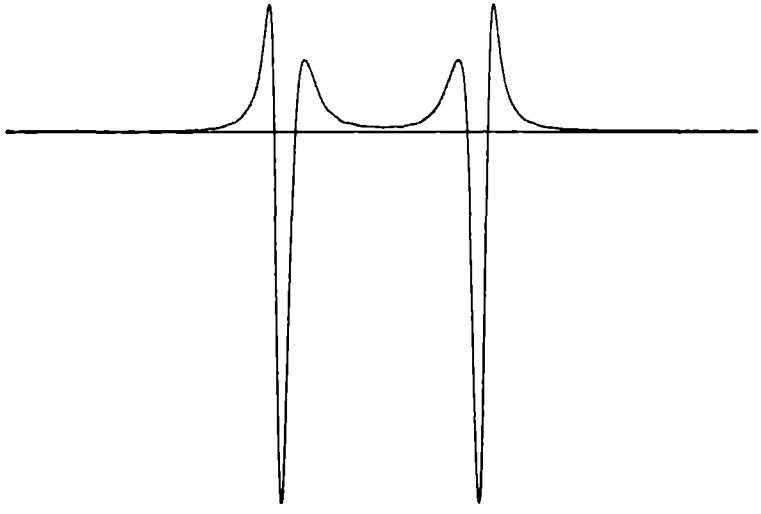

Figure III.3 : Potential distribution $\Phi_1(r,z)$ along the observation line.

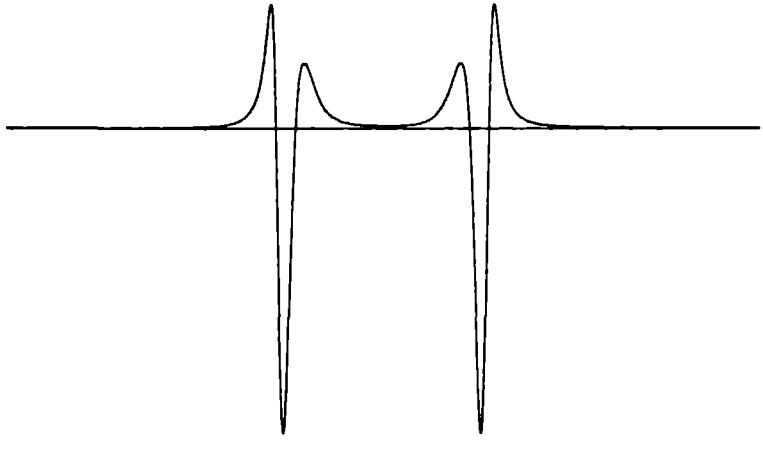

Figure III.4 : Homogeneous part of $\Phi_1(r,z)$ shown in fig. III.3.

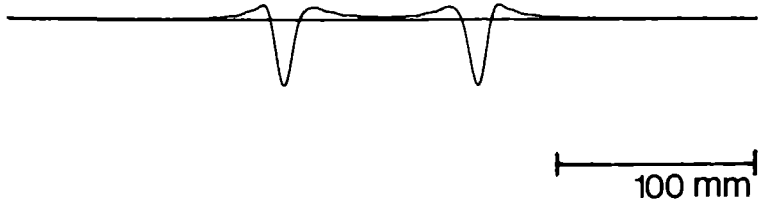

Figure III.5 : Finite volume conductor correction part of $\Phi_1(r,z)$.

III.3 Discussion

We have shown that two simple alterations in the solution method for a cylinder symmetrical potential problem facilitate the calculation of the potential fields in situations with eccentrically located sources and complicated combinations of boundary conditions. The first step is a better conditioning of the matrix equations that have to be solved. This conditioning can be recognised as one specific application of a method known from linear algebra: row equilibration. The specific choice of the scaling factors was inspired by the physics of the underlying problem. The second step is an application of the logarithm in the calculation of the modified Bessel functions. This step was necessary in order to avoid overflow or underflow problems in calculating the elements in the linear systems that have to be solved.

The conditioning of the matrix equation described in the previous section has done away with the problem of anisotropic conductivities that is so often encountered in potential field calculations. It appears, that in all the elements of the matrix the anisotropy ratio's (equation III.9) show up in the arguments of the Bessel functions in the counter as well as in the denominator of the fractions. The two-decade range we have mentioned above as practical limits for the ratio of the arguments can therefore directly be applied to a, b and ρ, independently of the anisotropy ratio's.

The advantage of the method described above is clear : analytically well-defined potential problems, whose solutions could not be obtained by numerical methods, can now be solved for a much wider range of orders of the Bessel functions and of their arguments. Since no restrictions are imposed on the general expressions describing the final solutions or on the boundary conditions, which determine the contents of the linear systems to be solved, this method opens up potential field calculations for all kinds of physical, cylinder symmetrical problems. In general, the two aspects of row equilibration and logarithmical scaling can be applied to all potential problems which have to be solved by series expansions. The disadvantage of the method is that expression III.15 has to be calculated not only for every n and k value but also for every field point (ρ, ϕ), whereas in the unconditioned situation in eq. III.8 the calculated coefficients are independent of the field point. In our opinion this disadvantage is amply counterbalanced by the new possibilities the method brings forward.

Chapter IV

Finite limb dimensions and finite muscle length in a model for the generation of electromyographic signals. [1]

Abstract

A volume conductor model is presented in which the aspects of finite volume conductor dimensions and finite muscle fibre length are combined. The effects of these aspects on single muscle fibre action potentials (SFAPs) and on motor unit action potentials (MUAPs) are shown and verified with surface recorded motor unit action potentials. It is demonstrated that the influence of the fibre length being finite is significantly enhanced by the finite limb dimensions of the volume conductor model, for single fibre action potentials as well as for motor unit action potentials. The model described is found to be capable of generating surface MUAPs which show a very good resemblance with measured surface MUAPs. Recorded MUAPs illustrate clearly the effects caused by finite muscle fibre length. The effect of finite limb dimension in simulated intramuscular MUAPs was evidently less dominant than in simulated surface MUAPs.

IV.1 Introduction

Almost all motor unit action potential (MUAP) simulation models presented in the literature are based on single fibre action potential (SFAP) waveforms in homogeneous volume conductors of infinite dimensions and muscle fibres of infinite length [14,62,63,87,129]. Only a single study concerns a more complicated volume conductor model [42]. Most of the studies on motor unit simulations have been directed towards finding proper values for the parameters describing the motor unit

[1] T.H.J.M. GOOTZEN, D.F. STEGEMAN and A. VAN OOSTEROM. *Submitted to Electroenceph. Clin Neurophysiol.*

structure, both in normal and in pathological situations. This has caused the volume conductor aspects of MUAP modelling to lag behind the latest developments in SFAP modelling (e g [3,106]).

We have indicated in a preliminary report that the finite dimensions of the volume conductor and the finite muscle fibre length have substantial influence on single fibre action potentials (Chapter II, [51]). When single fibre potentials are added in simulating an MUAP, as is allowed by the generally accepted summation principle, the influence of the finiteness of the volume conductor and of the muscle fibre may be expected to be present in the motor unit action potential as well.

In this chapter, we study the above influence of finite dimensions of a realistic muscle and its surroundings on MUAP waveforms recorded in intramuscular and surface EMG. An algorithm for the calculation of SFAPs from fibres having a finite length (Chapter II, [50]) is applied to an inhomogeneous volume conductor with finite radial extent. An improved method for the analytical calculation of the volume conductor weighting function for eccentrically located sources in a cylinder symmetrical inhomogeneous volume conductor geometry (Chapter III, [52]) allows the calculation of SFAPs with good accuracy. Special attention will be paid to the simulation of surface SFAPs and MUAPs, since in these simulations, the effects caused by the finite muscle fibre length and the finite muscle dimension are expected to be maximal.

After a recapitulation of the analytical calculation of the resulting potential fields in section IV.2.1, and of the description of the single muscle fibre source characteristics in section IV.2.2, the parameter selection for calculating MUAPs will be briefly reviewed in section IV.2.3. Most of the latter parameters have been taken from reports in the literature. In section IV.3, some fundamental SFAP simulations and various MUAP simulations will be presented. Simulated surface MUAPs will be compared with surface MUAPs recorded from human quadriceps muscle.

IV.2 Methods

IV.2.1 The volume conductor

The volume conductor used in this chapter for representing a muscle in a limb is a cylinder symmetrical configuration, consisting of two compartments (fig. IV.1).

The inner compartment represents the muscle tissue. Its conductivity is anisotropic and purely resistive. We have reconfirmed that capacitive effects can be neglected [50]. The second compartment, forming a layer around the muscle tissue, represents the subcutaneous fat tissue. Its conductivity is isotropic, having a value much lower than that of the muscle tissue. The volume conductor is surrounded by air as a 'third compartment' with conductivity zero and infinite extension.

In the muscle tissue, muscle fibres of finite length and zero diameter are located. When a muscle fibre is activated at the neuromuscular synapse, usually located somewhere halfway the muscle fibre, two action potentials start propagating towards the ends of the fibre. From this activity of the muscle fibre, represented by the transmembrane current source density $J_m(z)$ ($A.m^{-2}$) along the fibre (see

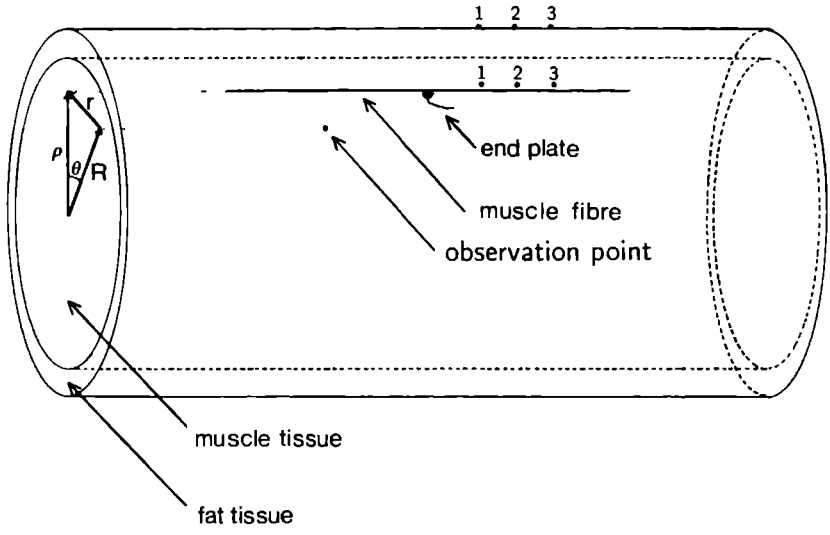

Figure IV.1 : Volume conductor configuration with finite length muscle fibre.

section IV.2.2), the potential fields Φ_1 and Φ_2 in respectively the muscle tissue and the fat tissue can be obtained.

The general solutions Φ_1 and Φ_2 from Laplace's equation read [72,95]

$$\Phi_1(r,k) = \frac{d}{\sigma_{1_r}} K_0(r\sqrt{\frac{\sigma_{1_z}}{\sigma_{1_r}}} \mid k \mid) J_m(k) \quad + \quad \sum_{n=-\infty}^{\infty} e^{-in\Theta}[A_n(k) I_n(\rho\sqrt{\frac{\sigma_{1_z}}{\sigma_{1_r}}}k)] \quad \text{(IV.1)}$$

$$\Phi_2(r,k) = \frac{d}{\sigma_{2_r}} K_0(r\sqrt{\frac{\sigma_{2_z}}{\sigma_{2_r}}} \mid k \mid) J_m(k) \quad + \quad \sum_{n=-\infty}^{\infty} e^{-in\Theta}[C_n(k) I_n(\rho\sqrt{\frac{\sigma_{2_z}}{\sigma_{2_r}}}k)$$
$$+ \quad D_n(k) K_n(\rho\sqrt{\frac{\sigma_{2_z}}{\sigma_{2_r}}} \mid k \mid)], \quad \text{(IV.2)}$$

where Φ_1 and Φ_2 are expressed in the spatial frequency domain. k equals $2\pi k'$, with k' indicating the spatial frequency (repeatency). d is the muscle fibre diameter which is effective as a scaling factor to the source strength. In the volume conductor model, the muscle fibre is treated as a line source.

Since the potentials Φ_1 and Φ_2 also have to be calculated for eccentrically located muscle fibres, the homogeneous terms

$$K_0(r\sqrt{\frac{\sigma_z}{\sigma_r}} \mid k \mid)$$

have to be expanded [24] as

$$K_0(r\sqrt{\frac{\sigma_z}{\sigma_r}} \mid k \mid) = \sum_{n=-\infty}^{\infty} e^{-in\Theta} I_n(R\sqrt{\frac{\sigma_z}{\sigma_r}}k) K_n(\rho\sqrt{\frac{\sigma_z}{\sigma_r}} \mid k \mid) \quad \rho \geq R \quad \text{(IV.3)}$$

In order to obtain the coefficients $A_n(k)$, $C_n(k)$ and $D_n(k)$, the following boundary conditions have to be applied to $\Phi_1(r,k)$ and $\Phi_2(r,k)$

$$\Phi_1|_{\rho=a} = \Phi_2|_{\rho=a} \quad , \tag{IV.4}$$

$$\sigma_{1_r} \left.\frac{\partial \Phi_1}{\partial \rho}\right|_{\rho=a} = \sigma_{2_r} \left.\frac{\partial \Phi_2}{\partial \rho}\right|_{\rho=a} \quad , \tag{IV.5}$$

$$\sigma_{2_r} \left.\frac{\partial \Phi_2}{\partial \rho}\right|_{\rho=b} = 0 \quad , \tag{IV.6}$$

resulting in a linear set of equations for every n and k. For higher values of n, numerical problems such as over- and under-flow in the Bessel-functions and an ill conditioning of the set of equations occur. By solving the set of equations for $A_n(k)I_n(r,k)$, $C_n(k)I_n(r,k)$ and $D_n(k)K_n(r,k)$ and by using logarithmic values for the Bessel functions, it has been shown that these numerical problems can be avoided (Chapter III, [54]). Bessel functions of orders up to 40 can then be used, which results in an accurate determination of the potential fields.

IV.2.2 Single fibre source characteristics

The common concept of uniform action potential propagation over infinite distances has been applied to SFAP simulations for a long time without a sound, quantitative knowledge on the consequences of this simplification of reality. It is obvious that the neuromuscular end-plate and the fibre endings are factors distorting this concept. We have shown that inclusion of the excitation and the extinction of the action potential can have important effects (Chapter II, [50,51]). The description of the start and stop phenomena as described there is applied in the present analysis as well. The principle involved was first described by Plonsey [97]. The extinction of an action potential is described as a current source compensation at the end of the fibre. The compensation is calculated such that the total transmembrane current $\int_{fibre} J_m(z)$ over the active part of the fibre is zero whereby propagation is normal up until the end of the fibre. Later measurements [65] and simulations [30,66] support this principle, which can also be applied to the end-plate excitation of the two action potentials propagating in opposite directions. A recent study based on a Hodgkin-Huxley type model, adapted to muscle fibre properties and including a fibre ending [74], has confirmed the compensation principle.

The total activity of a muscle fibre of finite length is limited in time and it is therefore possible to store the membrane current source density, as a function of time t and of location s, along the fibre in a matrix. With the time in the horizontal direction and the location in the vertical direction the above matrix is illustrated in fig. IV.2.

The current source density waveform, at locations along the fibre where no influence of the start or end effects occurs, is taken to be proportional to the second derivative of the intra-cellular action potential as measured by Ludin [81] and validated theoretically by Rosenfalck [103].

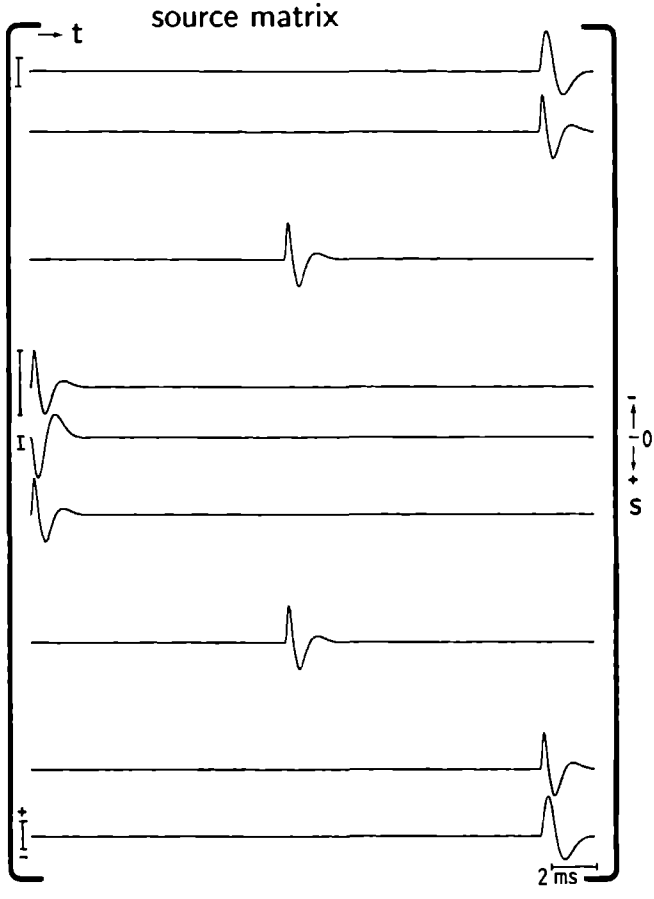

Figure IV.2 : Muscle fibre activity pattern represented by current source density as a function of time and place.

A column of the matrix is used for the calculations described in section IV.2.1 to represent the instantaneous membrane current source density distribution along the muscle fibre.

IV.2.3 Motor unit activity

From the algorithm for SFAP simulations, it is in principle a simple computational step to MUAP simulation. The structure of motor units in human skeletal muscle is qualitatively well known. Quantitative data, however, are difficult to obtain, and so several assumptions have to be made. It is inevitable that part of the assumptions on motor unit structure are based on animal skeletal muscle data, since human data are not always available. Summation of a set of SFAP's, each with its proper set of parameters, results directly in an MUAP. This summation principle

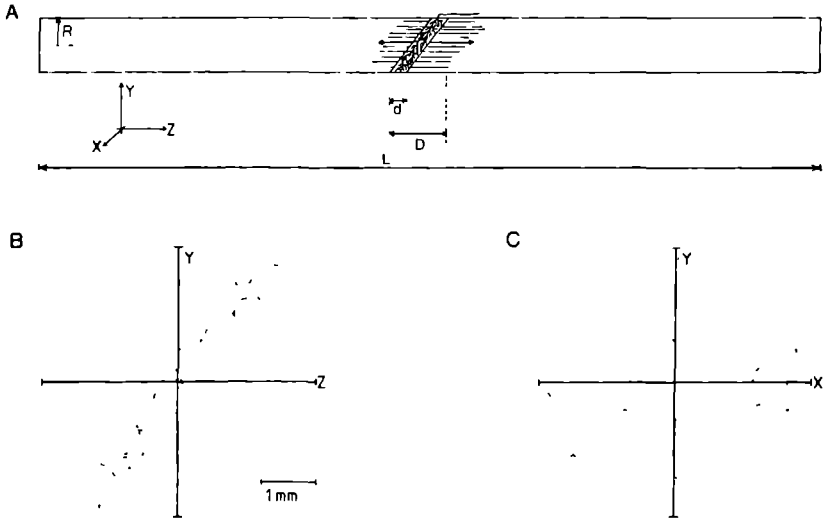

Figure IV.3 : Motor unit structure: A) motor unit territory, B) cross section of motor unit territory, C) end-plate locations.

has been generally accepted [12]. It may still be discredited with the existence of mutual influence of propagating action potentials along active muscle fibres. To our knowledge, however, this has never been observed in non-pathological muscle fibres.

The parameters, for which specific choices are made in the following subsections, represent the geometry of the motor unit and the dispersion within the temporal initiation of the individual SFAPs.

Motor unit geometry

As the first assumption, we take all muscle fibres constituting one motor unit to be distributed within a circular cross sectional area [17,44,117].

The cylinder of which a side view is drawn in fig. IV.3A outlines the motor unit area. Its domain is shared by muscle fibres from other motor units. The motor unit is placed in the muscle tissue compartment of the finite volume conductor.

The diameter of the cross section of the motor unit cylinder, usually called the motor unit territory, ranges from 3 to 10 mm. The distribution of the muscle fibres over the motor unit territory is taken as uniform [17] (fig. IV.3C), which we believe to be more accurate than the normal distribution as suggested by Gath [44]. Within the motor unit territory, 20 to 500 fibres [19], or even up to 2000 in larger limb muscles [37], belonging to that motor unit, can be found.

A second assumption concerns the geometry of the endplate region, i.e. that part of the muscle where the branches of the motoneuron end and where their endplates contact the muscle fibres. The shape of this region differs between muscles [23]. A simple example for its longitudinal cross section, found in several muscles,

is that of a parallelogram shaped area [25], lying halfway between the two tendons of the muscle, approximately 5 mm wide, and having a ratio of d/D (see fig. IV.3) of about 0.3 [9,40]. Within the width of this parallelogram, the locations of the endplates are assumed to be Gaussian distributed (fig. IV.3B). Bimodal distributions have also been suggested in literature (e.g. [87]), but have not been found in non-pathological situations. The above description will be suitable for each separate endplate region for muscles containing more than one endplate region.

Temporal dispersions

There are three factors which lead to a dispersion in the temporal behaviour in the set of SFAP's that form the MUAP [62,87,129].

The first factor arises from the variation in arrival times from the motoneuron action potential at the endplates, due to the different pathlengths and propagation velocities along the branches of the motoneuron.

The second factor is the variation in reaction time of the neuro-muscular synapse, known as the synapse jitter.

The third factor arises from the variation in propagation velocities of the muscle fibre action potentials. In normal, non-pathologic muscle, this variation is mainly due to the different diameters of the muscle fibres.

The first factor may be roughly estimated by dividing the motor unit territory dimension by the motoneuron action potential propagation velocity. In a more precise estimation, the way in which the motoneuron branches towards the endplates will play a role.

The second factor has been measured by the jitter measurements, as described by Stålberg [115]. It is the only dispersion factor which will take different values each time the motor unit is activated and leads to statistical variation within a specific MUAP waveshape. Normal jitter values range between 20 and 50 μs (mean 35 μm, sd 7.5 μm). Since in these jitter measurements the jitter in the arrival times at two mutually independent endplates is measured, for one synapse these values become 14 to 35 μs (mean 24.7 μm, sd 5.3 μm), under the assumption of a Gaussian distribution of the jitter.

For the variation in fibre diameter, causing the third dispersion factor, also a Gaussian distribution is assumed, with a mean diameter of 55 μm. The diameter influence is accounted for by the variable d in eq. IV.1 and IV.2. In the numerical implementation of the algorithm for calculating the expansion coefficients in eq. IV.1 and IV.2, the fibre diameter has its influence via the propagation velocity which plays a role in the evaluation of these expressions in de k-domain. The ranges indicated in the simulation results, which will be shown in the next section, correspond to a range from minus to plus three standard deviations. Although the muscle fibre diameter range in e.g. the human quadriceps muscle is 55 $\pm$ 9 μm (mean $\pm$ s.d.), the diameter range within one motor unit will be smaller. The propagation velocity v (m.s^{-1}) along the muscle fibre is modelled as a function of its diameter d (μm) according to the theoretical relationship [87]

$$v = 2.2 + 0.05 * (d - 25) \quad . \tag{IV.7}$$

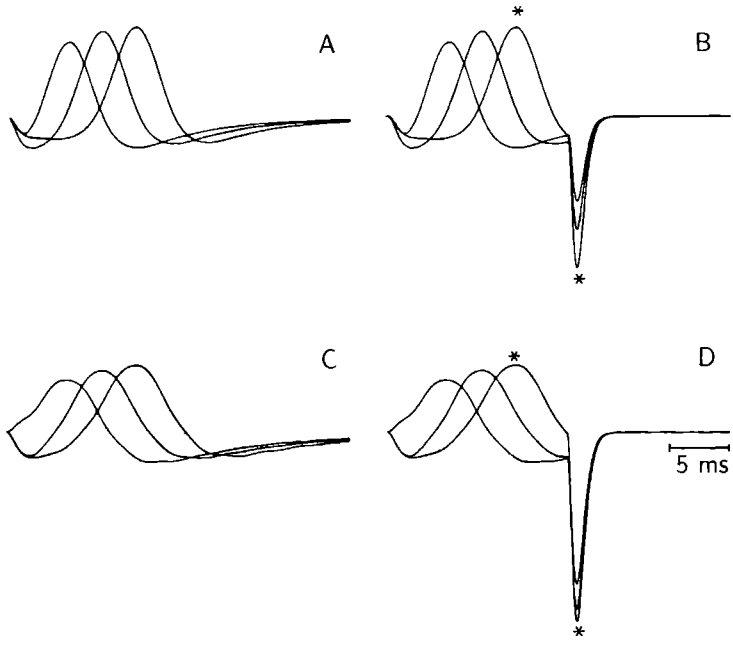

Figure IV.4 : SFAP triplets for four different modelling conditions. A) infinite fibre length in infinite volume conductor, B) finite fibre length in infinite volume conductor, C) infinite fibre length in finite volume conductor, D) finite fibre length in finite volume conductor. Distance between fibre and observation 1 mm, distance between end-plate and observation 14, 23 and 32 mm. For details see section IV.3.

For each individual muscle fibre in the MUAP simulations, the values for the parameters as described in this section and in the previous section are selected by a random sample taken from their respective statistical distributions. Except for the conduction velocity and the fibre diameter, all variables are independent of each other. With the obtained values individual SFAPs are calculated and these are added to obtain the MUAP.

IV.3 Results

The relative importance of the major aspects: 1) finite dimensions of the volume conductor, and 2) the finite propagation trajectory, depends on the distance between the muscle fibre and the recording electrode. This can most prominently be illustrated by comparing the simulation of an intramuscular observation point with the simulation for a surface electrode. Fig. IV.4 and IV.5 show, in each of the four parts, a triplet of SFAPs simulated at axial distances of 14, 23 and 32 mm to the end-plate and at a radial distance of 1 mm (i.e. intramuscular for the bounded

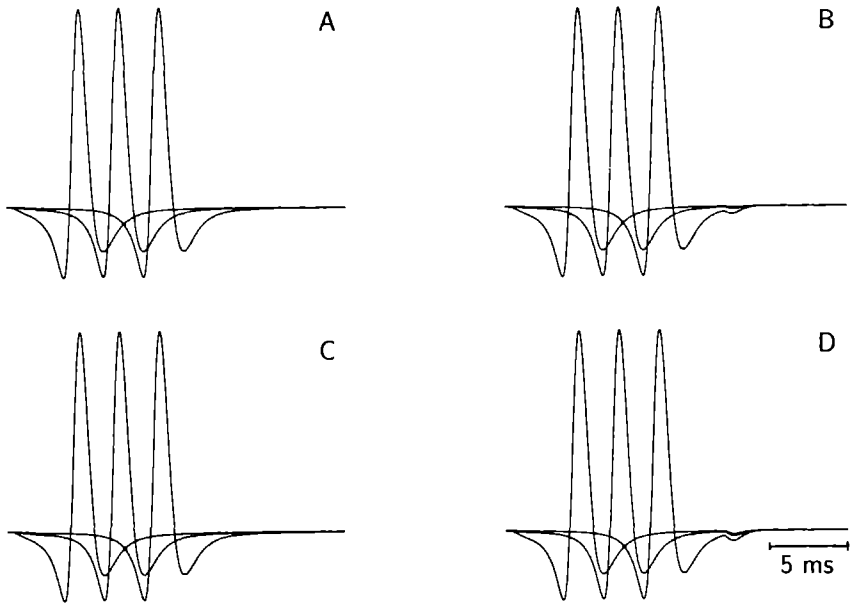

Figure IV.5 : SFAP triplets for the same modelling conditions as in figure IV.4. Distance between fibre and observation 7 mm.

volume conductor) and 7 mm (i.e. on the surface of the cylinder for the bounded volume conductor) respectively. In each of the parts A, B and C of fig. IV.4 and IV.5, one or two of the major aspects are omitted from the complete model of which the results are shown in part D of fig. IV.4 and IV.5. In the parts A, the muscle fibres have infinite length and are located in an infinite volume conductor. In parts B, the muscle fibres have finite length but the volume conductor is infinite. In parts C, the muscle fibres have infinite length again but the volume conductor is finite. In parts D, the finite muscle fibres are located in the finite volume conductor. The other model parameters are documented in table IV.1.

Table IV.1 Model parameters

parameter	value	unit	
a	27	mm	radius muscle tissue
b	30	mm	radius volume conductor
d	55	μm	fibre diameter
L	100	mm	fibre length
σ_{1_r}	0.1	$(\Omega\text{m})^{-1}$	radial conductivity muscle
σ_{1_z}	0.5	$(\Omega\text{m})^{-1}$	axial conductivity muscle
σ_{2_r}	0.05	$(\Omega\text{m})^{-1}$	radial conductivity fat
σ_{2_z}	0.05	$(\Omega\text{m})^{-1}$	axial conductivity fat

Fig. IV.6 shows the result of an intramuscular MUAP simulation in a bounded

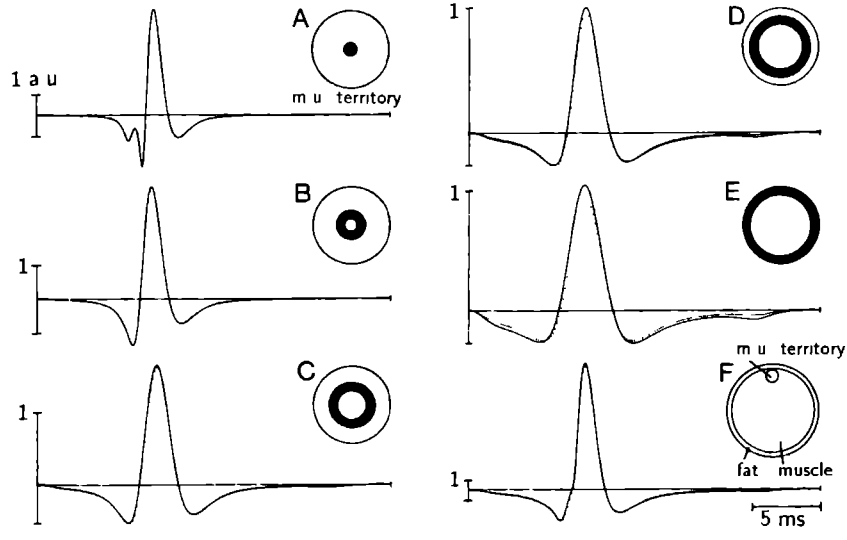

Figure IV.6 : A)-E) Contributions to MUAP from five concentric regions of the motor unit territory (inset: motor unit territory and shells), F) Total MUAP (inset: motor unit in configuration).

volume conductor geometry with a muscle tissue radius of 45 mm and a fat tissue thickness of 5 mm (see fig. IV.1). The conductivities are the same as for the simulations shown in fig. IV.4 and IV.5. The MUAPs arising from a motor unit with a territory of 2.5 mm radius, containing 150 muscle fibres with a total fibre length of 100 mm and fibre diameters ranging from 45 to 65 μm, an end-plate region with a total width of 5 mm and a $\frac{d}{D}$ ratio of 0.3 are simulated. The first two time dispersion factors described in section IV.2.3 are accounted for together by one time-shift which is Gaussian distributed (mean 0 ms, sd 0.1 ms). The observation point in the MUAP simulation is located at the center of the motor unit territory which is located 2.5 mm below the boundary between the muscle tissue and the fat tissue (see the inset in fig. IV.6F). So the boundary of the motor unit territory just reaches the fat tissue.

In order to show the influence of the finite volume conductor on the contributions from regions of the motor unit territory with different distances to the observation point, the MUAP is divided in separate contributions from five concentric shells, each with a thickness of 0.5 mm. The solid lines represent the MUAP contributions resulting from the finite volume conductor whereas the dotted lines represent the contributions from an infinite volume conductor (corresponding to fig. IV.4B and IV.5B). The complete MUAP waveshapes are shown in fig. IV.6F.

In order to show the influence of the location of the motor unit on the contribution from the outer shell of the motor unit territory to the MUAP, the same motor unit as in fig. IV.6 is also simulated shifted 2.5 mm deeper inside the muscle

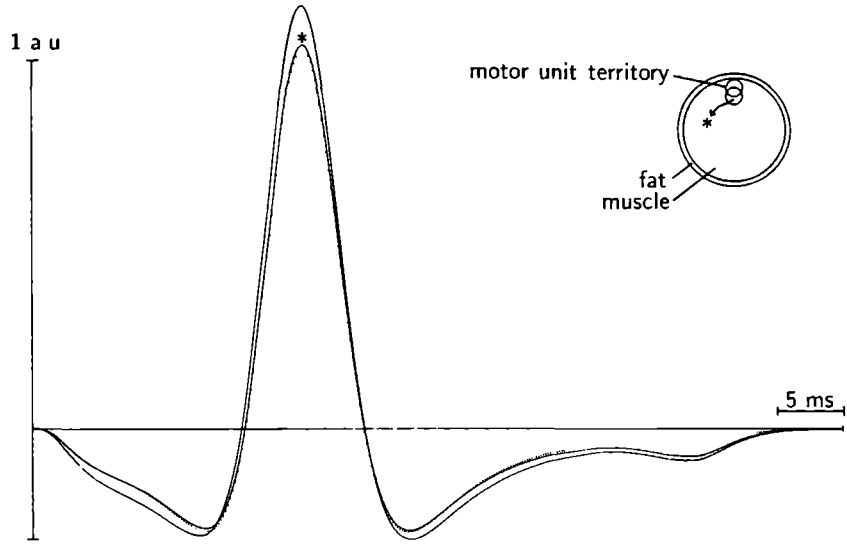

Figure IV.7 : Contribution from the outmost shell to MUAP in three different situations : motor unit in infinite muscle (dotted line), motor unit just below fat tissue (solid line), motor unit deeper in muscle tissue (solid line marked with *).

tissue compartment. Fig. IV.7 shows the contribution from the outmost shell (2 to 2.5 mm radius from the motor unit center) of this motor unit (the solid line waveshape marked with an asterisk). Also the two waveshapes from fig. IV.6E are shown (the unmarked solid line waveshape and the dotted line waveshape for the infinite volume conductor).

An experimental verification of the results found with respect to intramuscular motor unit activity is hardly possible because precise knowledge on the structure and the dimensions of a specific motor unit cannot be obtained. Such knowledge is necessary to reproduce the relatively small differences in intramuscular MUAPs between the finite and the infinite volume conductor configurations . Comparing fig. IV.4 and IV.5, the differences between the two approaches to motor unit action potential generation seem obvious when observing the motor unit from a great distance, as in surface EMG recordings.

In fig. IV.8A, an experimental set-up for measuring surface MUAPs is shown. From the human medial vastus muscle rows of surface recordings and an intramuscular recording were obtained simultaneously. The time marks obtained by ADEMG [85], decomposing the intramuscular recording into separate motor unit contributions, were used to obtain averaged surface MUAPs.

The results for one MUAP from one row of recording positions is shown in fig. IV.8B. Fig. IV.8C and IV.8D show two sets of simulated MUAPs, simulated in approximately the same geometrical configuration as in which the MUAPs

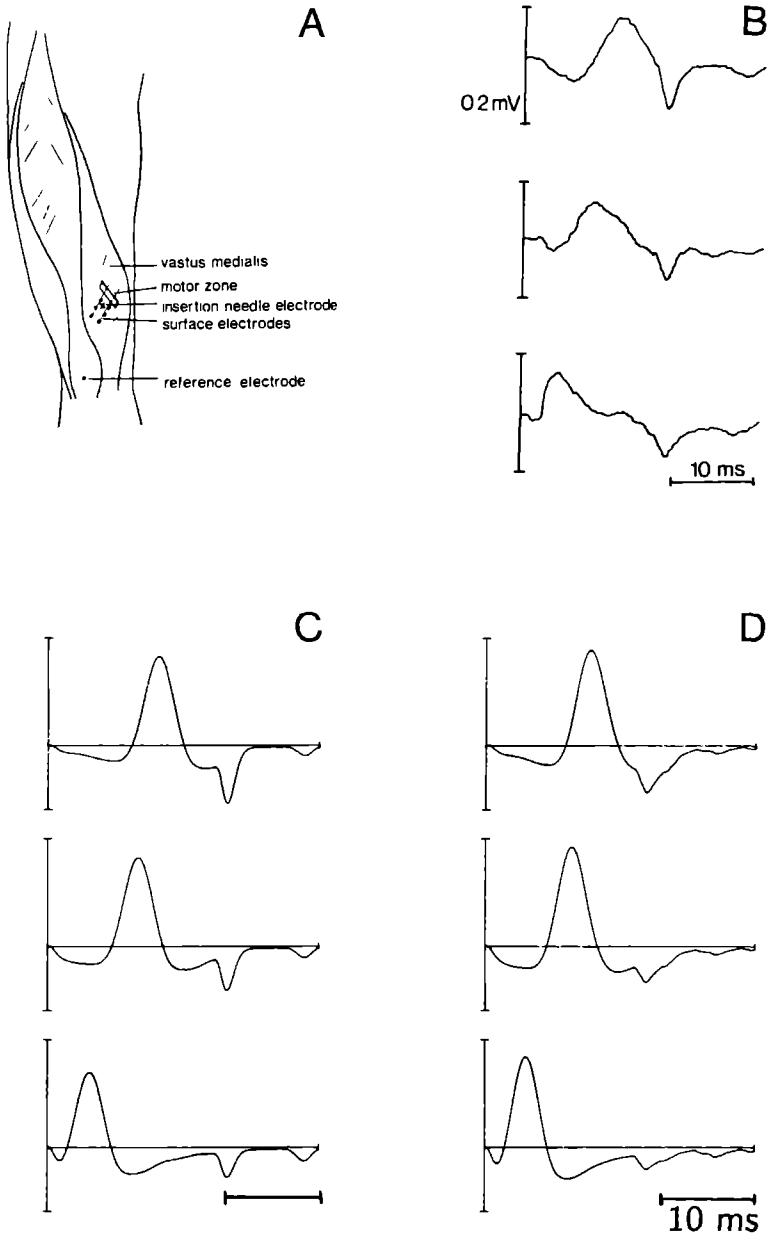

Figure IV.8 : A) Experimental set-up for recording surface and intramuscular MUAPs, B) Set of three surface MUAPs, C) Simulated MUAPs, diameter range 50 - 60 μm, D) Simulated MUAPs, diameter range 30 - 80 μm.

presented in fig IV 8B were recorded To show that variations in motor unit parameters can be visible in surface recorded MUAPs we simulated a motor unit with the fibre diameter ranging from 50 to 60 μm in fig IV 8C and ranging from 30 to 80 μm in fig IV 8D

IV.4 Discussion

A volume conductor model has been presented in which the finiteness of muscle fibre length and of volume conductor dimensions is included The ease of calculation when these properties are being neglected has caused a scarcity of studies in which such properties are incorporated Ganapathy et al [42] reported on an inhomogeneous volume conductor model for simulating surface MUAPs but in fact their volume conductor was infinite and therefore not suitable for MUAP simulations in which the finiteness of the limb is one of the aspects under study Important observations on SFAPs resulting from finite length muscle fibres have been reported by Dimitrov [29] and by Lateva [78] but they also used an infinite volume conductor To our knowledge, no studies have been published in which both aspects are considered simultaneously

IV.4.1 Single fibre action potentials

When the different parts of fig IV 4 and IV 5 are compared, it is easy to observe the increasing necessity to include the more complicated properties of finite limb and muscle dimensions in an SFAP model for larger electrode to-fibre distances The most prominent aspect caused by the finite fibre length is the appearance of a positive, constant latency peak It has a constant waveform and its amplitude is much less affected by the observation distance than that of the propagating part of the SFAP The latency of this peak corresponds to the moment at which the propagating action potential reaches the end of the muscle fibre In fig IV 5B, it can be seen that the amplitude of the peak increases with decreasing distance to the end of the fibre The finiteness of the volume conductor increases the amplitude of the constant latency peak and diminishes the influence of the distance between fibre-end and the site of observation From this observation, it can be expected that in bipolar surface recordings these non-moving components are largely cancelled The behaviour of the positive end effect peaks may seem confusing It is, however, exactly the field of a time-varying dipole located at the end of the fibre An equivalent dipole description for action potential extinction was validated in [74] The time-varying amplitude has the shape of the intracellular action potential This waveshape is, because of its non-propagating character, not influenced by the volume conductor properties

In principle, also the excitation of the action potential at the neuromuscular synapse would cause similar dipole effects But, since at the end-plate two action potentials start propagating in opposite directions, two dipoles will be present: close together and pointing in opposite directions Hence, the influence of the excitation is much less marked than that of the extinction of the action potentials at the fibre endings

The effects related to the action potential propagation stop are quite similar to observations about so-called far field phenomena in evoked potential measurements. In recent evoked potential literature also dipoles are considered to be the sources of far-field phenomena [122]

Another observation that can be made is the fact that the amplitude of the propagating part of the waveform is smaller and wider in fig. IV.5C and IV.5D compared to fig. IV.5A and IV.5B. This is caused by the low conductivity of the fat tissue that surrounds the muscle tissue. In the positive peaks the end-effect amplification we have mentioned, and which is caused by the finite volume conductor, predominates the attenuation by the fat layer.

IV.4.2 Intramuscular MUAPs

The bounded nature of the volume conductor clearly influences the MUAP waveforms. As can be expected from fig. IV.6 and IV.7, this influence appears to be small for intramuscular MUAPs . In fig. IV.6A to IV.6D the MUAP contributions calculated in the finite and the infinite volume conductor only differ in the enhancement of the relatively small positive end-effect peak. Only fig. IV.6E shows a noticeable difference between the two waveforms. As seen already in the SFAP simulations the greatest effects due to the finite volume conductor are present at greater observation distances. The contribution of the outer shell to the MUAP in the finite volume conductor has an amplitude which is about 10 % higher than the MUAP contribution of this shell in the infinite volume conductor.

In fig. IV.7, it can be observed that the differences between the two volume conductor descriptions disappear rapidly when the motor unit is shifted deeper inside the muscle. For a motor unit located 2.5 mm deeper than the motor unit from fig. IV.6, the contribution from the outmost shell differs less than 0.5 % in amplitude from the contribution by that shell when the same motor unit is placed in a homogeneous, infinite volume conductor. Together with the observation that the 10 % difference of fig. IV.6E is not visible at all in the total MUAPs in fig. IV.6F, this leads to the conclusion that for simulations of intramuscular motor units the finite volume conductor aspects need not be included for describing the main complex of the MUAP waveform. The influence of the finite volume conductor on the amplitude of the relatively small end-effect peak is pronounced however.

IV.4.3 Surface EMG MUAPs

For a correct simulation of surface MUAPs, the finite volume conductor description is indispenseable. This is obvious from the great resemblance between recorded MUAPs of which examples are shown in fig. IV.8B and the simulated MUAPs in fig. IV.8C and IV.8D. The presence of one propagating peak and of stationary peaks is clear in all three series of MUAPs. Details, such as the onset of the MUAPs and the presence of two positive end peaks at two different latencies (caused by an end-plate region location not exactly half-way the muscle fibres), are also in accordance. The widths of the positive end peaks in the simulated MUAPs in fig. IV.8C, are somewhat smaller than in the measured MUAPs, whereas in

fig. IV.8D the widths of the end peaks are greater than in the measurements of fig. IV.8B. This is caused by a smaller respectively a greater time dispersion of the SFAPs constituting the MUAP. In fig. IV.8C an underestimation and in fig. IV.8D an overestimation of the range of fibre diameters was used in the simulations. It is remarkeable that the range of the fibre diameters range appears to have no great effects on the shape of the propagating parts of the MUAPs. These findings are consistent with the SFAP triplets as shown in fig. IV.5. They reveal that for surface potentials the broadening of the propagating part of the waveshape due to volume conductor effects is so great that an extra time dispersion caused by a variation in propagation velocity and other time-dispersion factors will be of little importance. Broadening in the end-effect peaks can only be caused by time dispersion due to different arrival times at the muscle fibre endings because the waveshape of a single fibre end-effect peak is not broadened by volume conductor effects (see section IV.4.1) MUAP recordings as in fig. IV.8B might therefore be used for a rough estimation of the muscle fibre diameter variation within one motor unit.

IV.4.4 Conclusions

Although not all aspects about motor unit action potential simulation are clarified, some important inferences can be made from the volume conductor model presented in this chapter.

The model can simulate the behaviour of any given motor unit structure in a bounded, inhomogeneous volume conductor, incorporating the important effect of action potential propagation stop at the fibre endings. Although the problem of correct parameter selection for describing the motor unit structure still exists, the simulation results reveal that for surface MUAPs the influence of various geometrical parameters and of some of the time dispersion factors is not very strong.

It can be concluded that the resulting end-effect peaks are important for understanding errors occurring in surface EMG conduction velocity estimations from latency shifts from propagating MUAPs present in recordings from two different locations [16]. Since the end-effect peaks will be present in both recordings with the same latency a distortion of the velocity estimation can be expected.

Chapter V

Intramuscular potential changes caused by the presence of the recording EMG needle electrode.

Part I : Mathematical formulation and basic results. [1]

Abstract

Needle recorded electromyographic signals may be expected to be influenced by the metal electrode shaft, by the electrical double layer at the metal - electrolyte interface and by the presence of an oedematous layer around the needle electrode. The magnitude of these effects is derived from a cylinder symmetrical volume conductor model. Analytical solutions of Laplace's equation have been derived. These are used for simulating single muscle fibre action potentials (SFAPs) recorded by a typical single fibre electrode. The results indicate that, owing to the electrical double layer, the SFAP amplitudes decrease or increase when compared to a homogeneous situation. The amplitude changes depend on whether the muscle fibre is located at the same side or at the opposite side of the electrode as the leading-off point. Only slight SFAP waveform changes are found. The oedematous layer counteracts the effects caused by the electrical double layer. The amount of counteraction depends on the thickness and the conductivity of the oedematous layer.

[1] Adapted from The effect of needle electrodes on recorded action potentials revealed by an analytical model M M H J THEEUWEN, T H.J M GOOTZEN and D.F STEGEMAN *Submitted to IEEE Trans Biomed Eng*

V.1 Introduction

In the recording and modelling of electrophysiological phenomena such as single muscle fibre or motor unit action potentials, the determination of the influence of the recording electrode on the recorded potentials has always presented a problem. At very short recording distances, the dimensions of the standard needle electrodes, and hence probably also their influence on the recorded potentials, are not likely to be negligible.

In fundamental electrophysiological studies, some methods for describing electrode properties and results of measurements of electrode properties have been reported [13,47,61,100,101].

In (clinical) applications of the recording of electrophysiological phenomena, much attention has been paid to the use of standard electrode types, so that reported results could be compared although the exact influence of the (needle) electrode on the recorded potentials was not known [45,76,99].

Although the volume conductor models used to simulate electrophysiological phenomena are becoming more and more detailed and accurate, and some attempts have been reported to include the electrode influence in the models (e.g. [88]), the lack of a proper description of the influences of standard EMG electrodes has remained. This holds true especially for the recordings and simulations of clinical single fibre electromyography (SF EMG)

In this chapter we report on a volume conductor model which treats the effect of the presence of the needle, in particular of the impedance of an electrical double layer between the metal needle electrode and the surrounding muscle tissue on simulated single fibre action potentials (SFAPs). The characteristics of such a layer have been taken from the literature (see e.g. de Boer and van Oosterom [13]). Another aspect considered is the presence of an oedematous layer around the needle electrode after insertion of the electrode into the muscle tissue. The development of such a layer might cause the decreases in the SFAP amplitudes observed while an electrode is being kept in the same recording position for several minutes. Although the model described in this chapter represents the typical SF EMG recording situation, part of the results is certainly of interest for other bioelectric applications of metal electrodes.

After a description of the model in section V.2, some basic simulation results illustrating the influence of the needle electrode will be shown in section V.3.1. Results including the oedematous layer are shown in section V.3.2.

V.2 Theory

V.2.1 General description of the model

The box in the left part of fig. V.1 gives an illustration of the actual recording geometry in single muscle fibre action potential measurements. The standard single fibre electrode [115] consists of a metal shaft of about 5 cm length. Through the hollow cannula, filled with insulating epoxy resin, a thin wire (25 μm $\varnothing$) is lead. About 7 mm from the tip of the electrode shaft, this wire is brought to the shaft surface through a hole in the metal shaft. The wire is cut and its cross sectional

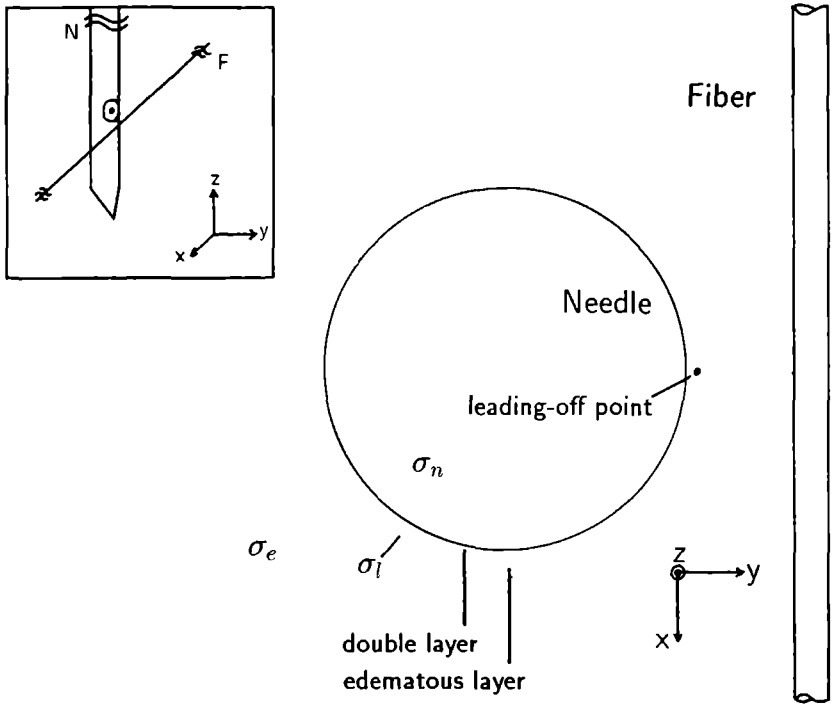

Figure V.1 : Model geometry. In the box the usual single fibre recording situation is sketched, while in the right part a cross section of the model in the plane $z = 0$ is depicted.

area is used as recording surface. Since the hole is also filled with insulating resin, the recording point is electrically isolated from the shaft. In order to be able to perform potential field calculations in the presence of such an electrode, several assumptions in the description of the needle electrode have to be made. The right part of fig. V.1 shows how the recording situation is described in the volume conductor model.

The metal electrode shaft is represented by a homogeneous cylinder with conductivity σ_n. This conductivity is so high that the influence of the insulating core can be expected to be negligible. The conductivity of the metal shaft is also very high when compared to the other conductivities in the model. The electrode shaft is completely surrounded by the electrical double layer. The thickness of the double layer, being of the order of a few Å[61], is neglected. Several reports exist on the electrical properties of this electrical double layer. It has often been described in terms of a frequency dependent resistance and capacitance in parallel (e.g. [101]). More appropriate is a mathematical description in somewhat more abstract terms of the frequency dependence actually found [13]. The impedance of this infinitesimally thin layer is described as a function of the angular velocity

$\omega = 2\pi\nu$, with ν the frequency, by [13]

$$Z(\omega) = \frac{K}{\left(i\frac{\omega}{\omega_0}\right)^m} \quad , \tag{V.1}$$

where $0 < m \leq 1$, and $\omega_0 = 2\pi$ rad/s for dimensional normalisation [57,126]. The constant K has the dimension Ωm^2. This relation was first proven by Fricke [41]. The value of m lies in practice between 0.4 and 0.9 (Geddes et al. [47] : 0.52, Hary et al. [67] : 0.75, De Boer and Van Oosterom [13] : 0.6-0.85, Schwan [111] : 0.45).

There is no consensus in literature which factor determines the value of m. The roughness of the interface appears to be an important factor which suggests that the material used is of second order importance. This can be made plausible with a so-called fractal surface structure model [80,125]. For our study, the values for the constants m and K are taken from [13] : $K = 0.125\ \Omega m^2$, $m = 0.75$ (Table V.1).

The recording surface, in the real needle electrode the bare end of the thin wire, is represented by an observation point lying in the medium surrounding the needle electrode, thus just outside the electrical double layer. By doing so, the double layer on the recording surface is not taken into account. This is allowed since the impedance of this small area of double layer, calculated by eq. V.1 is low compared with the input impedance of a high ohmic amplifier (2 MΩ versus 100 MΩ for $\nu = 100$ Hz). The potential variations that can be expected over the recording surface will be so small that it may well be considered as being infinitesimally small [34].

Since the potential field calculations are carried out in the spatial frequency domain (corresponding to the z-direction), the Fourier transformations imply that the needle shaft has an infinite length. The decrease in SFAP amplitude in the longitudinal direction of the needle electrode is so fast that, for usual distances between the electrode tip and the recording surface, the approximation of the needle shaft as being of infinite length will be appropriate.

For the surrounding medium, two different situations are modelled. In the first situation, the needle electrode is surrounded by an infinite homogeneous and isotropic medium with conductivity σ_e, representing the muscle tissue. The muscle tissue conductivity is taken to be temporal frequency independent, which has been proven to be valid in this kind of modelling (Chapter II, [50,53,94]). In the second situation, an oedematous layer of a thickness ranging up to 100 μm and with conductivity σ_l is present directly outside the electrical double layer. This oedematous layer is then surrounded by the muscle tissue.

A muscle fibre is located in the muscle tissue, in a plane perpendicular to the orientation of the needle shaft. Owing to the fact that the muscle fibre and the needle shaft are orientated perpendicular to each other, the muscle tissue cannot be described as anisotropic. This is of course not realistic, but in the next subsection it will be explained why this choice has to be made and in the discussion it will be estimated in which way the anisotropy might influence the results. The muscle fibre is represented by a line source [6] with an action potential propagation velocity of 4 m/s.

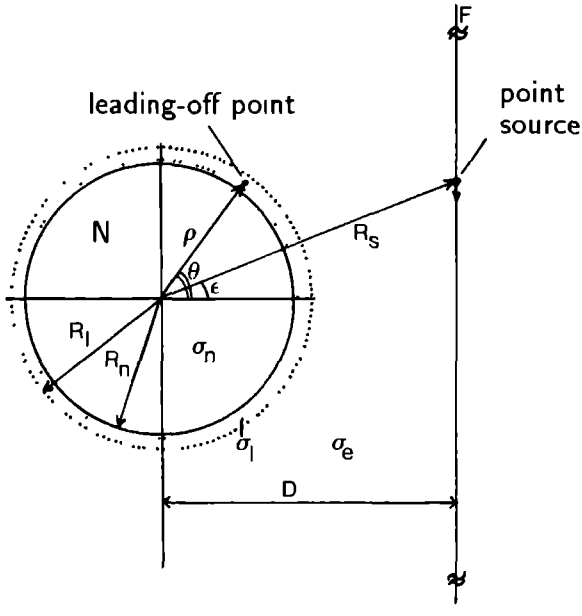

Figure V.2 . Geometrical parameters used in the model. Note that the fibre is considered as a line source The leading-off point is located at position (ρ, θ). Only results using $\theta = 0$ and $\theta = \pi$ will be presented in this chapter.

V.2.2 Analytical solution of the potential problem

By solving the potential problem for the observation point located just outside the double layer, the disturbance with respect to the homogeneous situation on a monopolar observation of the potential at this field point is calculated. This disturbance is caused by the presence of the metal needle shaft and the interactions of this shaft with its surroundings. The geometrical parameters of the model are indicated in fig. V.2.

Since the shape of the needle electrode is a cylinder, the potential field is best calculated in cylindrical coordinates with the symmetry axis, the z-axis, taken to coincide with the core of the needle. This choice dictates a different approach for the description of the source than usual when dealing with muscle or nerve fibres lying in cylinder symmetrical inhomogeneous volume conductors. In our approach, a monopolar current source of unit strength is taken to propagate uniformly along the line representing the muscle fibre. The solution of Laplace's equation for the potential at the observation point can be obtained in the classical way. The main difference with other models is that there is only one source point present of which the location in the plane perpendicular to the longitudinal axis is different for every time instant. So for every separate time instant the boundary conditions implied by the model geometry have to be applied.

Another consequence of the choice of the symmetry axis is that the muscle tissue conductivity has to be treated as isotropic. When the symmetry axis is parallel to the muscle fibre direction, which is the case in the cylinder symmetrical models presented in the past, the anisotropy can be included as a scaling of the radial distances in the model. In our model radial directions with respect to the muscle fibre are not the same as the radial directions with respect to the symmetry axis. To our knowledge there are no mathematical methods available to overcome this problem.

From fig. V.2, it can be seen that in this description the angle ϵ and the distance R_s have to be replaced by the time dependent functions $\epsilon(t)$ and $R_s(t)$. Since the frequency dependence of the electrical double layer impedance requires that part of the calculations are performed in the temporal frequency domain, also the Fourier transforms $\epsilon(\omega)$ and $R_s(\omega)$ of these functions have to be evaluated.

After completion of the calculations in the temporal frequency domain and inverse Fourier transformations to the regular spatial and temporal domain, the potential in the observation point (R_n, θ) owing to the moving monopole is obtained as a function of time. In the situation without the oedematous layer, this potential is given by $\Phi_e(t; R_n, \theta)$ and when the oedematous layer is present by $\Phi_l(t; R_n, \theta)$ (see next subsection). By a convolution of this potential waveform with a physilogical current source density distribution $S(t)$, the actual SFAP is obtained. This current source distribution corresponds to the second derivative of the intracellular action potential [103] and has often been used in SFAP modelling [86] (see fig. VIII.5A, dotted curve).

The potential $\Phi(\rho, \phi, z)$ in a source free region, obeys Laplace's equation. In cylindrical coordinates this reads [72]

$$\frac{1}{\rho}\frac{\partial}{\partial \rho}\left(\rho \frac{\partial \Phi}{\partial \rho}\right) + \frac{1}{\rho^2}\frac{\partial^2 \Phi}{\partial \phi^2} + \frac{\partial^2 \Phi}{\partial z^2} = 0 \quad . \tag{V.2}$$

Using standard solution methods (see e.g. [68,72]) one can obtain the following expression for the potential distribution in the surrounding medium

$$\Phi_e = \Phi_\infty + \sum_{n=-\infty}^{\infty} e^{-jn(\theta-\epsilon)} \mathcal{F}_z^{-1}\left[A_n K_n(\mid k \mid \rho)\right] \tag{V.3}$$

and for the potential distribution in the needle electrode

$$\Phi_n = \sum_{n=-\infty}^{\infty} e^{-jn(\theta-\epsilon)} \mathcal{F}_z^{-1}\left[B_n I_n(\mid k \mid \rho)\right] \quad , \tag{V.4}$$

where Φ_∞ is the potential in an infinite, homogeneous and isotropic medium resulting from a point source and $\mathcal{F}_z^{-1}$ the inverse Fourier transformation with respect to z. From fig. V.2, it can be seen that the source point is located eccentrically. In order to be able to solve the boundary conditions in this situation, the addition theorem for Bessel functions [60] has to be applied to the K_0 Bessel function which forms part of the solution in the homogeneous, infinite medium. In this way, the homogeneous solutions can be expressed with respect to the eccentric location of

the source point. For $\rho < R_S$ this leads to

$$\Phi_\infty(\rho,\theta,z;R_S,\epsilon) = \sum_{n=-\infty}^{\infty} e^{-jn(\theta-\epsilon)}\mathcal{F}_z^{-1}\left[\frac{I}{2\pi\sigma_e}K_n(\mid k \mid R_S)I_n(\mid k \mid \rho)\right] \quad , \qquad \text{(V.5)}$$

where ρ is the radial position of the leading-off point and R_S the radial position of the source point. The coefficients A_n and B_n can be solved using the boundary conditions [42]

1. continuity of current passing through the double layer

$$-\sigma_n \left.\frac{\partial\Phi_n}{\partial\rho}\right|_{\rho=R_n} = -\sigma_e \left.\frac{\partial\Phi_e}{\partial\rho}\right|_{\rho=R_n} \quad , \qquad \text{(V.6)}$$

2. Ohm's law for current passing through the double layer

$$-\sigma_n Z(\omega) \left.\frac{\partial\Phi_n(\omega)}{\partial\rho}\right|_{\rho=R_n} = \Phi_n(\omega)|_{\rho=R_n} - \Phi_e(\omega)|_{\rho=R_n} \, . \qquad \text{(V.7)}$$

Although it is appropriate to apply Dirichlet boundary conditions when metal electrodes are used as stimulation electrodes [72], in a passive application Neumann boundary conditions are prefereable. This has as extra advantage that the boundary conditions are consistent with earlier volume conductor studies of electrophysiological phenomena (e.g. [68,121]) and that a non-mixed boundary condition problem is maintained. The description of the second boundary condition is equivalent to a model reported in literature containing the description of a connective sheet surrounding a muscle [42].

Applying the boundary conditions, and straightforward calculus result in the following expression for the potential in the observation point located just outside the electrical double layer

$$\Phi_e(t;R_n,\theta) = \sum_{n=-\infty}^{\infty} \mathcal{F}_z^{-1}\left[\mathcal{F}_t^{-1}\left[P_n(\omega)I_n(\mid k \mid R_n)\right.\right.$$
$$\left.\left.\left(1 + \frac{1 - \frac{\sigma_n}{\sigma_e} + \sigma_n Z(\omega) \mid k \mid \frac{I'_n(\mid k \mid R_n)}{I_n(\mid k \mid R_n)}}{\frac{\sigma_n}{\sigma_e} - \frac{K'_n(\mid k \mid R_n)}{K_n(\mid k \mid R_n)}\left(\frac{I_n(\mid k \mid R_n)}{I'_n(\mid k \mid R_n)} + \sigma_n Z(\omega) \mid k \mid\right)}\right)\right]\right] \quad , \qquad \text{(V.8)}$$

with $\mathcal{F}_t^{-1}$ the inverse Fourier transformation with respect to t, I'_n and K'_n the first derivatives of I_n and K_n with respect to $\mid k \mid \rho$ for $\rho = R_n$ and

$$P_n(\omega) = \mathcal{F}_t\left[e^{-jn(\theta-\epsilon(t))}\frac{I}{2\pi\sigma_e}K_n(\mid k \mid R_S(t))\right] \quad . \qquad \text{(V.9)}$$

The second term in the round brackets in the lower part in eq. V.8 actually represents the presence of the needle electrode shaft and the electrical double layer.

V.2.3 Analytical solution of the potential problem including an oedematous layer

The conductivity of the oedematous layer with thickness $R_l - R_n$ (see fig. V.1) is taken to be frequency independent and to be equal to that of intracellular fluid (= physiological saline solution [130]). The observation point remains on the outer surface of the double layer, which is also the inner side of the oedematous layer. The muscle fibre lies completely outside the oedematous layer. The general expressions for the potential distribution inside the needle and the external medium still hold true. Inside the oedematous layer, which is a source free medium, the solution of Laplace's equation can be expressed as

$$\Phi_l = \sum_{n=-\infty}^{\infty} e^{-jn(\theta-\epsilon)} \mathcal{F}_z^{-1} \left[C_n K_n(|\, k \,|\, \rho) + D_n I_n(|\, k \,|\, \rho) \right] \quad . \tag{V.10}$$

By combining this with the boundary conditions

1. continuity of current passing through the double layer

$$-\sigma_n \left. \frac{\partial \Phi_n}{\partial \rho} \right|_{\rho=R_n} = -\sigma_l \left. \frac{\partial \Phi_l}{\partial \rho} \right|_{\rho=R_n} , \tag{V.11}$$

2. Ohm's law applied to the electrical double layer

$$-\sigma_n Z(\omega) \left. \frac{\partial \Phi_n(\omega)}{\partial \rho} \right|_{\rho=R_n} = \Phi_n(\omega)|_{\rho=R_n} - \Phi_l(\omega)|_{\rho=R_n} , \tag{V.12}$$

3. continuity of current through the boundary between oedematous layer and muscle tissue

$$-\sigma_l \left. \frac{\partial \Phi}{\partial \rho} \right|_{\rho=R_l} = -\sigma_e \left. \frac{\partial \Phi_e}{\partial \rho} \right|_{\rho=R_l} \tag{V.13}$$

and

4. continuity of potential across the boundary between oedematous layer and muscle tissue

$$\Phi_l|_{\rho=R_l} = \Phi_e|_{\rho=R_l} , \tag{V.14}$$

it can be shown, in analogy to the previous section, that

$$\Phi_l(t; R_n, \theta) = \sum_{n=-\infty}^{\infty} \mathcal{F}_z^{-1} \left[\mathcal{F}_t^{-1} \left[(f_n(k,\omega,R_n) + 1) P_n(\omega) I_n(|\, k \,|\, R_n) \right. \right.$$
$$\left. \left. \frac{\left(\frac{I'_n(|\, k \,|\, R_l)}{I_n(|\, k \,|\, R_l)} - \frac{K'_n(|\, k \,|\, R_l)}{K_n(|\, k \,|\, R_l)} \right)}{\left(\frac{\sigma_l}{\sigma_e} - 1 \right) f_n(k,\omega,R_n) \frac{K'_n(|\, k \,|\, R_l)}{K_n(|\, k \,|\, R_n)} \frac{I_n(|\, k \,|\, R_n)}{I_n(|\, k \,|\, R_l)} + \frac{\sigma_l}{\sigma_e} \frac{I'_n(|\, k \,|\, R_l)}{I_n(|\, k \,|\, R_l)} - \frac{K'_n(|\, k \,|\, R_l)}{K_n(|\, k \,|\, R_l)}} \right] \right] , \tag{V.15}$$

with

$$f_n(k,\omega,R_n) = \frac{\left(1 - \frac{\sigma_n}{\sigma_l} + \sigma_n Z(\omega) \,|\, k \,|\, \frac{I'_n(|\, k \,|\, R_n)}{I_n(|\, k \,|\, R_n)} \right)}{\frac{\sigma_n}{\sigma_l} - \frac{K'_n(|\, k \,|\, R_n)}{K_n(|\, k \,|\, R_n)} \left(\frac{I_n(|\, k \,|\, R_n)}{I'_n(|\, k \,|\, R_n)} + \sigma_n Z(\omega) \,|\, k \,| \right)} \quad . \tag{V.16}$$

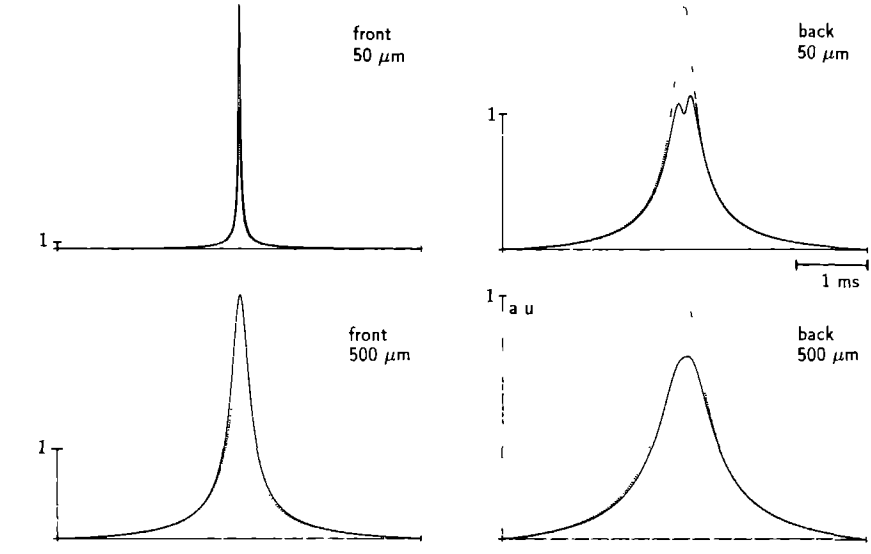

Figure V.3 : Point source potentials in the homogeneous situation (dotted lines) and with the presence of the electrode (solid lines) for muscle fibres located at distances of 50 and 500 μm from the electrode surface on the same side as the leading-off point (left column) and on the opposite side (right column). (a.u. = arbitrary units)

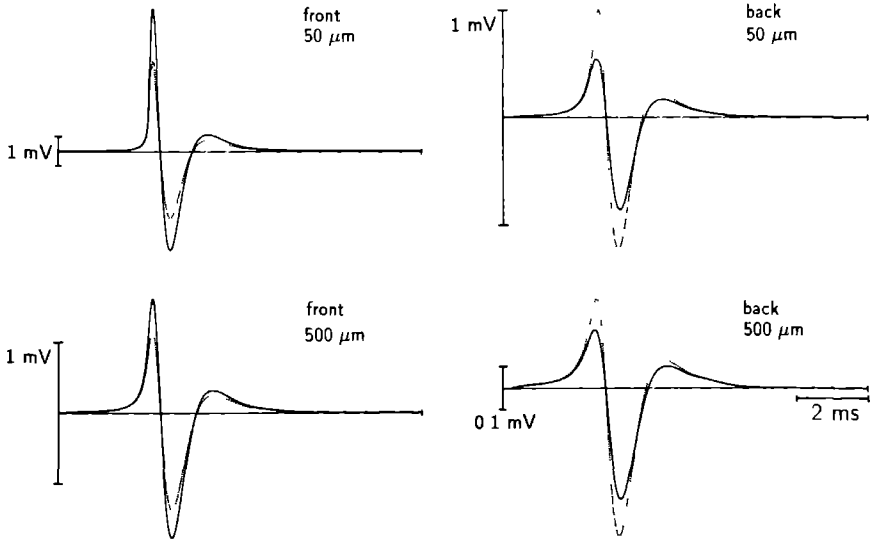

Figure V.4 : SFAPs corresponding to the point source potentials in figure 5.3.

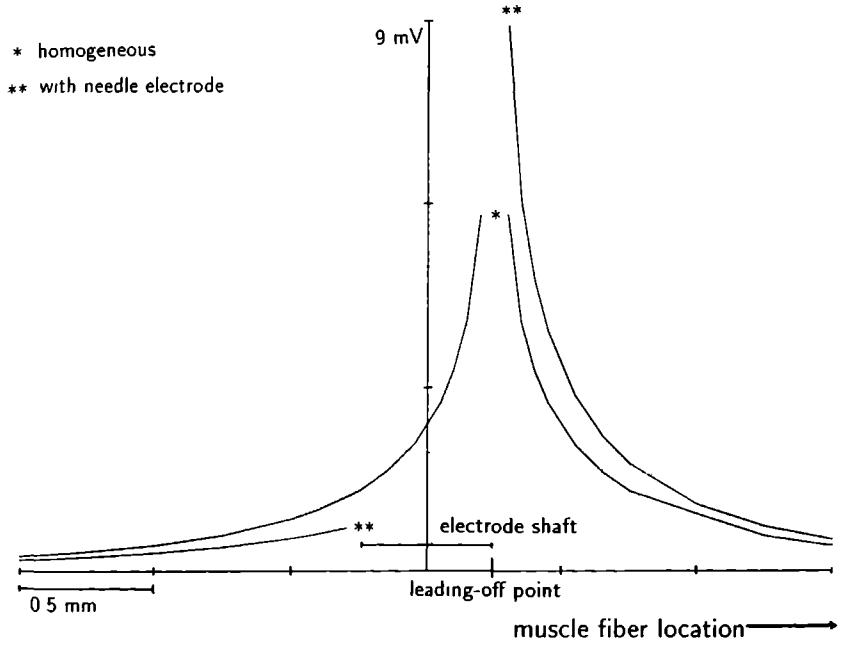

Figure V.5 : SFAP amplitude as a function of the location of the active muscle fibre with respect to the leading-off point.

V.3 Results

V.3.1 Results without oedematous layer

Fig. V.3 shows four potentials resulting from a point source propagating along a line with shortest distances to the needle electrode of 50 and 500 μm, for line sources (read: muscle fibres) lying on the same side of the electrode as the leading-off point as well as on the opposite side of the electrode. The parameters used in these simulations are documented in table V.1.

Table V.1 Model parameters

Parameter	Value	Unit	
σ_n	1000	$(\Omega m)^{-1}$	conductivity needle
σ_e	0.25	$(\Omega m)^{-1}$	conductivity muscle tissue
σ_l	1.0	$(\Omega m)^{-1}$	conductivity oedematous layer
R_n	0.25	mm	radius needle
R_l	0.25-0.35	mm	outer radius oedametous layer
K	0.125	Ωm^2	double layer constant
m	0.75		double layer exponent
ω_0	2π	rad s^{-1}	normalisation constant

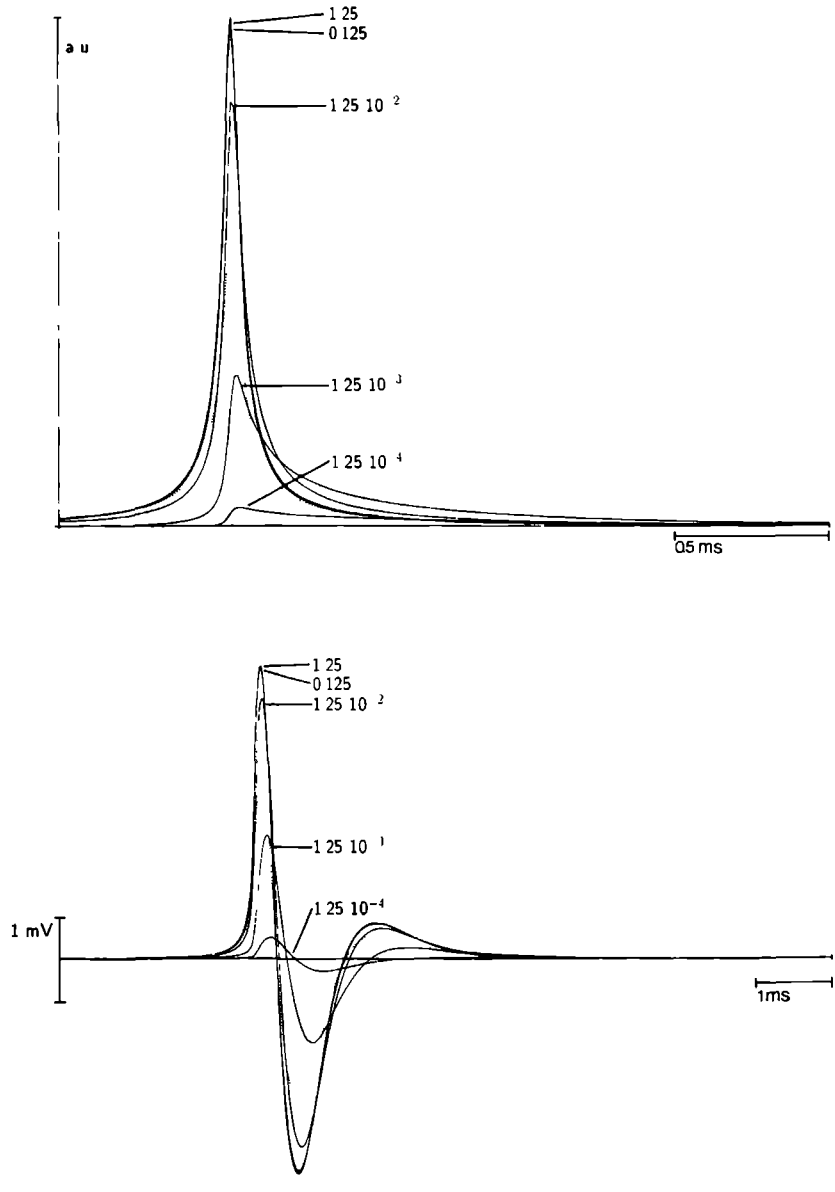

Figure V.6 : A) Point source potentials for the homogeneous situation (dotted line) and for different values of double layer impedance constant K (solid lines). B) SFAPs corresponding to the point source potentials from A.

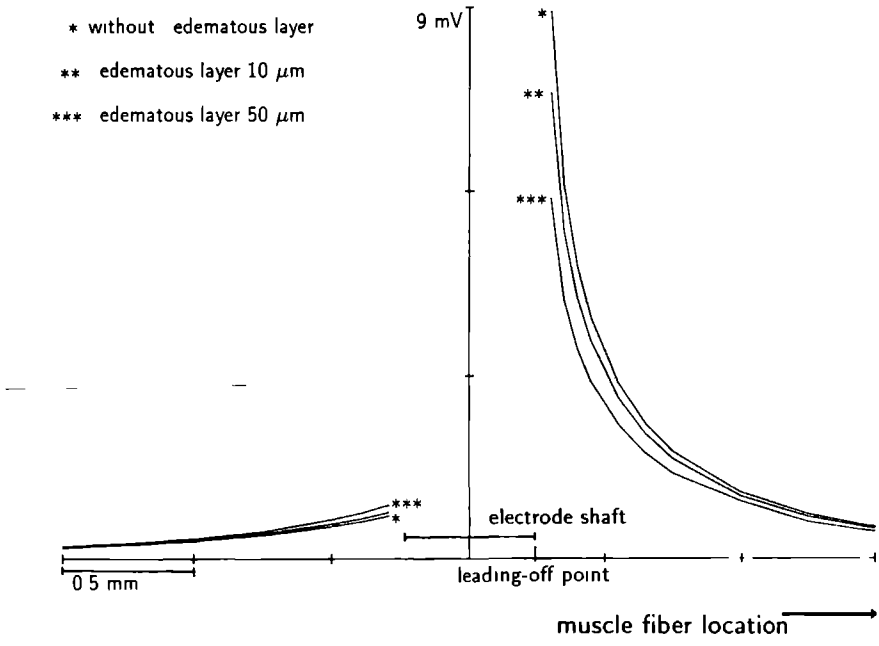

Figure V.7 : SFAP amplitude as a function of the location of the active muscle fibre with respect to the leading-off point for different widths of the oedematous layer.

Fig. V.4 shows the SFAPs, corresponding to the point source potentials in fig. V.3, which have been obtained by a convolution of the curves in fig. V.3 with the muscle fibre source function.

In order to get a complete view of how the SFAP waveform and especially of how the SFAP amplitude is changed due to the presence of the needle electrode, SFAPs have been simulated at a number of locations of the muscle fibre.

Fig. V.5 shows the peak-peak amplitudes of the SFAPs as function of the location of the active muscle fibre relative to the observation point. The observation point is located at + 0.25 mm. The distance ranges from close to the needle electrode (locations + 0.3 and − 0.3 mm) up to + 1.5 and − 1.5 mm distance to the cannula surface.

The influence of the high conductivity of the needle shaft relative to the influence of the double layer can be demonstrated if the value of K in the double layer impedance is varied.

Fig. V.6A shows point source potentials and V.6B the corresponding action potentials for several values of the K constant in the double layer impedance. K is varied from 10 times the default value (see table V.1) to 10^{-4} times the default value. The conductivity of the needle shaft has been kept at the value of table V.1.

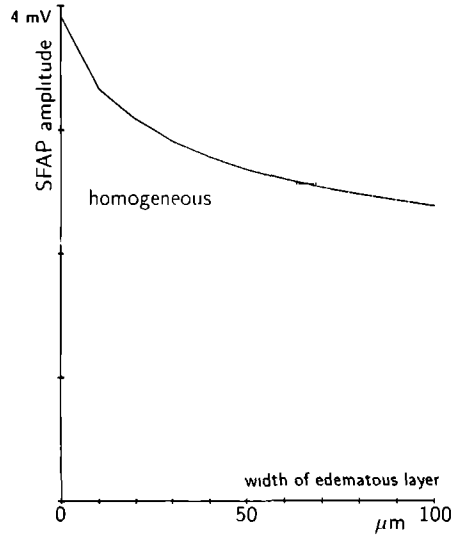

Figure V.8 : SFAP amplitude for a muscle fibre located at a distance of 150 μm from the leading-off point as a function of the width of the oedematous layer.

When the conductivity of the needle shaft σ_n is varied from 1 to 10^9 $(\Omega m)^{-1}$, while keeping K at the value from table V.1, no changes can be noticed in the SFAPs.

V.3.2 Results including the oedematous layer

Fig. V.7 shows the peak-peak amplitudes of the SFAPs as a function of the location of the active muscle fibre for situations without an oedematous layer (indicated in the figure by *), with an oedematous layer of 10 μm thickness (**) and with an oedematous layer of 50 μm thickness (***), observed at the leading-off point just outside the double layer at + 0.25 mm. The conductivity of the oedematous layer is 1.0 $(\Omega m)^{-1}$. All other parameters have the same values as used for the simulations shown in fig. V.5.

A gradual increase of the thickness of the oedematous layer causes a decrease in SFAP amplitude. Fig. V.8 shows the peak-peak amplitude of the SFAPs for a muscle fibre located at a distance of 150 μm from the front side of the electrode, as a function of the thickness of the oedematous layer.

V.4 Discussion

This model describes the influence of the presence of a metal electrode shaft of infinite length, surrounded by an electrical double layer and an optional oedematous

layer, in an isotropic, infinite and homogeneous medium on the potential recorded in the leading-off point. To keep the calculus feasible, several assumptions had to be made. These assumptions and their implications are discussed in subsection V.4.1. The validity of the values of several parameters in the model will be discussed in section V.4.2. The results obtained with the model are discussed in section V.4.3.

V.4.1 Geometrical aspects

To describe the properties of an infinite cylindrical needle, a cylindrical coordinate system with the central axis of the needle as z-axis is the most suitable. Having chosen this system of coordinates, it is very hard to include axial symmetries around any axis other than the chosen z-axis. Such would be required if the anisotropy or the finiteness of the medium were to be taken into account because these two aspects usually have their symmetry axis parallel to the direction of the muscle fibres. Neglecting these properties of the medium is the price one has to pay when working with coordinates suitable for describing the needle itself. Any other system of coordinates would result in very cumbersome expressions. The results, however, indicate that major alterations of SFAP amplitudes occur with muscle fibres located at relatively small distances from the needle electrode. At these distances the influence of the finiteness of the medium will be relatively small (Chapter IV) so the assumption of an infinite medium in the model described in this chapter seems appropriate. Although it could not be incorporated in the model, some remarks on the influence of the anisotropy of the muscle tissue can still be made. In a homogeneous unbounded volume conductor a change in anisotropy can be considered as a virtual change in the observation distance and of the effective conductivity. When an anisotropic medium is characterised by its transversal and longitudinal conductivities σ_T and σ_L the effective conductivity is $\sqrt{\sigma_T \sigma_L}$ and the radial distances are scaled with a factor $\sqrt{\frac{\sigma_L}{\sigma_T}}$ [6]. As first approximation for the influence of the anisotropy this principle can be applied to our model for the observations with $\Theta = 0$ or 180 degrees by scaling the distance to the location of the muscle fibre relative to the location of the observation point. When the effective conductivity is taken constant, the curves in fig. V.5 and V.7 will then be squeezed along the horizontal axis with the factor given above. The amplitude values will be change inverse proportional to changes in the effective conductivity. As we have mentioned already in the methods section of this chapter, there are, unfortunately, no analytical methods known to us to validate this approach.

The fact that in practice the needle does not have an infinite length will not cause great disturbances on the calculated potentials. The potential at the cannular ending will be decreased drastically due to the relatively great distance from the active fibre. Moreover, owing to the use of an discrete FFT algorithm to perform the Fourier transformations along the z-axis, an implicit periodicity has already been incorporated in the present computations, and the obtained solutions represent just the length of one spatial period as if it is electrically isolated. The extension of this finite length is equal to the number of datapoints multiplied with the spatial resolution in z-direction. In our algorithm, this results in a length of 51.2 mm.

The location of the leading-off point just outside the double layer appears to be acceptable. As desired, the double layer impedance completely insulates the leading-off surface from the cannula. When using sufficiently high ohmic amplifiers the voltage drop over the impedance of the double-layer formed on the leading-off surface itself will be negligible.

Numerical solutions methods using the boundary element technique [68] are able to describe the exact shape of both the electrode shaft and of the leading-off surface but cannot easily include the effects of the electrical double layer. Just like the model presented in this chapter the boundary element method cannot include anisotropic conductivities in a three-dimensional model. Using a finite-element method is then a logical, next step in a numerical assessment of this problem.

V.4.2 Model parameters

The constant K in the double layer impedance can be varied over about two decades around the measured value [13] without causing great variations in the amplitudes of the calculated SFAPs (fig. V.6). An increase of its value causes no substantial changes and only when it is decreased by a factor 10 or more a significant decrease in point source potential and SFAP amplitudes can be noticed. This decrease is caused by the high conductivity of the metal shaft of the needle electrode. For realistic values of K, however, the conductivity of the electrode shaft has hardly any influence on the simulated potentials. The value used for the shaft conductivity is 1000 $(\Omega m)^{-1}$, which is rather low for metal, but no changes in point source potentials and SFAPs were found when it was varied between 1 and 10^9. The assumption of a homogeneous needle is therefore justified and the value taken for its conductivity acceptable.

Fig. V.6 shows that only for the extreme low values of K a phase lag of the waveform and a suppression of the third phase of the SFAP is observed. For acceptable values of K no effects of the frequency dependent characteristics of the double layer can be observed. It can therefore be concluded that no time-dependencies other than those caused by moving sources have to be incorporated in the model. For the frequency dependencies in the muscle tissue this was evident already (Chapter II, [53,94]).

Both effects discussed in this subsection will also hold true for other metals than platinum, such as stainless steel and nickel. These metals have similar frequency dependencies and impedance values [47,100,101].

The parameters describing the oedematous layer remain uncertain in the practical situation. The values used in the simulations shown in fig. V.8 span, in our opinion, a realistic range.

V.4.3 Interpretation of the simulations

For the situation without an oedematous layer the following observations can be made:

In the case of an active muscle fibre located at the same side of the needle as the leading-off point, the point source potential is amplified (fig. V.3) by a factor which increases with decreasing distance between needle and muscle fibre.

The theoretical limit is formed by an amplification factor 2 in case of a planar boundary separating two semi-infinite spaces, one of which having conductivity zero, according to the method of electrostatic images [72].

When muscle fibre and leading-off point are located at opposite sides of the needle, the point source potentials are attenuated due to the shielding by the needle (fig. V.3). The point source potentials in this situation are slightly asymmetrical (most clearly in the upper right part of fig. V.3, solid line). This asymmetry is caused by the frequency dependence of the double layer impedance. In the corresponding SFAPs (fig. V.4), however, the asymmetry does not show up for the present choice of the source function. The influence of the source function will be discussed in Chapter VI.

The attenuation and amplification of the SFAPs (fig. V.4) is less than those of the point source potentials, owing to the convolution in which source points at greater distances, and thus with smaller attenuation or amplification, also contribute to the observed potential.

Where the presence of the needle shaft and its double layer amplifies the amplitudes, the presence of an oedematous layer decreases the amplitudes. Increasing the thickness of this layer results in decreasing amplitudes (fig. V.7 and V.8). At a thickness of about 60 μm and with the chosen conductivity σ_l (table V.1), the oedematous layer completely counteracts the amplification due to the double layer for the case when muscle fibre and leading-off point lie on the same side of the needle (compare fig. V.5 and V.8). When the muscle fibre is located at the opposite side of the electrode shaft with respect to the leading-off point, the SFAP amplitudes increase when the thickness of the oedematous layer increases. Owing to the fact that the conductivity of the oedematous layer is higher than that of the muscle tissue, the shielding by the presence of the electrode shaft becomes less effective.

The effects caused by the presence of the oedematous layer can qualitatively be explained well. The quantitative implications for practical situations depend on the values of the parameters involved, in particular the width of the layer. No experimental data, however, are available on this parameter.

V.4.4 Conclusions

The model presented in this chapter allows an analytical evaluation of the influence of the presence of a metal needle shaft on the potentials recorded at a given leading-off point. The solutions contain the frequency dependence of the electrical double layer characteristics. The results reveal that the electrical double layer acts as an insulating shield around the highly conducting metal electrode shaft. The effect of the frequency dependent characteristics of the electrical double layer are hardly observeable for realistic parameter selctions. The oedematous layer counteracts the influence of the double layer, i.e. where the double layer causes an increase of amplitudes the oedematous layer decreases the amplitudes (when the muscle fibre is located on the same side of the electrode as the leading-off point) and vice versa (when the muscle fibre is located at the opposite side of the electrode).

Chapter VI

Intramuscular potential field changes caused by the presence of the recording EMG needle electrode. [1]

Part II : Evaluation and practical consequences.

Abstract

A comprehensive volume conductor study of a single fibre needle EMG (SF EMG) recording has been made. The electrode shaft is described as a passive inhomogeneity in the volume conductor. The most important observation is a substantial increase in single fibre action potential (SFAP) amplitude (up to 70 %) for muscle fibres observed from a short distance. For SFAPs from muscle fibres located on the back of the SF electrode a shadow effect occurs which can result in a maximal amplitude decrease of 50 %. SFAP waveforms changes are observed in situations which are of limited practical interest only. The presence of the needle shaft causes an anisotropy-like behaviour of the relation between leading-off point to muscle fibre distance. The observed amplification decreases faster in the direction parallel to the cannula than in the direction normal to the cannula owing to the presence of the needle cannula. Due to the amplification of SFAPs from muscle fibres observed from a short distance, the maximal distance from which SFAPs are included in fibre density measurements (amplitude greater than 0.2 mV) is raised from 380 μm to 460 μm, for the situation where no oedematous layer is present.

[1] Adapted from *Intramuscular potential changes caused by the presence of the recording EMG needle electrode* T H J.M GOOTZEN, D F STEGEMAN and H J M. VINGERHOETS Submitted to Electroenceph Clin Neurophysiol

VI.1 Introduction

Metal electrodes of different types and shapes are used extensively in various electrophysiological investigations (e.g. [61,91]). Electrodes used in everyday clinical electrophysiology are the needle EMG electrodes (e.g. concentric needle electrodes, single fibre needle electrodes, macro electrodes). When using needle EMG electrodes a physician is aware of the fact that insertion of an EMG needle in a muscle will be noticed by the neuromuscular system in the broadest sense of the word. Structural displacement, damage and perhaps reactions of the central nervous system will affect an EMG recording.

To circumvent the need for knowledge of the exact character of all influences mentioned in routine electromyography, attention is paid to the use of standard electrode types (e.g. [82]). Although useful in clinical practice, such an approach fails when experimental and theoretical knowledge on the level of the muscle fibre membrane or the single muscle fibre is related to clinical EMG studies. This relation has been the subject of study in a number of papers using the theory of volume conduction [6,62,86,88]. Hitherto, all such studies have lacked a proper, theoretically verified description of the influence of the standard EMG electrodes. In this chapter such a description will be presented. The full description of the theoretical aspects of this analysis has been presented in Chapter V and in [52,126]. Here we concentrate on the implications for the clinical applications of metal needle electrodes. Since single muscle fibre activity is usually recorded by so-called single fibre EMG electrodes in clinical practice [115] (fig. VI.1A) we base our study on a model presentation of this type of electrode.

The results of the model are described in general, non-mathematical, terms in this chapter. In section VI.2 the different aspects of the model are briefly reviewed. Section VI.3 shows simulation results for various modelling situations. In the discussion, an attempt is made to interprete the simulation results, from which a better understanding of routine EMG recordings can be derived.

The first aspect related to the presence of a needle electrode in the muscle tissue is the mechanical disturbance of the tissue. The displacement of muscle fibres was taken into account in the simplest possible way in one EMG simulation study. Where the needle is inserted, the fibres are "ploughed" [88] to one side of the electrode.

Another important theme of both the previous and the present chapter is the electrode shaft which is considered as an inhomogeneity in the muscle tissue with a deviating electric impedance. This effect is mostly discussed on the basis of intuitive insights (e.g. [115]). The fact that the dimensions of the electrode are an order of magnitude greater than the cross section of the muscle fibre as the elementary unit of electric field generation is felt to be an important point, moreover.

Two of the various needle electrode characteristics are expected to be of substantial importance in the present context. One is the polarising electrochemical process at the interface between a metal electrode and the electrolyte, the electric double layer [61]. The other is a reaction of the muscle tissue which may form an oedematous layer around the electrode [33].

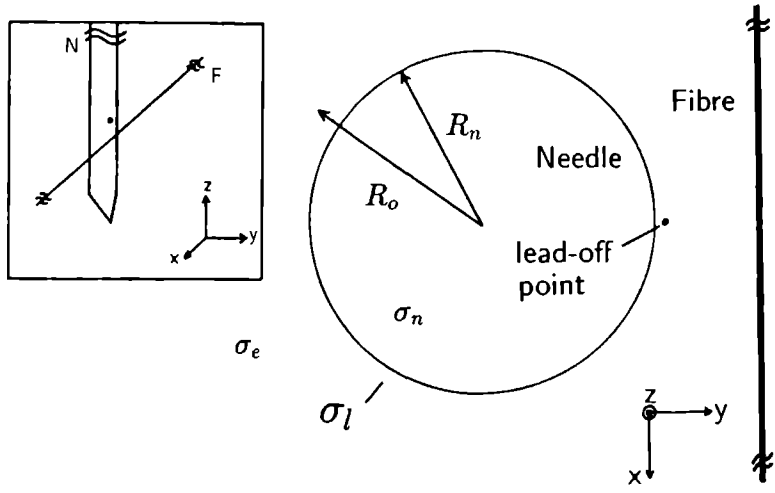

Figure VI.1 : A) frontal view of a standard single fibre electrode. B) frontal view of the infinite length electrode used in our model. In the model the leading-off surface is insulated from the electrode shaft by the electrical double layer.

VI.2 Model of a single fibre EMG recording configuration

The single fibre EMG needle electrode

The single fibre EMG needle electrode, as first proposed by Stålberg (see fig. VI.1A), consists of a stainless steel cannula 0.4-0.6 mm in diameter, inside which an insulated thin wire (25 μm diameter, usually platinum or silver) is placed and taken out at a hole at the side opposite to the bevelled surface of the needle shaft. The cannula and the side hole are filled with epoxy resin [115].

The description of the needle electrode in this section is based on considering the needle shaft as a part of an inhomogeneous volume conductor configuration. Our model of the electrode shaft (fig VI.1B) consists of an infinitely long homogeneous metal cylinder with a very high electric conductivity σ_n, i.e. several orders of magnitude higher than that of all other conductivities.

Muscle tissue and single fibre activity

The muscle tissue is modelled by a homogeneous, frequency independent, isotropic conductivity σ_e. The well known anisotropy of the muscle structure [46] is neglected. This is obviously a violation of reality. The choice of the mathematical solution principle in cylinder coordinates oriented to the needle shaft, which has very pronounced advantages [126], will lead to almost unmanageable complications when anisotropy in another coordinate system has to be taken into account. As

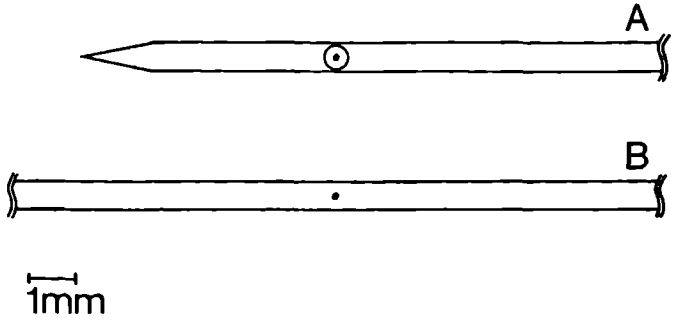

Figure VI.2 : Upper left : schematic representation of the recording geometry of a single fibre recording. Right : geometry of the volume conductor model. Cross-section trough the electrode at the z=0 plane. (R_n radius electrode, R_l radius outer boundary oedematous layer, σ_n, σ_l and σ_e electrode shaft, oedematous layer and muscle tissue conductivity)

was shown in Chapter V, the essential conclusions of the model are not undermined by this simplification.

The muscle fibres are orientated perpendicularly to the needle shaft (fig. VI.2). The action potential propagates at a constant velocity of 4 m/s along the muscle fibre that is located parallel to the x-axis. The electrophysiological source is modelled as a line source [6]. In Chapter V, the action potential wave shape (= the transmembrane action potential) was taken from [86] (fig. VIII.5A, dotted curve). In this chapter, an adapted version of that source function has been used (fig. VIII.5A, solid curve). This adaptation, which will be described in detail in Chapter VIII has been performed to obtain simulated single fibre action potentials (SFAPs) which are better comparable to experimentally recorded SFAPs.

Unless otherwise stated, the z-level of the fibre (fig. VI.2) is equal to that of the leading-off surface (see section "The leading-off surface").

The electrode-electrolyte interface

An infinitesimally thin interface layer is formed between a metal electrode and the tissue fluid in which it is placed. This is a result of complicated electrochemical reactions [61]. The impedance of this electrical double layer is usually described by the relation [13,41] :

$$Z(\omega) = \frac{K}{(i\frac{\omega}{\omega_0})^m} \quad , \tag{VI.1}$$

where $0 < m \leq 1$, and $\omega_0 = 2\pi$ rad/s for dimensional normalization (Chapter V, [57,126]). The constant K has the dimension Ωm^2. For our study, the constants m and K are taken from de Boer and van Oosterom [13] ($m = 0.75$, $K = 0.125$ Ωm^2, Table V.1). Fortunately, variations of K and m within physically reasonable limits have appeared not to be of importance in the present study [126].

The leading-off surface

As can be observed in fig. VI.2, this leading-off surface, which is located on the needle electrode surface in the real needle electrode, is located outside the double layer and is considered as being a (infinitesimally small) point. At first sight, a location just inside the double layer might appear to be more justified. A property of the mathematical expressions describing our model is that the insulating resin area around the leading-off surface (fig. VI.1A) cannot be implemented. The leading-off surface would then become part of the needle cannula. It has been proven in Chapter V that the location of the observation point outside the double layer is suitable [126]. The coordinates of the leading-off point are, by definition, (x,y,z)=(0,0,0).

The oedematous layer

In long-term (longer than approximately 1 minute) needle EMG recordings, it is often observed that the signal amplitude decreases with time. A similar phenomenon was described by Ekstedt [33] who found it impossible to record high amplitude SFAPs with a slightly bent or blunt electrode. Histological alterations found in muscle biopsies investigated by needle EMG previously ("needle myopathy" [93]) suggest that an unspecified number of muscle fibres is damaged or injured by the investigation. Without having further evidence, we hypothesise, as Ekstedt already speculated, that because of intracellular fluid release from compressed muscle fibres, or leakage from crushed fibres in the vicinity of the electrode, a layer of intracellular fluid, rich of potassium ions, may form around the electrode shaft. The relative importance of the presence of such an extra inhomogeneity in the configuration cannot easily be predicted and was therefore made part of the volume conductor model description (fig. VI.2). A layer with a thickness of the order of one fibre radius ($R_l - R_n = 25\mu$m) was assumed to be present and to have a conductivity σ_l which is equal to the conductivity of intracellular fluid.

"Monopolar" simulations

It is stressed that the results to be shown in the next sections, all concern the simulated potential waveform as picked up by the leading-off point indicated in fig. VI.2. The reference in the simulations can be conceived of as lying distant from the recording electrode. Hence the usual bipolar configuration with the cannula as a reference is not considered here, which means that all influences of the needle shaft and the layers around it concern their passive presence as inhomogeneities in the volume conductor formed by the muscle tissue. For the simulation of an SFAP, the difference between a remote reference electrode and the cannula as reference can expected to be small. The potential recorded from the cannula is the averaged potential over the large surface of the cannula. In this average, the regions with noticeable activity are small compared to the large regions with almost no electrical activity. Actual monopolar recordings of SFAPs from muscle fibres located on a short distance from the leading-off surface support this prediction (Chapter VIII).

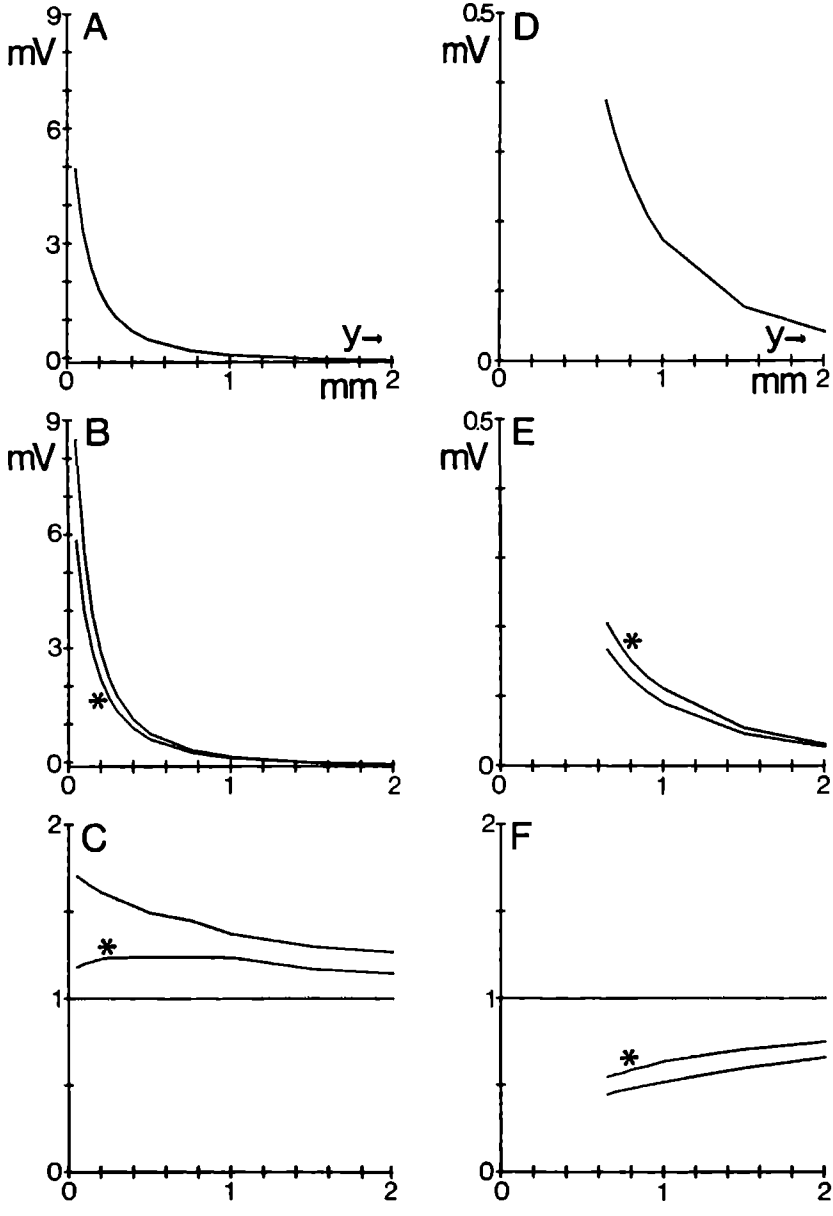
A
mV
9
6
3
0
y→
0
1
2
mm
D
mV
0.5
0
y→
0
1
2
mm
B
mV
9
6
3
0
*
0
1
2
E
mV
0.5
0
*
0
1
2
C
2
1
0
*
0
1
2
F
2
1
0
*
0
1
2

Figure VI.3 : Peak-to-peak amplitudes and amplitude ratios as a function of muscle fibre location. The unmarked curves represent the situation without an oedematous layer. The curves marked with * contain data for the situation with an oedematous layer (width 25 μm) present.

A) Peak-to-peak amplitudes for the homogeneous situation as a function of y (y > 0) for muscle fibres in the z=0 plane.

B) Peak-to-peak amplitudes for the same situations as in A but with the presence of the electrode cannula.

C) Ratio of peak-to-peak amplitudes between electrode model and homogeneous model for both curves from B.

D) Peak-to-peak amplitude for homogeneous situation, now for muscle fibre locations with y < 0, also in the z=0 plane.

E) Peak-to-peak amplitudes for the two model situations as described under B, now for muscle fibre locations with y < 0.

F) Ratio of peak-to-peak amplitudes for the two curves from E with respect to the homogeneous amplitude curve in D.

VI.3 Results

VI.3.1 Peak-to-peak amplitudes

Observation distance in the direction normal to the cannula

Fig. VI.3A shows how, in absence of the needle electrode shaft, the SFAP amplitude decreases with increasing distance between the muscle fibre and the leading-off point. The muscle fibre remains in the z=0 plane (fig. VI.2), on the same side of the needle electrode as the leading-off point. Fig. VI.3B shows for the same distance range the SFAP amplitude decrease, when the observations are affected by the presence of the needle cannula and its electrical double layer. The radius of the cannula R_n is 300 μm. The line marked with * shows the SFAP amplitudes when an oedematous layer with a width of 25 μm is present as well (R_l = 325 μm). Fig. VI.3C represents, as a function of the distance between the muscle fibre and the leading-off point, the ratios between the two amplitude curves in fig. VI.3B and the homogeneous amplitude curve in figs VI.3A. Figs VI.3D, VI.3E and VI.3F give the same information as VI.3A, VI.3B and VI.3C respectively, but now for the situation in which the muscle fibre is located at the opposite side of the needle electrode with respect to the observation point. In this case, the observation distances are evidently restricted to values greater than the needle cannula diameter (600 μm).

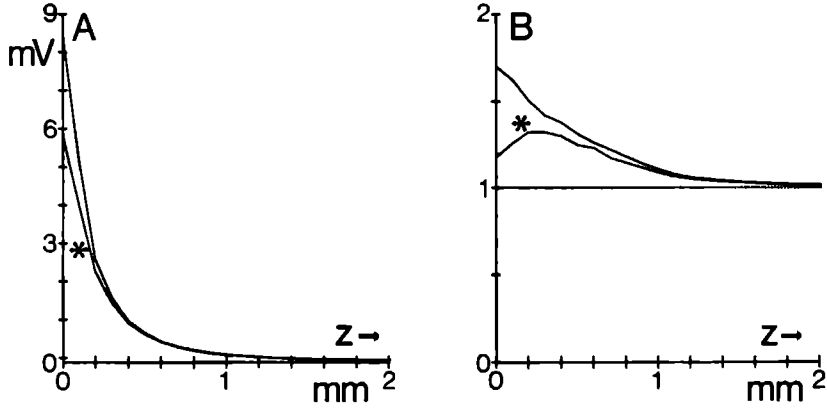

Figure VI.4 : A) Peak-to-peak amplitude as function of z ($z > 0$) for muscle fibre location y = 50 μm. Model situation without and with (*) oedematous layer (width 25 μm). B) Ratio of peak-to-peak amplitudes between the two curves in A and the homogeneous amplitude curve (fig. VI.3A).

Observation distance in direction parallel to the cannula

Fig. VI.4A shows the SFAP amplitudes for situations where the radial distance between the needle electrode and the muscle fibre is kept constant at 50 μm, but where the location in the z-direction of the observation point is varied. The muscle fibre remains in the $z = 0$ plane. The result can be interpreted as the amplitude characteristic when the action potential of a fibre close to the needle shaft fades away as a function of the insertion depth of the electrode, after it has been observed with a maximal amplitude in the plane z=0. The line marked with * again represents the situation in which also an oedematous layer of 25 μm width is present. In fig. VI.4B, the amplitude ratio as a function of the location of the leading-off point is presented for the two situations described above.

Double layer and cannula impedance

The shielding-off of the high conductivity of the shaft by the double layer can be studied by varying the constant K in eq. VI.1. The peak-to-peak amplitude of the SFAP at a transversal observation distance of 100 μm (fibre coordinates (y,z)=(100,0), see fig. VI.2) is presented in fig. VI.5 as a function of K on logarithmic scales. The default value (Table V.1) is encircled.

As a consequence of the results presented in fig. VI.5, the conductivity of the metal needle shaft has to be almost irrelevant at the default value $K = 0.125\ \Omega m^2$. The same conclusion has been drawn in Chapter V where the influence of σ_n was tested by varying the shaft conductivity σ_n. With $Z(\omega)$ at the default setting, the value of σ_n could be varied over 9 decades ($10^0 - 10^9$) without any noticeable change in the SFAP waveforms. This result implies that the nature of the needle

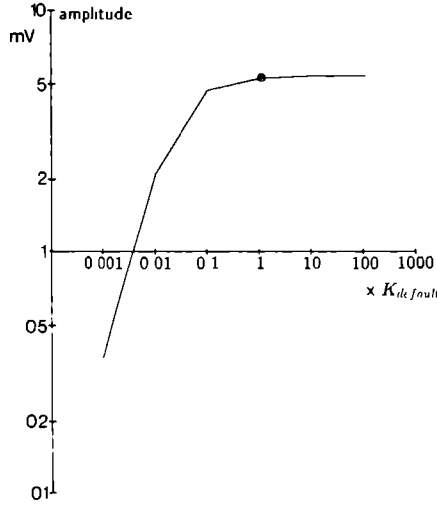

Figure VI.5 : Double logarithmic plot of the SFAP peak-to-peak amplitude as a function of the double layer impedance constant K. The data point marked by the small circle represents the default value of K as listed in table V.1.

itself, being an inhomogeneous cannula filled with almost insulating epoxy resin, need not to be considered.

VI.3.2 Wave shapes

Point source

In most of the simulations shown in this study, SFAP waveshapes are presented. The model describes how these SFAPs are changed due to the presence of a needle cannula and the two effects caused by this presence : the double layer and the oedematous layer. To show, however, some of the properties of this complicated volume conduction geometry, it is preferable to study the waveshapes generated by a propagating point source. These waveshapes are generated by taking just one current source point moving along the fibre (Chapter V, [57,126]), instead of a complete current source density distribution propagating [6] along the muscle fibre. The point-source waveforms can be considered as the volume conduction weighting functions and form the basis of the mathematical formulation of the model as derived in Chapter V (see section 5.2.2). By using the point-source waveshapes, the pure behaviour of the volume conductor configuration can be studied without any "fogging" effects caused by the inclusions of the complete source distribution related to the propagating action potential. Such point-source waveforms are presented in fig. VI.6B.

In fig. VI.6A, the simulation configuration in which the leading-off point is fixed

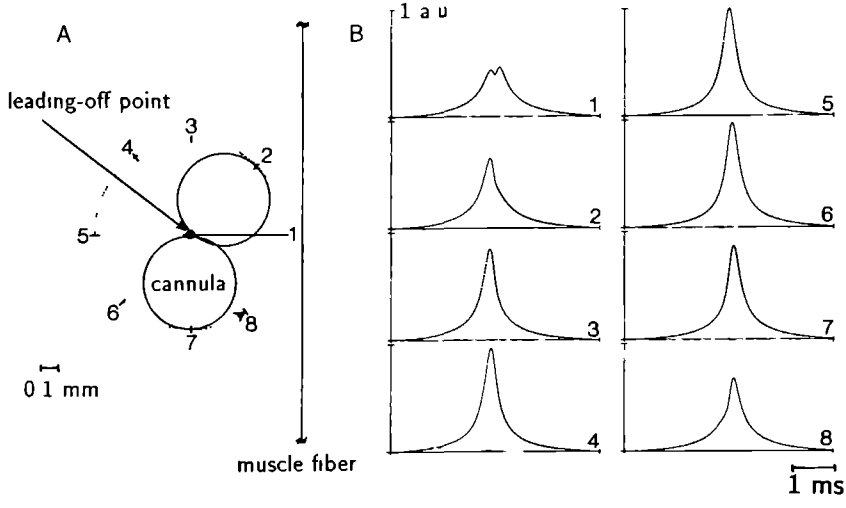

Figure VI.6 : A) Simulation results from a cannula circling around a leading-off at a fixed distance of 650 μm to the muscle fibre. The rotation step between subsequent simulations is 45 degrees. B) Point-source waveforms corresponding to the eight situations defined in A.

at a location on a distance of 650 μm transversal to the muscle fibre is presented. Eight different positions of the cannula relative to the fixed leading-off point are considered, such that the needle cannula circles around the leading-off point in steps of 45 degrees. In fig. VI.6A, only the situation corresponding to the second and the seventh waveshape is presented. Note that in a real recording each of these situations would correspond to a different insertion channel. The point-source waveforms resulting from these eight situations are shown in fig. VI.6B. Since no physiological meaning can be attached to a single source point, the amplitudes are indicated in arbitrary units. All eight waveforms are plotted on the same scale.

Physiological source

The simulations of physiological SFAPs, corresponding to the eight different situations as presented in fig. VI.6A, are shown in fig. VI.7. The results comparable to those of fig. VI.6 and VI.7 for the situation including the oedematous layer do not reveal interesting, new aspects and are therefore omitted.

VI.4 Discussion

It is more than twenty-five years ago since the first extensive discussion on the various aspects of recording single muscle fibre activity with a needle electrode was published. Ekstedt [33] and later also Stålberg and Trontelj [115] gave their view

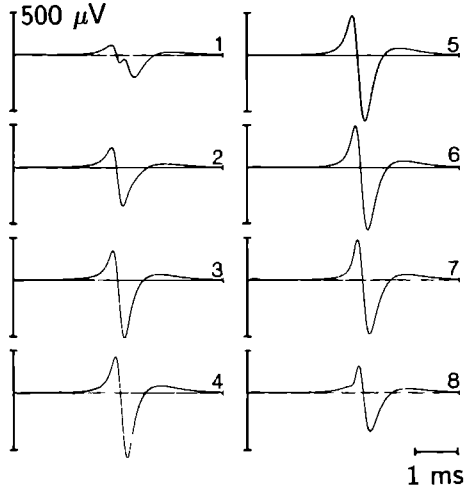

Figure VI.7 : Eight SFAPs corresponding to the eight situations defined by fig. VI.6A.

of the influence of the needle characteristics on the recorded SFAPs. They paid attention to the hole where the leading-off surfaces are surrounded by insulating resin. From that insulating part of the cannula, they expected the so-called "wall effect" by which the amplitude would have been enhanced by a factor of two. Figs VI.3C and VI.4B predict that this factor will not be reached (≤ 1.7) because of the difference between an infinite, insulating flat wall and our model for the needle shaft. This applies, irrespective of our finding that the whole needle shaft can actually be conceived as an insulating inhomogeneity in the volume conductor. The double layer insulates to such an extent, that even its frequency dependent behaviour (eq. VI.1) does not find expression in the results. An insight into what such a frequency dependence "could have looked like" (fig. V.6, [126]) may only be obtained by an unrealistic decrease of the double layer impedance.

This justifies the conclusion that omitting a complicated description of the needle characteristics around the leading-off surface can be justified retrospectively. It also obviates a discussion on the values chosen for the constants K and m. As stated before, the same applies to a precise description of the cannula.

Recently, Nandedkar et al. [88] assumed in their motor unit action potential simulations, that all the fibres actually passing behind the cannula with respect to the leading-off surface, are not observed electrically. Our results indicate that there is, at most, an amplitude decrease of 50 % for the muscle fibres located closest to the needle electrode (see fig VI.3F). The point-source waveforms in fig. VI.6 show that one can describe the volume conduction characteristic in that case as a "shadow" phenomenon which induces a dip in the point-source waveforms. Fig. VI.7 indicates that the SFAP simulated in situation 1 also shows this shadow phenomenon. The amplitude of this SFAP, however, is so low (slightly

above 100 μV) that this waveshape will not be included in a clinical single fibre EMG study. If it is observed, it is possible to decide by simply rotating the needle electrode whether the recording is due to a superposition of two SFAPs or to the shadow phenomenon described here. In case of a superposition of two SFAPs, the SFAP waveshape will remain "complex", while a regular bi or triphasic SFAP will appear in the case of an electrode shadow.

The source function which was used in Chapter V was broader than the source function used in this chapter and therefore the SFAP waveform change described here has not been noticed in the SFAPs presented in Chapter V.

In our presentation of the model, we mentioned the absence of the anisotropy in the muscle tissue description. If the influence of the anisotropy is considered as a virtual scaling of all distances perpendicular to the muscle fibre, the amplitude curves in figs VI.3 and VI.4 have to be stretched or squeezed corresponding to a decrease or increase of the anisotropy (Chapter V, [56,126]). The location of the leading-off surface is the central, fixed point in such a distance scaling.

When comparing the results of figs VI.3B and VI.3C with figs VI.4A and VI.4B, one can observe a slight additional anisotropy-like behaviour caused by the presence of the needle shaft. The enhancing effect of the insulating double layer is noticeable over a longer range transversally than in the cannula direction.

Removal of the double layer is the most drastic way of testing its influence. Fig. VI.5 clearly proves that a considerable SFAP amplitude decrease may a priori be expected from this removal. In the model, the SFAP amplitude is indeed reduced by as much as a factor of 10^6. The observation point for these simulations has to be slightly moved away from the cannula or else it would become part of the cannula (see section VI.2). It was found that the observed SFAP amplitudes decreased drastically when the double layer was removed, even if the observation point was moved away transversally over a distance of 200 μm. This distance is of the same magnitude as that on a real electrode surface between the leading-off point and the edge of the hole in the cannula. It should be realised that removing the double layer for a short time is made possible by movements of the electrode. In clinical EMG this effect is known as the "movement artifact". It is caused by sudden changes in the half-cell potential [91] following such mechanical removal of the double layer. This movement artifact also introduces a complete short-circuiting around the cannula, by temporarily breaking down the shielding-off by the double layer. In a volume conductor model, this short-circuiting is described by maintaining the potential of the cannula at zero [72]. The short-circuiting can be described as a "negative wall effect". Another method to break down the double layer is applying the relatively great voltage difference of approximately > 700 mV [13] between the cannula and the electrolyte medium. Such a potential difference is easily obtained when electrodes are used for stimulation purposes.

Many of the assumptions in our model appear to be applicable to describing a typical single fibre electrode. Several of the assumptions will not be valid for another type of electrode familiar in clinical EMG, the concentric needle electrode. Whereas, on the single fibre electrode the leading-off surface is located so far from the cannula tip that the entire length of the cannula can be considered as infinitely long, the leading-off surface of the concentric needle electrode is located at the tip of the electrode. The conclusions drawn from the behaviour of the electrical double

layer, however, are useful when we consider the concentric needle electrode. For this type of electrode, also some amplification or attenuation can be expected for muscle fibres located at the front and the back of the electrode respectively. The magnitude of these effects is expected to be smaller than in the single fibre electrode model described here.

VI.4.1 Conclusions

The amplification and attenuation effects as shown in figs VI.3 and VI.4 may, on first sight, look like a complex distance scaling since the relation between amplitude and distance is altered with respect to a homogeneous situation with no needle electrode present. Such a distance scaling, however, would be a scaling which is in contradiction with the volume conduction theory. In the volume conduction of propagating action potentials a change in distance would indissolubly be connected to a change in waveform. The only waveform changes found in this study are attributed to the shadow effect caused by the presence of the needle cannula and are only present in action potentials from muscle fibres located behind the electrode shaft with respect to the leading-off point.

An increase in the size of the pick-up area as defined by Stålberg [118] is another effect caused by the SFAP amplification for muscle fibres observed from a short distance, since the argumentation of Stålberg's definition was based on a homogeneous volume conductor model. From our model it can e.g. be derived that in a homogeneous situation an SFAP with an amplitude of 0.2 mV is recorded from a muscle fibre at a distance of about 380 μm from the leading-off surface, assuming an anisotropy ratio of 5. An SFAP recording from the same muscle fibre with the same amplitude in the needle electrode model implies that the muscle fibre is now located at a distance of 460 μm. Such effects need to be taken into account when the results from "fibre density" measurements [115] are translated in to a real densities (number of muscle fibres per cross-sectional unit area of muscle tissue).

Chapter VII

Electrophysiological Investigation of Motor Unit Structure by means of Scanning EMG. [1]

Abstract

The technique of scanning EMG has been used to obtain information on the structure of motor units from the human quadriceps muscle. Besides a group of healthy volunteers two groups of patients with proven neurogenic or myogenic neuromuscular disorders have been studied. In total 86 scans have been recorded. The obtained scanning EMG data are parametrized by the motor unit extension and the temporal dispersion of the entire motor unit. The motor unit extension parameter appears powerful in separating the two patient groups. The vast majority of myogenic patients shows motor unit territories of less than 4 mm whereas almost all the neurogenic patients show motor unit territories greater then 4 mm. Both patient groups show a greater temporal dispersion than the volunteers. Some special scanning EMG recordings are shown to illustrate the influence of the volume conductor and the recording electrode on the scanning EMG recordings. From this part of the analysis it can be concluded that recording scanning EMG signals with a concentric needle electrode will not have a disturbing influence on the parametrisation of the scanning data.

VII.1 Introduction

In the research of neuromuscular disorders, it is well known that the structure of motor units is subject to changes which can take on a wide variety of appearances for different kinds of pathology [21]. The most difficult aspect to obtain infor-

[1] T.H.J.M. Gootzen, H.J.M. Vingerhoets and D.F. Stegeman. *Submitted to Muscle & Nerve.*

mation about is the organisation of the end-plate region. From standard clinical motor unit action potential (MUAP) recordings, information about the temporal dispersion within a motor unit can be obtained [36] but no unambiguous information on the spatial characteristics of the motor unit is available. Although data on motor end-plate topography in human muscle are available [9], clinical histochemical analysis also fails in visualising this kind of information for a complete motor unit.

An electrophysiological method, the scanning EMG, which is able to measure both the temporal and the spatial structure of an entire motor unit, has been described a decade ago by Stålberg and co-workers [8,117], and it has been successfully applied to support their EMG research [69,70,86,119,120]. However, since this technique has been found to be experimentally difficult and time consuming, compared with the standard clinical EMG examination, it has not been widely used so far. In our research programme on muscle electrophysiology we needed information on the structure of motor units under both normal and pathological conditions. Therefore we built new scanning EMG equipment based on an AT personal computer. In the design of the system a maximal technical flexibility was pursued in order to minimise the experimental difficulties mentioned above.

In general, every electrophysiological recording of an MUAP is determined by three aspects. The first is the structure of the motor unit [15,20,104,114]. This structure can be characterised by geometrical parameters such as the (i) motor unit territory [18], (ii) the fibre distribution within this territory [77], (iii) the fibre diameters and (iv) the locations of the motor end-plates [23,26]. The third and fourth parameter also have a clear influence on the temporal behaviour of the recorded MUAP. Similar to the geometrical structure described above, the parameters underlying this temporal behaviour of the MUAP can be considered as determining the temporal structure of the motor unit.

The second aspect is the volume conductor. The SFAPs of the active muscle fibres are summed to form the MUAP and the activity of all the muscle fibres results in a potential field which spreads throughout the entire muscle. The way in which this potential field is influenced by the properties of the volume conductor has been a major subject in our own research, e.g. [55], and in that of many others, e.g. [14,6,42].

The third aspect is the influence of the recording electrode on the MUAP recording. There is no doubt that a needle electrode recording may not be idealised by a recording obtained from a point shaped electrode. The finding of a proper description for a needle electrode recording has been a subject of discussion since the very beginning of electrophysiological modelling [33,34]. The search for it is still continuing [88,126].

In this chapter, we report on a study in which scanning EMG has been performed on 11 healthy volunteers and on 10 patients with known neuropathic or myopathic disorders. In total 86 scans have been recorded. The experimental protocol and the signal processing are similar to the methods used by Stålberg and co-workers. The patient-selection, the equipment, the protocol and the signal analysis are reviewed in the sections VII.2.1 to VII.2.4. The scans obtained are parametrised by defining the spatial extension S as a measure of the motor unit territory and the temporal dispersion T as a measure of the over-all time dispersion

in the motor unit. The definitions of these parameters are elaborated in section VII.2.5. Examples of recorded scans, and the results of the parametrisation are shown in section VII.3.

The influence of the volume conductor and the recording electrode has also been studied for a more basic understanding of the scanning EMG results. To this end, two kinds of special scanning EMG recording have been made. The first concerns scans that are performed with a standard single fibre electrode. From these scans, single muscle fibre potentials can be extracted sometimes. The second kind is used for studying the influence on the recorded MUAPs of the use of the concentric needle electrode shaft as the reference electrode. Insight into this aspect is obtained by a simultaneous registration of a standard bipolar recording and a monopolar recording of the needle shaft signal, during the scanning. Results from these special recordings will also be shown in section VII.3.

VII.2 Methods

VII.2.1 Patient selection

For our study 10 patients with well known neuromuscular disorders have been selected. All the patients have been diagnosed by means of clinical examination, classical EMG and a muscle biopsy from the quadriceps muscle. In all cases a pure neurogenic (5 cases) or pure myogenic (5 cases) disorder has been diagnosed. On the medial vastus muscle of the selected patients scanning EMG recordings have been performed according to the experimental protocol described in section VII.2.3.

Table VII.1 Selected patients

sex	age (y)	pathology
		neurogenic:
F	32	radicular syndrome L4
F	38	Kugelberg-Welander atrophy
F	59	Kugelberg-Welander atrophy
M	35	poliomyelitis
M	50	radicular syndrome L4
		myogenic:
F	35	limb-girdle myopathy
F	36	nemaline rod myopathy
F	43	limb-girdle dystrophy
M	27	Becker dystrophy
M	48	polymyositis

VII.2.2 Equipment

Electrodes: During a scanning EMG recording, two needle electrodes are recording signals (for details see section VII.2.3). The first electrode, which will be referred to as the triggering electrode, is a standard single fibre electrode. For the second electrode, the scanning electrode, usually a concentric needle electrode is

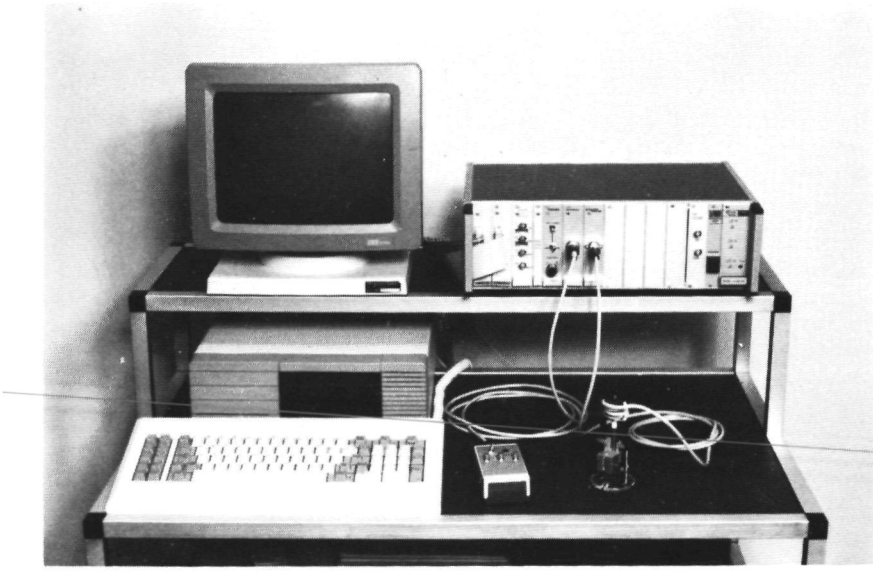

Figure VII.1 : The scanning EMG equipment.

used. For some recordings, a single fibre electrode has been used as the scanning electrode.

EMG amplifier: A Medelec MS-6 EMG system equipped with two AA6 Mk III amplifiers is used for amplification of the signals. For obtaining a trigger pulse from the triggering electrode signal, the module SD56 from the MS-6 system is used.

Data acquisition: The amplified scanning electrode signal is read into an IBM AT-compatible personal computer (ITT Xtra-XP) by a Metrabyte DASH 16-F 12 bits A/D converter card. Interface modules for handling the trigger pulse, the stepper motor control and remote control unit are mounted in a separate rack and can be controlled by the computer through a Metrabyte PIO-12 digital I/O card.

Stepper motor: An Airpax 92121-P2 linear stepper motor, controlled by an SAA 1027 integrated circuit, is used for moving the scanning electrode during recordings. The smallest stepsize of this stepper motor is 50 μm.

Fig. VII.1 shows a photo of the data acquisition equipment and the stepper motor device.

VII.2.3 Experimental protocol

Scanning EMG has been performed on the medial vastus muscle of 11 healthy volunteers without any known sign of neuromuscular disorders (8 male, 3 female, age 25 - 45 years) and of 10 patients with known neuropathy (5) or myopathy (5). The volunteer or patient is sitting upright or lying in supine position. Before the needle electrodes are inserted, two extra determinations are carried out in order to

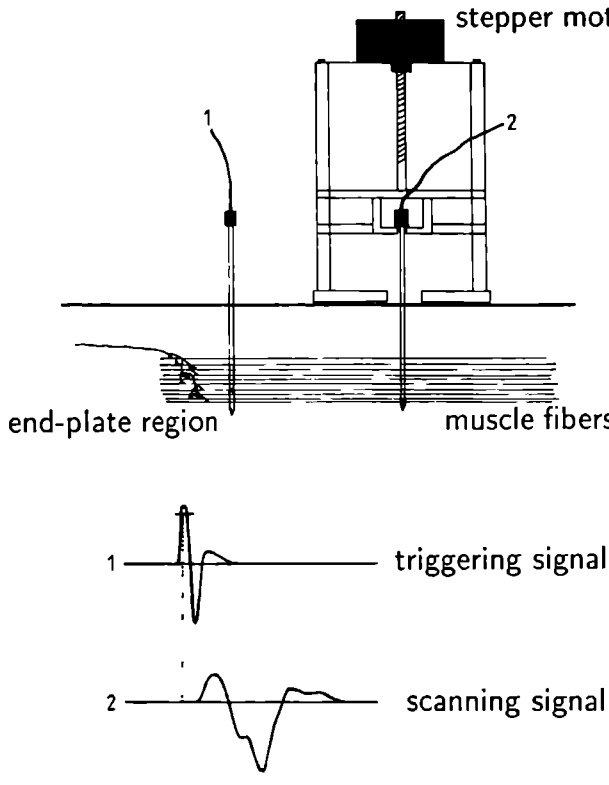

Figure VII.2 : Schematic drawing of the experimental set-up. Electrode 1 records the triggering single fibre potential and electrode 2 records the traces of the scan. It is moved upwards by the stepper motor after each trace recording.

obtain an insight in the global, longitudinal structure of the muscle. With surface electrical stimulation, the location of the motor point is determined. By doing so, the placement of the triggering and the scanning needle electrodes on the same side of the endplate zone is secured.

The finding of time-locked activity on both the triggering and the scanning electrode (functions are explained below) is essential in scanning EMG. A correct alignment of the two electrodes with the muscle fibre direction largely facilitates finding the desired time-locked activity. Therefore, this longitudinal direction of the muscle fibres is also determined. This is done by recording EMG signals from two bipolar surface recordings from a row of four small (diameter 2 mm) and sharp ended electrode points. When there is an optimal likeness between the two signals, the direction of the line on which the four electrodes are located will correspond well with the direction of the muscle fibres. This principle is based on a technique for determining the muscle fibre conduction velocity [16] and is commonly used in surface EMG recordings .

After having obtained this information on the global longitudinal structure of the muscle, the actual scanning EMG recording is performed. The set-up of this recording is drawn in fig. VII.2. A standard single fibre electrode is inserted into the muscle, approximately 1 cm distal to the motor point. The subject is asked to maintain a constant contraction of the quadriceps at a low to moderate force level. With the trigger electrode, a stable single fibre action potential is searched for. When a stable triggering SFAP is found, the second electrode is inserted in the muscle, approximately 1.5 cm distal from the triggering SF electrode. This second electrode, which is either a concentric needle electrode or a single fibre electrode, is moved manually while searching for activity that is time-locked to the triggering SFAP. When such activity is found, the scanning electrode is moved deeper inside the muscle until the time-locked waveshape on this electrode has disappeared or has decreased drastically. Then, the scanning electrode is coupled to the stepper motor device and the scanning procedure is started. After a triggering potential of the first electrode, a signal is read from a circular buffer in the computer memory where the signal from the second electrode is sampled continuously. This allows a pre-trigger interval which is long enough to ensure a recording of the complete motor unit action potential. The stepper motor pulls up the scanning electrode over a distance of 50 μm or a multiple of this distance after the signal is read. This sequence is stopped when the MUAP disappears from the scanning electrode signal.

VII.2.4 Signal analysis

The recorded signals are filtered by the MS-6 system. The filter settings are 8 Hz high-pass and 8 kHz low-pass for signals recorded with the concentric needle electrode as the scanning electrode and 16 Hz respectively 8 kHz for scans recorded with the single fibre electrode. The signal from the triggering electrode are filtered with a 500 Hz high-pass and 3.2 kHz low-pass setting which corresponds to the standard clinical filter settings for most single fibre recordings. No anti-aliasing filters have been used during data acquisition. For one complete scan about 200 traces are recorded. Each trace contains 625 samples: 25 ms recording time at a sampling rate of 25 kHz.

Once the raw scanning EMG data are stored in the computer, several processing options are available for improving the signal quality. The first one is removing the DC offset per recorded trace for elimination of movement artifacts. The second option is a three point smoothing in the time-direction of each trace for noise reduction. The third, and most important option, is a median filtering over 3, 5 or 7 points in the depth direction for elimination of non time-locked activity. This procedure was introduced by Antoni et al. [8]. In a N-point median filtering the amplitude value $A_{i,j}$ from a certain trace i at a certain time instant j is replaced by the median value of the N amplitude values $A_{i-n,j}$ to $A_{i+n,j}$, where n is the integer part of $\frac{N}{2}$. One or more of these procedures are performed, depending on the quality of the recorded scan.

From the entire scan, or from a selected region of interest, a three dimensional plot of amplitude (z-axis) versus time (x-axis) versus depth (y-axis) can be made. The amplitude information can also be coded using a colour-scale or a grey-scale.

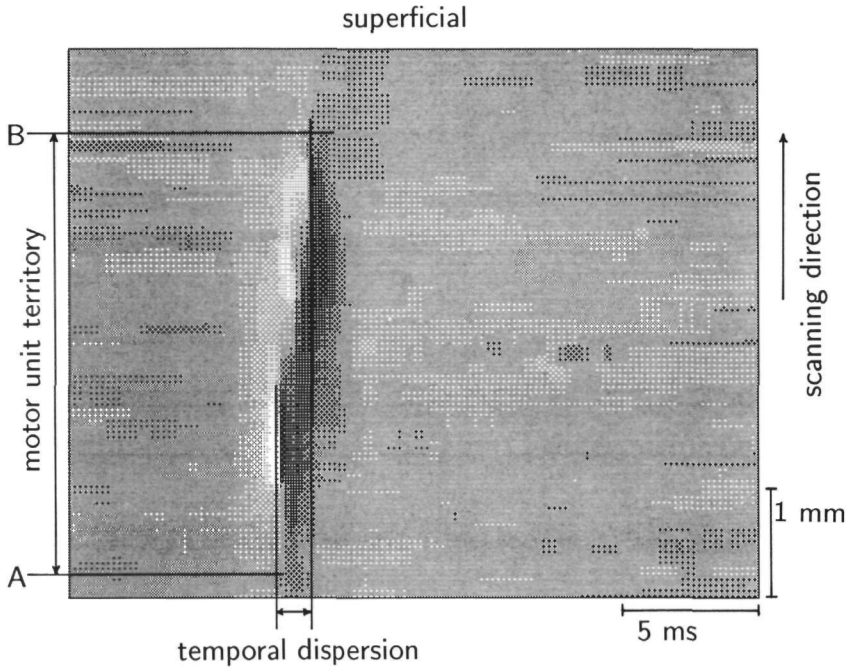

Figure VII.3 : Example of a grey-scale plot of scanning EMG data, containing 100 traces with a tracelength of 25 ms. The points A and B used for the determination of the motor unit extension are indicated. Also the two latencies used for measuring the motor unit time dispersion are indicated. Note that positive amplitudes are represented by lighter shades of grey and negative amplitudes by darker shades.

Fig. VII.3 shows an example of such a grey-scale plot. The horizontal axis is the time axis and the vertical axis the depth axis. The scanning direction is from the bottom to the top; the top of the plot represents the traces recorded in the most superficial position of the scanning electrode. The corresponding three dimensional representation of this scan is shown in fig. VII.5A.

VII.2.5 Scan parametrization

From a colour-scale plot of a recorded scan the motor unit territory and the temporal dispersion are derived by hand in the following way :

The spatial extension S of the motor unit territory is derived as the distance in depth between the two points A and B in fig. VII.3. Point A is defined as that trace were the maximal positive amplitude of the MUAP in that trace decreases below 15 % of the maximal positive MUAP amplitude observed over the entire positive area located deepest in the scan plot. In the colour plots this corresponds

to one colour level above zero when the scaling is adapted to the scanning data such that an optimal use of all colour levels is made. This criterium is applied to the positive amplitudes because usually a negative peak is recorded over a long distance below the motor unit territory. A similar criterium is applied to point B but now for the most superficial negative area in the scan plot.

The motor unit time dispersion T is defined as the latency difference between the earliest and the latest steep downward slope in the MUAP waveshapes, regarded over all traces of the scan between the points A and B (see fig. VII.3). The locations of these slopes are also determined by hand from the colour plots and can clearly be distinguished by sudden colour changes at the same latency in several succeeding traces. In ambiguous cases the three-dimensional plots are used as a control to distinguish between motor unit activity and artifacts. The two vertical lines in fig. VII.3 indicate the two latencies wich determine the time dispersion for this scan and from which region of the scan the two latencies are derived.

The time dispersion measure is not to be confused with the dispersion of individual SFAPs together forming an MUAP recorded at a fixed observation point. That kind of dispersion will be different for MUAPs recorded from different parts of the same motor unit. The parameter T defined here quantifies the time dispersion over the entire motor unit and is an new parameter in EMG analysis.

VII.3 Results

In fig. VII.4A, the raw data of an example of a scanning EMG recording from a healthy volunteer are shown. Fig. VII.4B shows the same scan after removal of the DC offset per individual trace . Fig. VII.4C shows the data of fig. VII.4B after a subsequent 5 point median filtering. The stepsize in this scan is 50 μm and 100 traces are displayed. (scan distance = 0.5 cm).

Fig. VII.5 shows three scans, one from a healthy volunteer, one from a patient with a myogenic pathology (polymyositis) and one from a patient with a neurogenic pathology (poliomyelitis). The latter scan is recorded with double stepsize (100 μm) so its scan distance is 1.0 cm. On the scan in fig. VII.5A, a 5 point median filter has been applied. The scan in fig. VII.5B, was corrected for DC offset and subsequently filtered by a 3 point median filtering. The scan in fig. VII.5C was corrected for DC offset, 5 point median filtered and finally smoothed. The motor unit extensions S as observed in these scans are 0.4, 0.15 and 0.85 cm respectively. The time dispersions T are 1.3, 2.6 and 6.4 ms.

In total 42 scans from volunteers (11 subjects), 23 scans from neuropathic patients (5 subjects) and 21 scans from myopathic patients (5 subjects) have been recorded. A scatter diagram of motor unit extension S versus time dispersion T of all these scans is shown in fig. VII.6.

From the scans obtained with a single fibre electrode as the scanning electrode, two typical examples are shown in fig. VII.7. Fig. VII.7A show 60 traces of a scan where the activity of two single muscle fibres can be recognised. The largest one is selected (selected region indicated with the bars marked with *). Fig. VII.7B

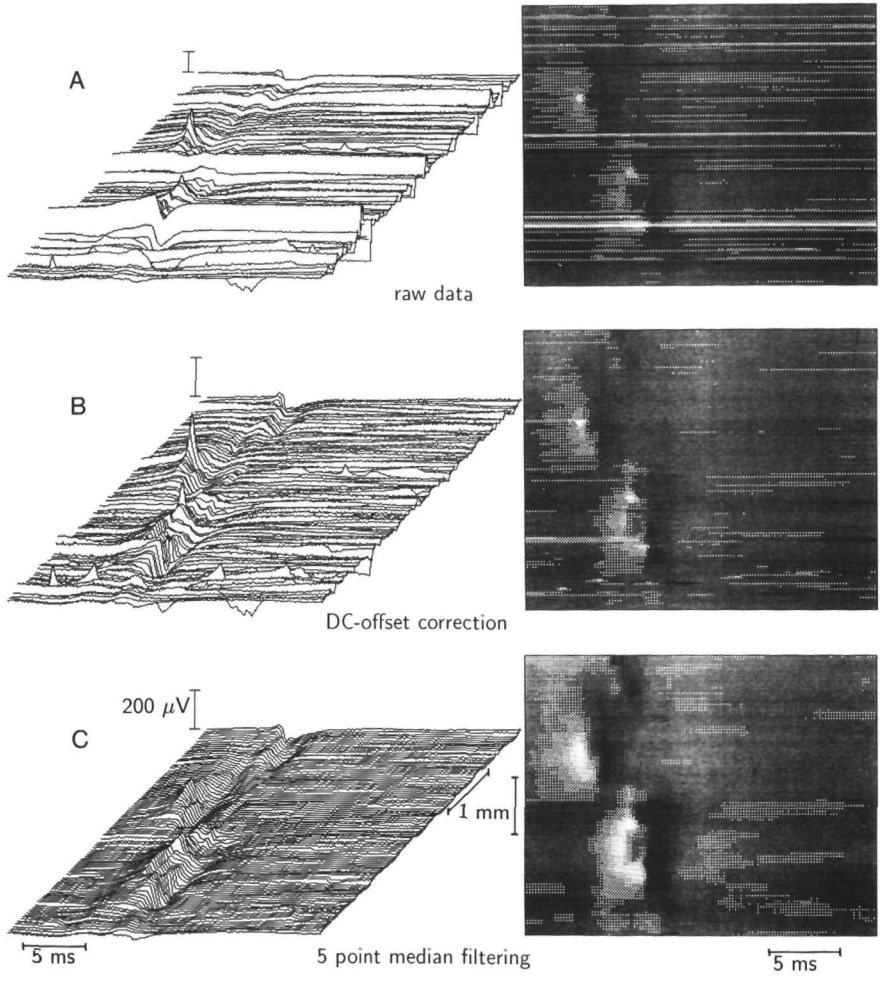

Figure VII.4 : Three dimensional and grey-scale plots of 100 traces from a scan recorded from a healthy volunteer (male, 38y). A) Raw data, B) Same data as A after removal of DC-offsets, C) Same data as B after a 5 point median filtering. Note that the amplitude of the sharp peak in the upper left part of the scan has been reduced due to the median filtering.

shows this region of interest, containing 20 traces (scan distance 1 mm) with a trace length of 4 ms. In this representation, it can be seen clearly how the amplitude ofthe SFAP rapidly increases and decreases when the recording electrode is pulled up by the stepper motor. The fast amplitude change and the short duration of the action potential confirm that this is a single fibre recording. Fig. VII.7C shows a recording where, over a relatively long distance, an almost monophasic SFAP of slowly varying amplitude can be seen. There is hardly any change in waveshape for the different observation points. This recording probably originates from a muscle fibre where the action potential propagation is blocked by compression of the muscle fibre by the needle electrode or by damage caused to the muscle fibre membrane. Such waveshapes are found regularly when an attempt is made to record such scanning EMG SFAPs from a short distance to a muscle fibre.

In a second special scanning EMG procedure, the influence of the needle electrode shaft as a reference electrode has been studied. Two signals, a standard bipolar recording and a monopolar shaft recording, are obtained simultaneously. Adding the data from these two recordings results in the signal that would have been recorded by a monopolar needle tip recording. This way of obtaining a monopolar tip recording is evidently not the most straightforward one.

However, a direct monopolar recording of the tip signal produces signals with a very poor signal to noise ratio, since the amplifier is unbalanced by the great difference in impedance of the small tip surface and the surface reference electrode. In order to overcome these problems, we recorded the signals as described above. Fig. VII.8 shows the two monopolar signals and the bipolar signal from the same scan. Fig. VII.8A shows the scan as it would have been recorded by a monopolar recording from the tip of a concentric needle electrode. Fig. VII.8B shows the monopolar recording from the shaft of the concentric electrode. Fig. VII.8C shows the bipolar recording. The scan contains 200 traces, which corresponds to a total scan distance of 1 cm. In the deeper half of the scan the tip of the concentric needle electrode is outside the motor unit territory, i.e. it is located deeper than the motor unit territory. Over a scanning distance of more than 5 mm the recorded signals from both the needle tip and from the needle shaft hardly change. When the motor unit territory is reached the signal from the tip records the motor unit activity from a short distance. The recording from the needle shaft signals does not show great waveshape changes but does show a gradual decrease in amplitude.

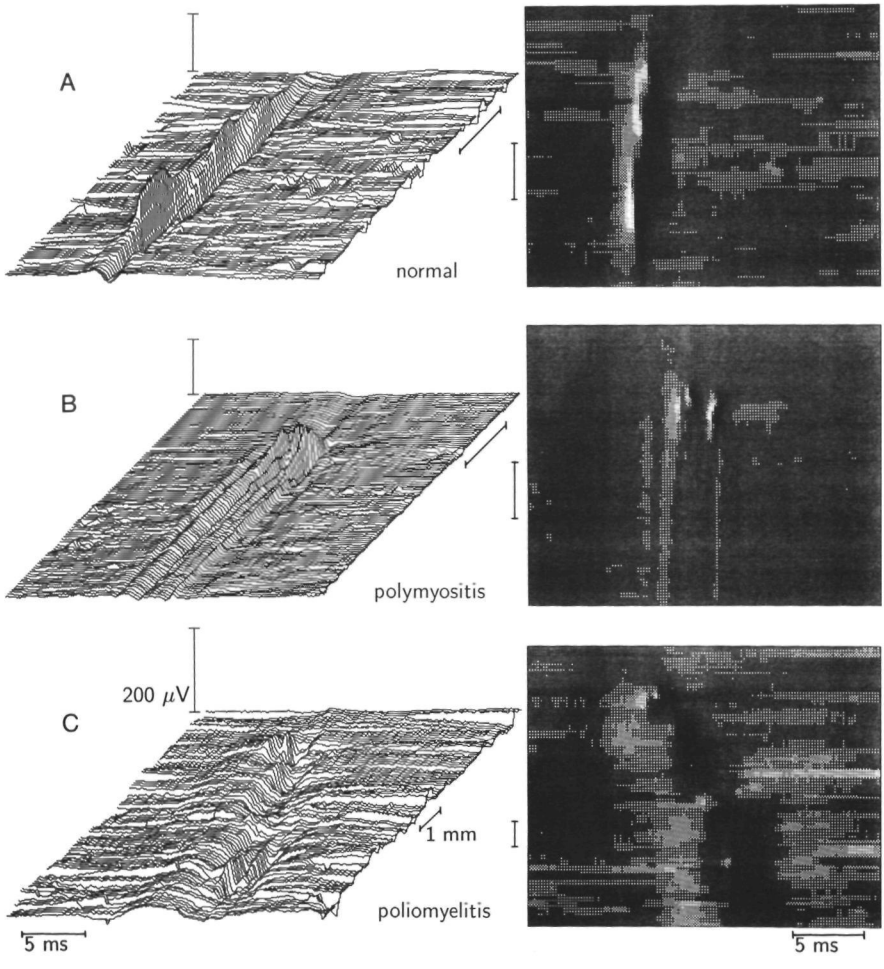

Figure VII.5 : Three dimensional and grey-scale plots of 100 traces selected from scans of the medial vastus muscle from one volunteer and two patients. A) Scan from a healthy volunteer (male, 30y). B) Scan from a myogenic patient (polymyositis, male, 48y). C) Scan from a neurogenic patient (poliomyelitis, male, 35y).

VII.4 Discussion

VII.4.1 Method

The scanning EMG equipment used in our experiments showed a great technical flexibility and ease in use. Data acquisition can be performed at such speed that a scan of 200 traces can be read into the computer within 45 seconds. In practice, this recording duration appeared to be well bearable to the subjects and did not cause difficulties in maintaining a stable positioning of the stepper motor device or of the triggering electrode.

As can be seen in fig. VII.4A, the chosen filter settings of the EMG amplifier can result in DC offsets varying over the different traces, caused by movement artifacts at the tissue - electrode interface (Chapter VI). We decided to maintain the chosen filter settings in order to be able to record motor unit action potential waveforms which are minimally distorted by the filter settings of the EMG equipment. The software DC offset correction introduced in the signal analysis procedures appears to be an efficient method to eliminate the movement artifacts. Note that our filter settings, when using a single fibre electrode as scanning electrode, differ substantially from the filter settings that are used in clinical routine single fibre recordings (approximately 500 Hz high-pass and 5 kHz low-pass). These latter filter settings are used, however, in applications of single fibre EMG where the moment of appearance of an action potential is of more interest than its precise waveshape (e.g. jitter measurements [115]).

The use of the median filtering, as described already by Antoni [8], again appears to be very useful for extracting a clear view of the motor unit structure from a scan distorted by incidental activity, not time-locked to the MUAP signal studied. On the other hand, when regarding the MUAP waveshapes of individual traces, the influence of this filtering technique is not negligible. This can be seen clearly when comparing the sharp positive peak in the upper half of the scans in fig. VII.4B and VII.4C.

Due to the median filtering, the amplitude of this peak is reduced by about 30% in comparison to the raw data. When the 3 point median filter is applied the amplitude decrease is about 10% but the not time-locked activity will not be removed adequately.

VII.4.2 Motor unit structure

The three typical examples shown in fig. VII.5, give a good impression of the variation of motor unit structures that can be found between healthy volunteers and patients with different kinds of pathologies. In order to be able to quantify the motor unit structure and to compare the different groups considered, two empiric measures have been defined. The results from this analysis, applied to a total of 86 scans, are plotted in the scatter diagram of fig. VII.6. This figure shows that the myopathic scans can, mainly based on the size of the motor unit territory S, be separated well from the neuropathic scans. In a clinical EMG examination, this parameter is not investigated. Both myopathic and neuropathic patients show a great variation in the time dispersion parameter T. The healthy

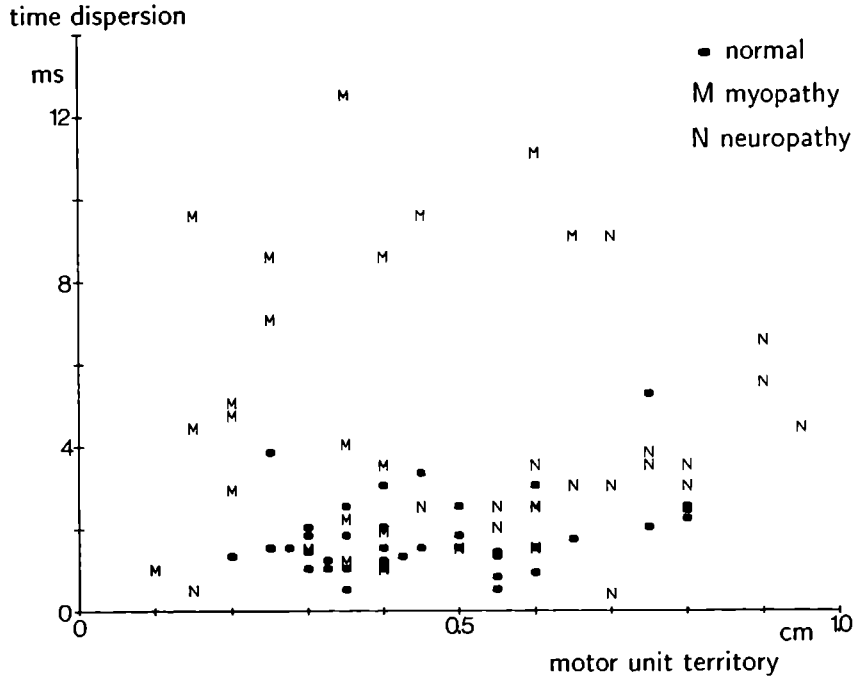

Figure VII.6 : Scatter plot of motor unit territory S versus time dispersion T of scans from 11 healthy volunteers (indicated by •), 5 myopathic patients (M) and 5 neuropathic patients (N). Scanning EMG was performed on the medial vastus muscle.

volunteers show a great variation in the motor unit territory and compared to the two pathological groups a small variation in the time dispersion. In the scatter diagram, a considerable region of overlap exists between the healthy volunteers and the two classes of patients considered.

The time dispersion measurement is influenced by the skewness of the end-plate region and of the insertion direction of the scanning electrode relative to the muscle fibre direction. The disturbance of the time dispersion parameter induced by the fact that a needle electrode may not be inserted exactly orthogonal to the muscle fibres appears to have a limited influence. This can be illustrated as follows. If a relatively narrow end-plate zone of a certain motor unit is orientated perpendicularly to the longitudinal direction of the muscle fibres, the time dispersion would only measure the skewness of the needle insertion direction relative to the muscle fibre direction. For a needle inserted under an angle of 45 degrees, this would result in a time dispersion of 2 ms for a motor unit with a territory of 0.8 cm (action potential propagation velocity 4 m/s). A deviation of 45 degrees from the optimal insertion direction can undoubtedly be accepted as an upper boundary for this insertion error. The maximal time dispersion caused by the insertion error as

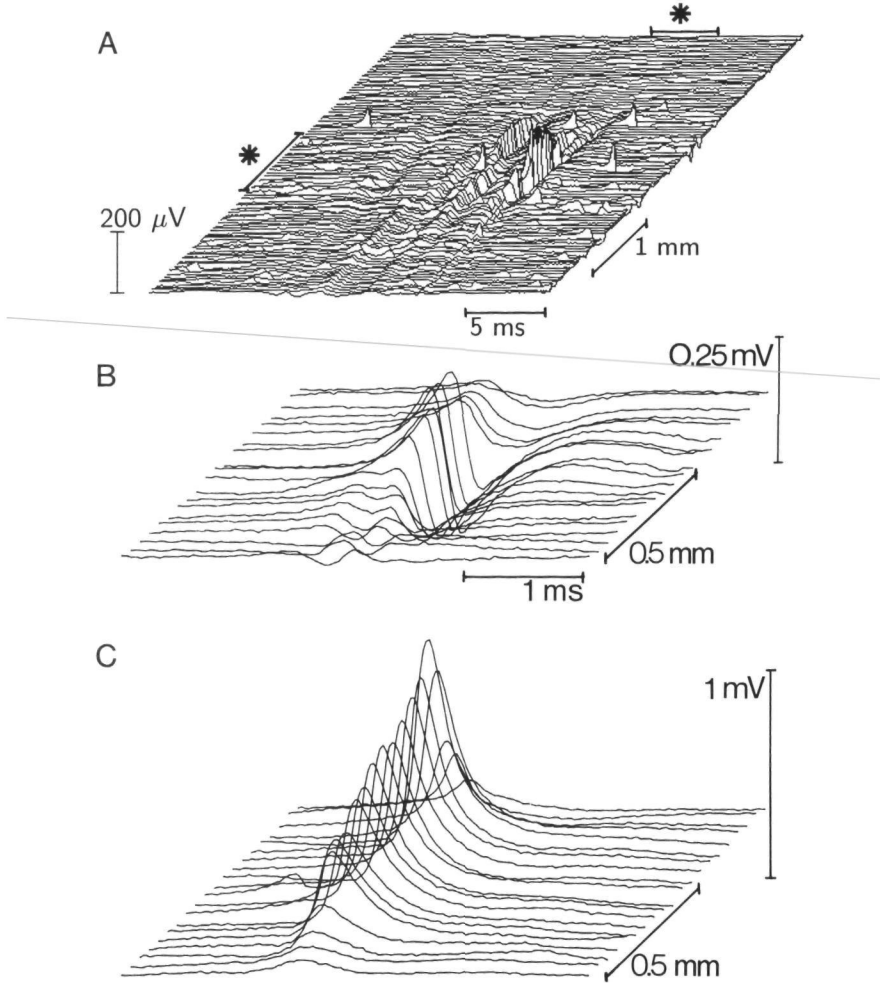

Figure VII.7 : Examples of two scans recorded with a single fibre electrode as scanning electrode during the passing of an isolated muscle fibre action potential. A) 60 traces from a total scan. The bars marked with * indicate a selected region of interest. B) Selected region of interest as defined in A. C) Part of another scan where an SFAP has been recorded from a muscle fibre where blocking of the action potential propagation has occurred.

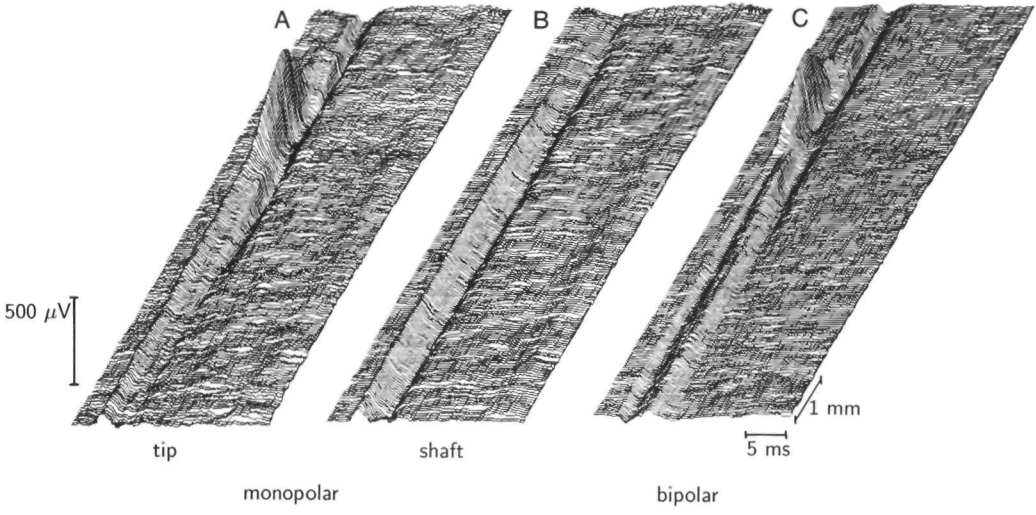

Figure VII.8 : Scan with simultaneous monopolar recordings of the concentric needle electrode tip signal and the electrode shaft signal (reference electrode on the knee) and a bipolar recording between electrode tip and shaft. A) Monopolar tip signal, B) Monopolar shaft signal, C) Bipolar signal.

a function of the motor unit territory will then always lie below the line trough the origin of fig. VII.6 and the point (0.8 cm, 2 ms). Almost all the values shown in fig. VII.6 are relatively large compared to the values determined by this line. This indicates that the time dispersion measure is dominated by the skewness of the end-plate zone relative to the muscle fibre direction and by the width of the end-plate zone.

An aspect that may cause erroneous estimations of the motor unit territory is the fact that the insertion channel of the scanning electrode may not pass through the center of the motor unit territory. If the shape of the motor unit territory is assumed to be cylindrical, the motor unit territory parameter S determined from the scanning EMG data will in that case be smaller than the actual diameter of the motor unit territory. From some of the volunteers, we recorded three scans from the same motor unit. The triggering electrode was kept at the same location, assuring that the same SFAP was used as triggering signal all the time. For each of the three scans, the scanning electrode was inserted in a new insertion channel such that the insertion angle was different for each scan. The variation in the S values for such a set of scans was in all cases less than 1 mm. This reproducibility suggests that the influence of the eccentric scanning of a motor unit may turn out smaller than was expected. An explanation for this may be that when the experimenter is manually positioning the scanning electrode, during the search for time-locked activity on both electrodes, he is biased towards searching an insertion

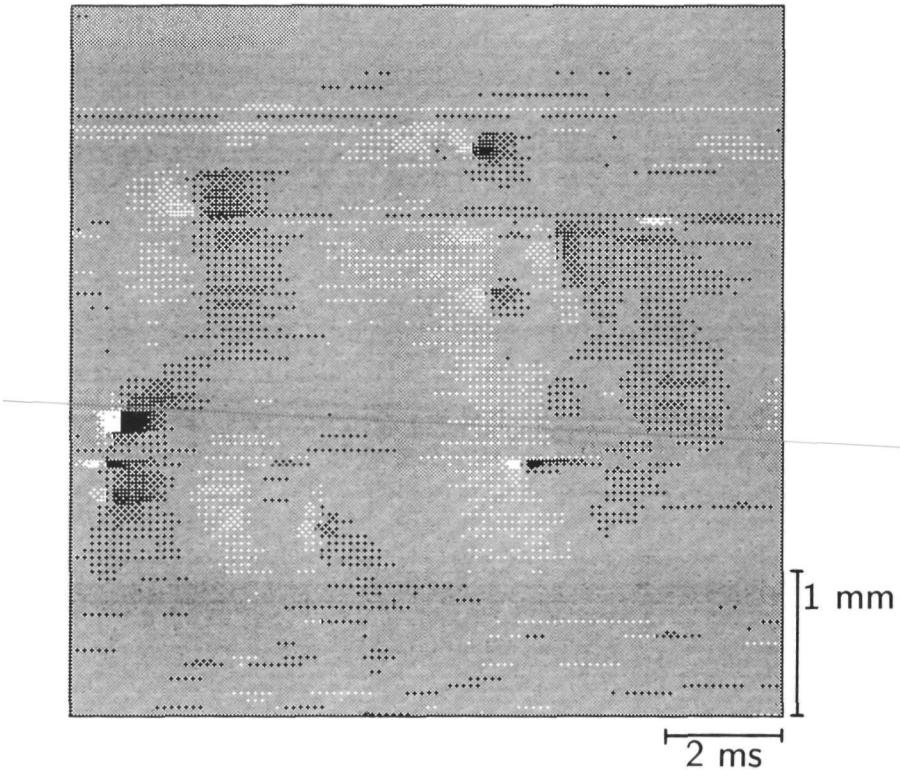

Figure VII.9 : Grey-scale plot of a myogenic motor unit recorded from the medial vastus muscle of a patient with nemaline rod myopathy (female, 36 y). The muscle biopt of the quadriceps showed a high degree of fibre splitting.

direction in which a maximum of time-locked activity is found.

VII.4.3 Volume conductor and recording electrode

The results in fig. VII.7 and VII.8 show that the scanning EMG technique can be used in fundamental studies concerning the volume conduction of muscle fibre and motor unit action potentials. Some volume conductor aspects on which conclusions can be drawn from the data shown will be discussed.

The first aspect is the observation of single muscle fibre action potentials in a scanning EMG recording. Fig. VII.7B shows a detailed example of such a recording. The increase and decrease of the SFAP amplitude can be used to verify SFAP volume conductor models. Since in Chapter VIII [59] this aspect will be treated extensively, we shall restrict the discussion here to some general remarks. When the SFAP amplitude from these scanning EMG SFAP recordings is plotted as a function of the trace number, the amplitude profile often appears to be skew, i.e.

the increase in amplitude when the fibre is approached is slower than the decrease in amplitude. Another finding is that, when SFAPs can actually be discriminated from the MUAP scan, often monopolar SFAPs are observed. The suggestion arising from these two findings is that SFAPs can only be observed in (scanning) EMG recordings when the distance between the needle electrode and the muscle fibre is very small. In some cases, apparently, this distance is so small that either the muscle fibre is moved by the motion of the needle electrode or that the action potential propagation is blocked. In the first case a skew amplitude profile will be found and in the second case a monophasic SFAP will be recorded. It was shown before that in case of action potential blocking the recorded SFAP waveshape corresponds to the waveshape of the intracellular action potential (Chapter II, [53,74]).

Other interesting aspects of volume conduction can be illustrated from the monopolar and bipolar scanning EMG data shown in fig. VII.8. From fig. VII.8A and VII.8B, it can be seen that in the lower half of the scan the tip and the shaft record a potential of almost constant amplitude and with the same polarity in both signals. For the electrode tip recording, this observation demonstrates that defining a pick-up area for a concentric needle electrodes might be more difficult than is suggested in literature [34,116], since the tip electrode appears to record activity from distances greater than expected. The short latency of the positive part of this activity suggests that it arises from dipole sources which are present at the locations of the end-plates during the excitation of the muscle fibres. A monopolar recording of the electrode shaft signal of a scanning EMG recording was also shown by Stålberg, to explain the positive knob that can be seen in the scans over a long distance when the tip of the needle electrode is below the motor unit territory but the shaft of the needle electrode remains within the motor unit territory. Our findings indicate that this so-called "trough" is not exclusively caused by the electrode shaft.

In that part of the scan where the main motor unit complex is present, the amplitude of the tip signal is much greater than that of the shaft signal. The monopolar tip signal and the bipolar signal look very much alike in the essential part of the scan, except for the amplitude of the main complex in the bipolar recording being somewhat lower than in the monopolar signal. This finding indicates that the measures of the motor unit extension and of the time dispersion will not differ between a monopolar tip signal recording and a standard bipolar recording.

In the two monopolar recordings, a small curvature is seen in the last 5 ms of each trace. This extra component in the recorded signals is caused by the end-effect from the propagation stop of the muscle fibre action potentials at the transition from muscle tissue to tendon. The appearance of this end-effect [66] has been studied theoretically (Chapter IV, [55]) and experimentally [51]. In the bipolar recording this component is absent, since its amplitude is almost equal in the two monopolar recordings. The latency of this component should, obviously, not be incorporated in the time dispersion measurements since it is mainly determined by the muscle fibre length and the action potential propagation velocity (Chapter IV).

VII.4.4 Conclusions

The two parameters defined in this chapter for describing the motor unit structure indicate how the motor unit structure of the myopathic and neuropathic patients is altered with respect to that of healthy subjects. The two patient groups can clearly be separated from each other by the new parameter S. A clear separation from the healthy volunteers is not found. The scanning EMG data, especially from the myopathic patients, suggest that a parameter should be devised that measures the "integrity" of the motor unit. Such a parameter describing the complexity of the end-plate zones of the scanned motor units should be able to achieve a better discrimination between the healthy subjects and the patients.

The major conclusions from the special scanning EMG registrations, as discussed in the previous subsection, are 1) SFAP scanning EMG data can be used for verifying volume conductor models but great care has to be taken to eliminate the artifacts from fibre movement or action potential blocking, and 2) bipolar recording of scanning EMG data with a standard concentric needle electrode will not disturb the parameters that can be derived for describing the motor unit structure.

Acknowledgement

We would like to thank M. Massa and G. van Voorst from the Development Section of the Instrumentation and Electronics Department (Head : S. Mientki) for developing and building the scanning EMG equipment.

Chapter VIII

Parameter estimation on single muscle fibre action potentials. [1]

Abstract
Multi-electrode single muscle fibre action potential (SFAP) recordings have been used in a parameter estimation procedure on muscle tissue and single muscle fibre properties. The implied (forward) model includes the influence of the presence of a metal needle electrode on the SFAP recordings. In spite of the complicated relation between the electrode-to-muscle-fibre distance and the anistropy ratio of the muscle tissue conductivities, stable estimates are found for these parameters. The method uses the extra information that can be obtained from multiple SFAP recordings and succeeds in deriving functional parameters from measured data. The average recording distance estimated by the procedure is 164 μm and the average anisotropy ratio 5.0. The average estimated muscle fibre diameter is 58 μm, assuming an effective muscle tissue conductivity of 0.25 $(\Omega\mathrm{m})^{-1}$.

VIII.1 Introduction

In the recording of single muscle fibre action potentials (SFAPs) many parameters influence the waveshape and the amplitude of the recorded signal. These parameters can roughly be divided into three groups :

1) **Parameters of the active source.**

The first group contains the parameters describing the properties of the muscle fibre as a current source injecting current into the surrounding tissue. A very important parameter in this group is the fibre diameter because it determines the propagation velocity of the action potential along muscle and nerve fibres [43,87]. The strength of the muscle fibre as a current source also depends on this diameter

[1] T H J M. Gootzen, D F. Stegeman and A van Oosterom. *Submitted to IEEE Trans. Biomed Eng*

[6,103]. Other parameters in this group are the intracellular conductivity and the ion channel parameters in the Hodgkin-Huxley type of models, describing the fibre membrane properties [42,74].

2) **Parameters of the tissue in which a potential field is generated.**

This group of parameters describes the properties of the surrounding tissue and it therefore determines the potential field around the active muscle fibre. For SFAP recordings which are usually performed at a very short distance from the muscle fibre the surrounding tissue can be characterised satisfactorily by its anisotropy ratio and its effective conductivity. The muscle tissue conductivity can be considered as purely resistive (Chapter II, [50,107]). The dimensions of the volume conductor (muscle and limb) are so large compared with the recording distance that, in this type of recording, the influence of the finite volume conductor dimensions can be neglected (Chapter IV, [51]).

3) **Parameters specifying the recording configuration and the disturbance of the recording electrode on the generated field.**

The third group of parameters characterises the configuration related to the recording of the SFAP. In this group all the parameters determining the location of the recording electrode with respect to the active fibre and the parameters characterising the properties of the recording electrode itself are contained.

The division of the parameters into these three groups is straightforward. However, in the actual recorded signals their influences largely intermingle. An SFAP of a given amplitude can be recorded from either a thick fibre at a great distance or from a thinner fibre at a shorter distance. The rapid decrease in SFAP amplitude, when the recording electrode is moved, may be caused by the fact that the electrode was moved over a relatively great distance or by the fact that the anisotropy ratio is greater than in an average recording.

An additional problem is that the parameters in the third group are usually unknown and have previously been too difficult to take into account. Therefore, no reports exist on simultaneous estimations of the parameters of the first and second groups, which are the parameters that may be different under normal and pathological conditions.

These problems can be overcome in two ways. The first is to use more, simultaneous recordings of the same SFAP. This can be realised by a multi-electrode. The second is a volume conductor model which describes the influence of the presence of the needle electrode near the active muscle fibre. In this chapter we report on the combination of a multiple SFAP recording with a sophisticated volume conductor model, realistically describing an SFAP recording. An estimations is made of three parameters which determine the recording geometry (group 3, see above), one parameter that characterises the muscle tissue (group 2) and one concerning the active muscle fibre (group 1).

In the methods section VIII.2.1 the data acquisition is described. Section VIII.2.2 gives a short review of the volume conductor model which has previously been described in greater detail (Chapter VI, [52,126]). Section VIII.2.3 describes the parameter estimation procedure. The results from this procedure are shown in section VIII.3 and discussed in section VIII.4.

VIII.2 Methods

VIII.2.1 Multiple SFAP recordings

Multiple SFAP recordings have been obtained by two different techniques. The first method uses an 9 channel multi-electrode (Medilog SN-6). On this electrode 8 recording surfaces similar to the standard single fibre needle electrode are mounted in a linear array with an inter-electrode distance of 100 μm (see fig. VIII.1). The ninth recording surface is placed aside of the array, between electrode 4 and 5, at a distance of 100 μm from the line on which the other electrodes are located.

During experiments which were performed on the human vastus medial muscle, the electrode is positioned manually so that a clear SFAP waveform is visible in the signal from either electrode 1 or from one of the central electrodes 4 or 5. When a good SFAP waveshape is found all eight channels, which are amplified and band-filtered 5 Hz to 5 kHz by own designed amplifiers, are recorded for a few seconds on a Philips EL 1016 FM tape recorder (bandwidth DC - 30 kHz). The signals are read into a computer off-line where 15 to 20 SFAPs are averaged for all channels. An example of such a recording is shown in fig. VIII.1.

The second method for obtaining multiple SFAP recordings uses the scanning EMG technique (Chapter VII, [8,117]). In a scanning EMG recording, a needle electrode is pulled through the area of a motor unit by a stepper motor. The signal acquisition and the stepper motor movements are controlled by a trigger pulse obtained from a separate SFAP recording from one single fibre of that same motor unit. Usually in scanning EMG, a concentric needle electrode is used as moving electrode. In our experiments, however, we have used a standard single fibre electrode as moving electrode. Under manual control a clear SFAP waveshape which is time locked to the SFAP recorded on the triggering electrode is searched. When this SFAP is found the electrode is moved slightly deeper and subsequently the stepper motor is attached to the electrode while care is taken that the electrode remains in the same direction. A scanning EMG recording from one or more single muscle fibres can be obtained in this way. An example of such a recording is shown in fig. VIII.2. The stepsize in scanning EMG is 50 μm which is 50 % of the inter-electrode distance of the multi-electrode. From the 20 traces shown in fig. VIII.2A 8 traces are selected to obtain a multi SFAP recording comparable to the multi-electrode recordings described above.

VIII.2.2 Volume Conductor Model

The volume conductor model used in this study consists of a cylinder symmetrical geometry of two or three coaxial compartments (see fig. VIII.3). The properties of this model have been extensively studied and documented in Chapter V and VI. The inner compartment represents the metal needle electrode shaft. It has a conductivity σ_n which is very high (10^6 $(\Omega m)^{-1}$) compared to the conductivity of the surrounding tissue and a radius R_n.

The second compartment, representing the muscle tissue, is considered to be homogeneous and infinite and to have an isotropic, purely resistive conductivity σ_e (0.25 $(\Omega m)^{-1}$). Between the metal electrode shaft and the surrounding com-

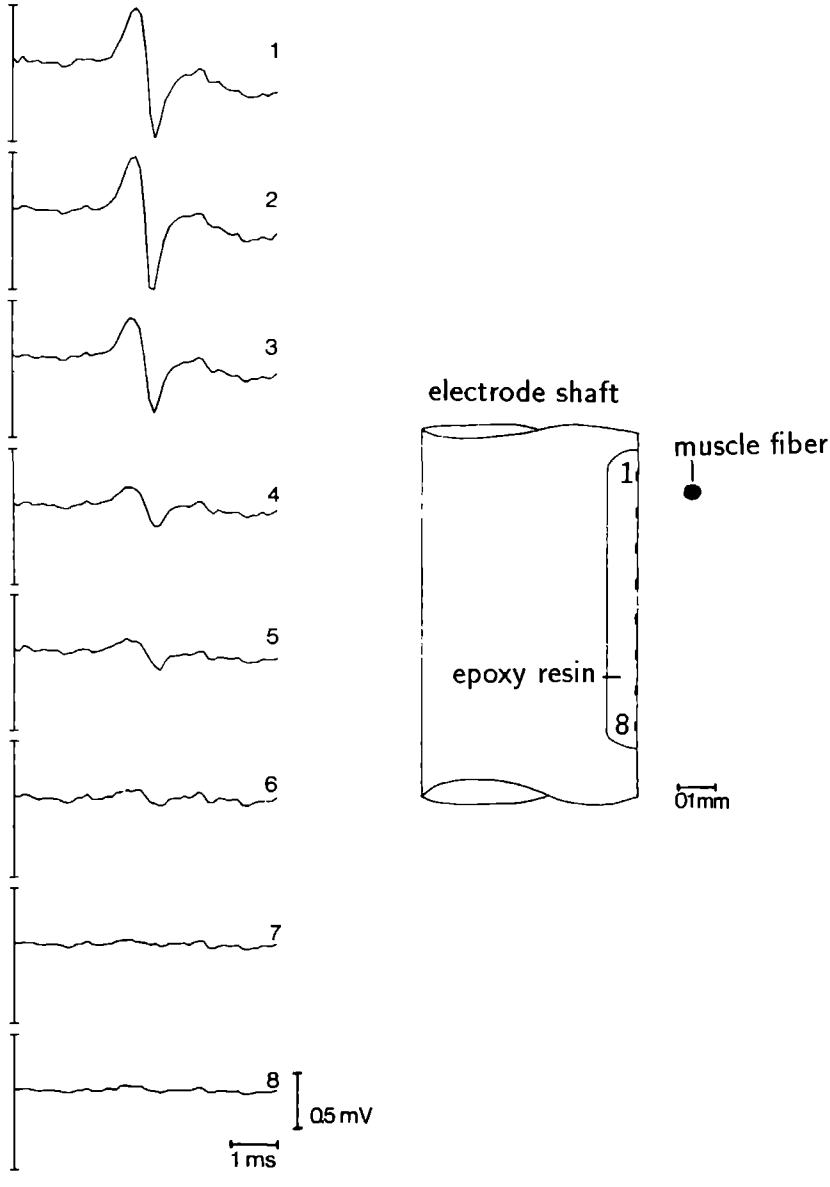

Figure VIII.1 : Right : systematic representation of the multi-electrode and a muscle fibre (on the same scale). Left : an example of a multi-electrode SFAP recording (averaged over 15 firings).

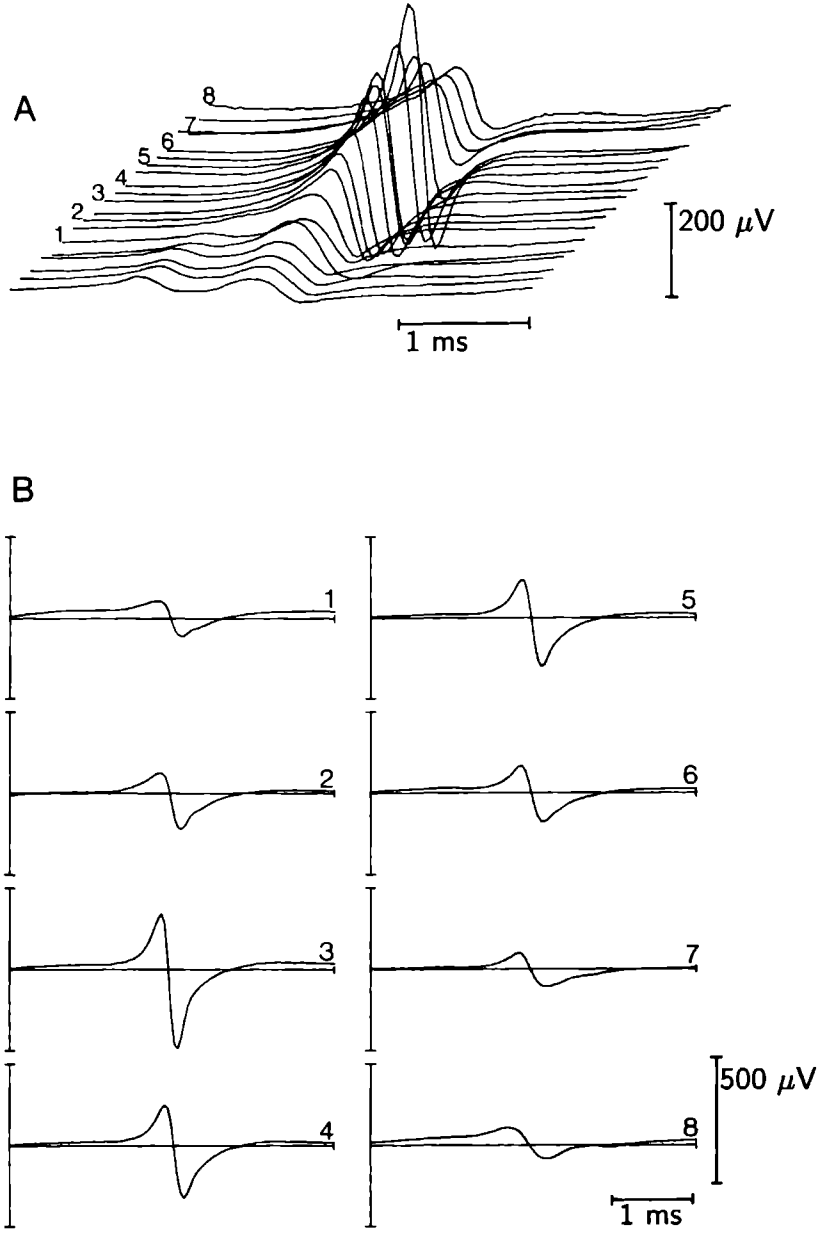

Figure VIII.2 : Example of a multiple SFAP recording used for the parameter estimation procedure, extracted from a scanning EMG recording. A) 3-D representation of scan data. B) Eight SFAPs with inter-recording distance of 100 μm as selected from A.

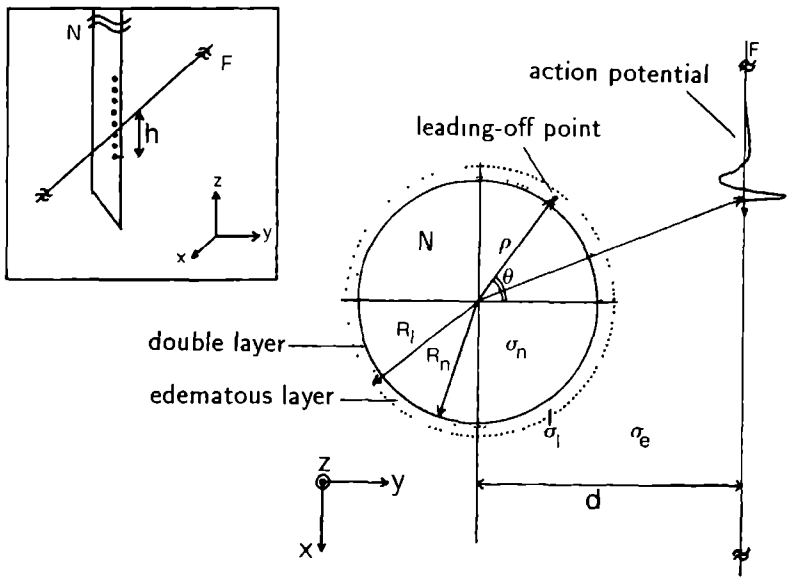

Figure VIII.3 : Systematic representation of the volume conductor model. The box in the upper left corner show the coordinate system and the geometry of the multi-electrode recording The parameter h (see section VIII.2.4) which is one of the estimated parameters is indicated in the figure. The right part shows a cross section through the plane z=0 with the main characteristics of the volume conductor model. (N = needle electrode, F = muscle fibre). The parameters d and Θ indicated in the figure are also parameters which will be estimated.

partment an electrical double layer is formed due to electrochemical reactions [61] between the metal and the free electrolytes in the surrounding tissue. In Chapter V [52,126] it was shown that the impedance of this layer is very high.

The third compartment represents a layer of oedematous fluid. This layer of fluid can be formed between the first (needle electrode) and the second (muscle tissue) compartment when the muscle fibres become irritated or damaged by the presence of the needle electrode and start releasing tissue fluid [33]. The conductivity of the oedematous layer σ_l is therefore assumed to be equal to the conductivity of intracellular fluid (1.0 $(\Omega m)^{-1}$). The outer radius of the oedematous layer is R_l. By taking the conductivity of the oedematous layer σ_l equal to σ_e the model reduces to the two compartment situation.

Perpendicular to the electrode, a muscle fibre is located along which an action potential propagates at a constant velocity of 4 m/s.

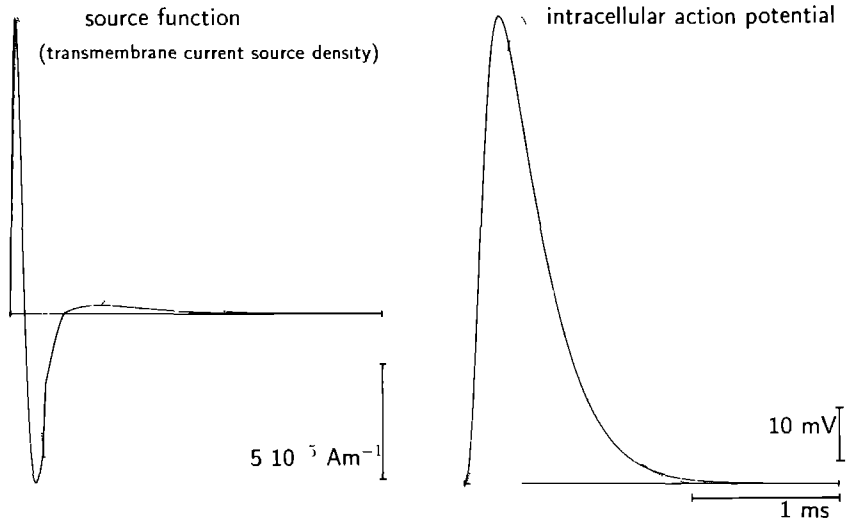

Figure VIII.4 : Original and adapted waveforms of A) the transmembrane current source density per unit length and B) the intracellular action potential. The dotted curves represent the waveforms used by Nandedkar et al. 1983 and the solid curves the adapted waveforms used in the model described in this chapter.

VIII.2.3 Source function

In the model, the action potential is represented by the transmembrane current source density. The waveshape of this source function corresponds to the second derivative of the intracellular action potential. The source function used in our model is an adapted version from the current source distribution described by Nandedkar [87]. It has been adapted to ensure that the resulting SFAP simulations have a smaller third phase and a shorter peak to peak latency, which makes them more comparable to action potentials recorded close to human muscle fibres. From volume conduction theory it is known that the waveshapes of SFAPs recorded close to an active fibre are similar to the waveshape of the transmembrane current source density distribution [96].

The first step in the adaptation performed on this source function is a stretching in time by a factor 2 of the third phase of the standard source function. After this stretching, the negative and positive source points in the discretised form of the source function are balanced to ensure that the total monopole and dipole moments remain zero. Fig. VIII.4A shows the original source function from Nandedkar (dotted line) and the adapted source function (solid line). The source strength of these source functions corresponds to a muscle fibre with a diameter of 55 μm. Finaly the total source function is compressed in time so that the peak to peak duration from the first (positive) to the second (negative) peak corresponds with

the shortest peak to peak times found in our multi-electrode recordings. These recordings can be expected in recordings at a very short distance to the muscle fibre and to demonstrate an optimal likeness with the second derivative of the intracellular action potential.

There are no detailed data on human intracellular muscle fibre action potentials which can support the performed, empirical adaptation of the source function. Twice integrating the adapted source function should result in an waveshape which has similar characteristics as the standard intracellular action potential waveshape. Fig. VIII.4B shows the intracellular action potential used by Nandedkar et al. [86] (dotted line) and the intracellular action potential corresponding to the source function used in our model (solid line).

VIII.2.4 Optimalisation Procedure

The parameters of which the values are estimated by the optimalisation procedure are

1. the radial distance d from the electrode center to the muscle fibre,
2. the distance h in z-direction between the electrode closest to the needle tip and the muscle fibre,
3. the angle of rotation Θ of the linear array of electrodes with respect to the shortest radial distance to the muscle fibre,
4. the anisotropy ratio a of the conductivities of the muscle tissue,
5. a scaling factor s which is proportional to the diameter of the muscle fibre and inverse proportional to the effective conductivity of the muscle tissue.

The parameters d, h and Θ are indicated in fig. VIII.3 Note that the actual distance between the electrodes and the muscle fibre is $d - R_n$ ($R_n = 300\ \mu$m) and that the value of h will be negative if the electrode closest to the tip lies below the plane in which the muscle fibre is located.

In a parameter estimation procedure, a measurement comprising n measured values b_i, $i = 1, n$ is compared to a model that calculates from m parameters p_j, $j = 1, m$ the function values ϕ_i, $i = 1, n$ This model vector $\vec{\phi}$ forms an estimate for $\vec{b}$. After a first estimation with a parameter vector $\vec{p_0}$ an iterative procedure is started which search for a parameter vector $\vec{p}$ so that

$$\left|\vec{\phi}(\vec{p}) - \vec{b}\right| < \varepsilon \quad . \tag{VIII.1}$$

In our implementation of the parameter estimation procedure, an optimised version of the Marquard algorithm [84] is used.

As the actual error value at a given stage of the optimalisation procedure the relative residual is used. This error measure, indicated as RELRES, is defined by

$$\text{RELRES} = \sqrt{\frac{\sum_{i=1}^{n}(\phi_i(\vec{p}) - b_i)^2}{\sum_{i=1}^{n} b_i^2}} \tag{VIII.2}$$

A strong data reduction is performed on the SFAP data in the implementation of the optimalisation procedure in our study. For reasons to be discussed in the last section of this chapter, only the positive and negative peak amplitudes of the 8 recorded SFAPs are used instead of the 8 complete SFAP waveforms. This results in a measurement vector $\vec{b}$ containing $n = 2 \times 8$ elements.

From the volume conductor model described in the previous subsections a database of positive and negative SFAP amplitudes is obtained. In this database, the ranges over which the parameters d, h, Θ and thickness of the oedematous layer $R_l - R_n$ will vary under physiological conditions, are discretised. During the optimalisation procedure, subsequent interpolations (cubic spline's [39]) over the angle, the distance and the height range give the proper data for the desired parameter values. The thickness of the oedematous layer is not varied during one optimalisation procedure. If results for different values of this parameter are desired, more optimalisations are performed subsequently, each with a fixed chosen value for this parameter.

Although the anisotropy ratio can, for mathematical reasons, not be implemented in the model described in the previous subsection, the data from this model are used as if they have been obtained from a model with an anisotropic muscle tissue by a scaling of all distances perpendicular to the longitudinal axis of the muscle fibre and by adapting the conductivity of the muscle tissue. For an infinite, homogeneous volume conductor with radial conductivity σ_r and axial conductivity σ_z this adaptation can be achieved by scaling the radial distances by $a = \sqrt{\frac{\sigma_z}{\sigma_r}}$, and by defining the effective muscle tissue conductivity σ_e as $\sqrt{\sigma_r \sigma_z}$ [6]. In the optimalisation procedure, only the scaling from the distances perpendicular to the muscle fibre : $d - R_n$ and h is implemented. The adaption of the muscle tissue conductivity is accounted for by the scaling factor s.

VIII.3 Results

VIII.3.1 Multi-electrode data

Two examples of successful parameter estimations are shown in fig. VIII.5. The asterisks indicate the negative and positive peak amplitudes obtained form the SFAP recordings. The data in fig. VIII.5A are obtained from the recording shown in fig. VIII.1. The solid lines connect the peak amplitudes of the best fitting SFAPs as they are returned by the optimalisation procedure. The parameter values found by the optimalisation procedure for the two examples from fig. VIII.5 are listed in the first and second data column of table VIII.1. Also the estimated parameters from 4 other multi-electrode recordings are listed.

Table VIII.1 Estimated parameters.

d	(μm)	463	501	399	450	481	489
h	(μm)	52	205	-61	232	306	314
a		6.866	2.632	4.259	3.577	3.800	5.650
s		1.213	1.231	1.854	1.000	0.650	1.100
RelRes		0.107	0.065	0.224	0.136	0.248	0.176

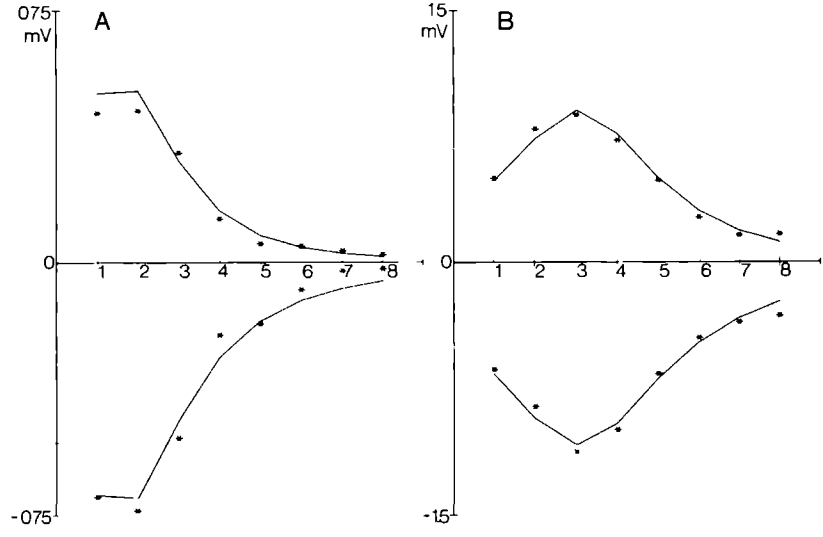

Figure VIII.5 : Two examples of the results of an optimalisation procedure are shown. The asterisks indicated the peak amplitudes obtained from the measured SFAPs. The solid lines connect the peak amplitudes of the best fitting SFAPs from the volume conductor model. The corresponding parameter values are listed in table VIII.1. The numbers along the abcissa represent the numbers of the recording surfaces on the multi-electrode.

The values for the distance d indicate that for all these recordings the distance between the electrode surface and the muscle fibres ($d - 300$) is estimated to be in the range from 100 μm to 200 μm (mean 164 μm, standard deviation 37 μm). In all cases the estimation of the distance h was very stable. The values for the parameter Θ are not listed. This parameter appeared to be an insensitive parameter in the optimalisation procedure. In all estimation procedures were an acceptable relative residual was found, the value of Θ was less than 5 degrees. The values estimated for the anisotropy ratio (mean 4.998, standard deviation 1.750) correspond surprisingly well with the generally accepted value of 5 (e.g. [6]). The scaling parameter does not show great deviations from the reference value 1. This indicates that no SFAPs from muscle fibres much thicker or thinner than an average fibre with a diameter of 55 μm have been recorded or/and that the conductivity of the muscle tissue has not been much higher or lower than the assumed default value of 0.25 $(\Omega\text{m})^{-1}$.

In fig. VIII.6 the solid line waveforms show the measured SFAPs corresponding to the data from fig. VIII.5B and the dotted lines the SFAPs calculated by the volume conductor model with the parameters estimated by the optimalisation procedure.

One aspect that can be studied in a parameter estimation procedure is whether or not a successful optimalisation procedure can be performed on a smaller set of

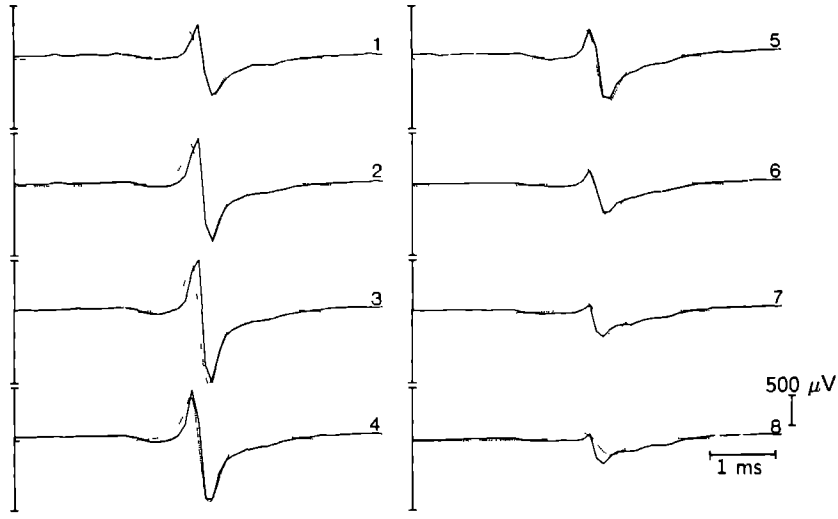

Figure VIII.6 : Recorded SFAPs (solid curves) and model SFAPs (dotted curves) for the amplitude data shown in fig. VIII.5B.

data. Knowledge of this aspect can be useful in practical situations when no high-quality SFAPs can be recorded from all electrodes of the multi-electrode. To study this the number of SFAPs that can be used in the parameter estimation is reduced from 8 to 6 or 4. This corresponds to reducing the length n of the measurement vector $\vec{b}$ which is the input to the optimalisation procedure from 16 to 12 and subsequently to 8. Table VIII.2 shows the results from this analysis for one multi-electrode recording.

Table VIII.2 Estimated parameters fig. VIII.7

		4 electrodes	6 electrodes	8 electrodes
d	(μm)	340	385	399
h	(μm)	-113	-99	-61
a		4.493	4.322	4.259
s		1.956	1.913	1.854
RelRes		0.179	0.194	0.224

For many multi-electrode recordings reducing the size of the data set only has a small influence on the results of the optimalisation procedure. The variation in the estimated parameters is usually below 10 %. Reducing the number of data points will, in general, lead to a decrease of the residual of the fit. For the majority of the multi-electrode recordings this decrease was only a few percent. The data shown in fig. VIII.7 and table VIII.2 represent an example where the quality of the fit increases above average, and the variation in the parameters is above aerage, when the number of data points is reduced. This can be explained by the fact

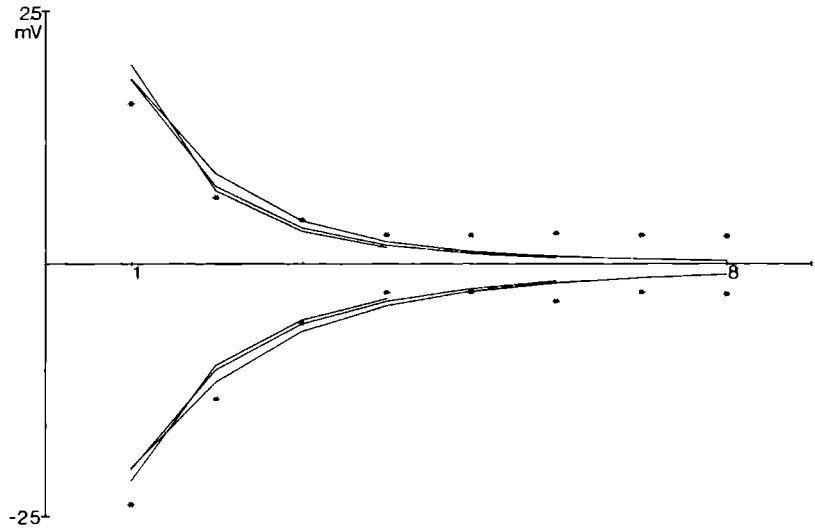

Figure VIII.7 : Peak amplitudes (*) and resulting amplitudes (solid lines) from the optimalisation procedure for a different number of electrodes incorporated in the procedure. The corresponding parameter values are listed in table VIII.2.

that the amplitudes recorded on electrodes 4 to 8 hardly change in amplitude. For the model this is, of course, an irreproduceable situation. In practice, this kind of recordings are found quite regularly since it is not always possible to separate the SFAP waveform completely from the activity from other muscle fibres belonging to the same motor unit. The observation that changing the size of the data set does not lead to great variations in the estimated parameters and the observation that on 4 SFAPs also parameter estimations with high quality fits can be performed makes that these "disturbed" recordings still can be used. Reliable input data for the optimalisation procedure can be obtained by discarding those traces in which the single SFAP cannot clearly be separated from the activity of the rest of the motor unit .

The influence of the oedematous layer on the parameter estimation appears to be marginal. For almost all recordings a successful fit can be obtained using reference data from the model with no oedematous layer present. Adding an oedematous layer in the successful cases causes changes in the parameter values of less than 10 %. In the few cases where no successful fit can be obtained using the reference data without the oedematous layer, the inclusion of the oedematous layer does not produce better results.

Estimations for the cases listed in tables VIII.1 and VIII.3 have also been performed using a homogeneous volume conductor model. For 2 of the cases no successful fit could be made by using the homogeneous model. For the other recordings the parameters estimated by the homogeneous model showed a sig-

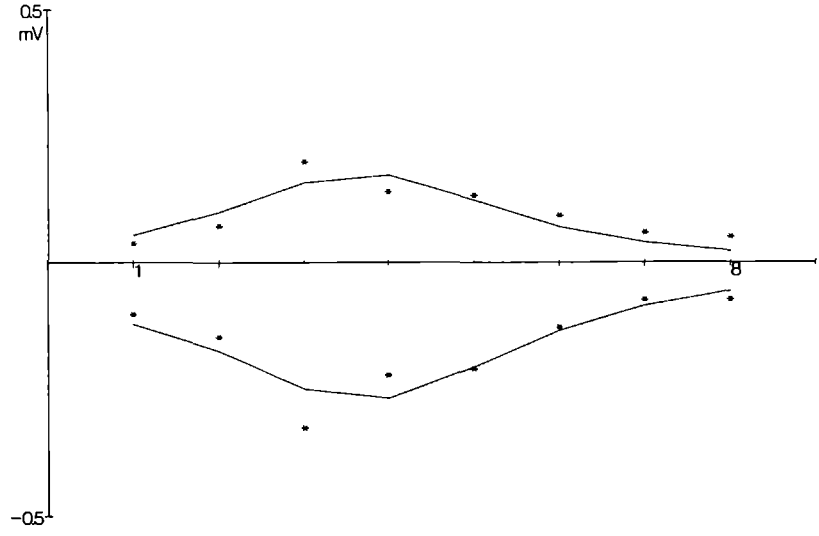

Figure VIII.8 : Measured SFAP amplitudes (*) and optimalisation results (solid lines) obtained from data from a scanning EMG recording. The corresponding parameters are listed in the left data column of table VIII.3.

nificant decrease in the estimated distance d (average decrease 9.3 %), a (not significant) decrcase in anisotropy ratio a (average 6.9 %) and a (not significant) increase in the scaling factor s (average 18.9 %) was found. For the anisotropy ratio a a significant increase of the standard deviation of 39.7 % was found.

VIII.3.2 Scanning EMG data

Table VIII.3 shows the parameters estimated on two multiple SFAP recordings extracted from scanning EMG data. The recorded and estimated positive and negative peak amplitudes corresponding to the first column are shown in fig. VIII.8.

Table VIII.3 Estimated parameters fig. VIII.8			
d	(μm)	504	425
h	(μm)	269	228
a		7.783	5.416
s		0.655	0.690
RELRES		0.205	0.142

The relatively high residual of the fit on the data corresponding to the first column can probably be explained by the almost equal amplitudes recorded on electrodes 4 and 5.

VIII.4 Discussion

VIII.4.1 Methods

The technique of multi-electrode recordings, which was described already by Buchthal for motor unit recordings [17] and by Ekstedt for single fibre recordings [33], has shown to be a powerful method for obtaining simultaneous information from the activity of one single muscle fibre from different observation points. An optimal utilisation of all this information, however, needs a volume conductor model which adequately describes the recording of single muscle fibre recordings with a metal needle electrode. Once the recorded data and the volume conductor model are available, the combination of both in an optimalisation procedure based on the Marquard algorithm is quite straightforward calculus. The Marquard algorithm has proven its value on many occasions, among which also other bio-electric modelling studies at our laboratory [92,110,123,127].

Fig. VIII.6 shows that a fair correspondence exists between the simulated SFAP waveforms and the recorded SFAPs. It can be seen from fig. VIII.6 that the major differences between the recorded and the simulated SFAPs are present in the final part of the action potentials.

Unfortunately, the sampling rate by which the multi-electrode recordings can be read into the computer is at the moment limited to 10 kHz per channel. Regarding the spectral contents of recorded SFAPs this sampling rate is marginally acceptable. When this hardware problem is solved, it should become possible to perform estimations on essential parameters from the first group of parameters defined in the introduction: the source description of the muscle fibre activity. As stated in the introduction of this chapter, and illustrated in section VIII.2.3 by the lack of detailled information on the actual source characteristics of an active muscle fibre, obtaining this information has to be a major goal for future investigations. The intracellular action potential corresponding to the adapted source function we used in our model does show a physiologically realistic appearance. In spite of this, we decided to use only the two peak amplitudes of the recorded SFAPs as measurement data at this stage of the development of the parameter estimation procedure, and not the entire SFAP waveforms.

Not only on real multi-electrode data, but also on SFAP data obtained from scanning EMG recordings can the parameter estimation be applied. Sometimes, recordings are disturbed by movement artifacts. The optimalisation procedure estimates that the average distance between the electrode surface and the muscle fibre is about 150 μm, which corresponds to just 2 or 3 fibre diameters. The diameter of the scanning electrode is about 3 times greater than this distance. Therefore, it should not be surprising that, when the scanning needle electrode is moved upwards the fibres close to the electrode may also be shifted. The data from fig. VIII.8, showing an almost equal amplitude in recording 4 and 5, may be explained by the fact that when the needle electrode is pulled from position 4 to position 5 the muscle fibres close to the electrode are also shifted over about the same distance. When the electrode is subsequently pulled to position 6, the mechanical contact is lost and the amplitude suddenly decreases. The relatively high estimate for the anisotropy ratio for this recording may be an illustration of

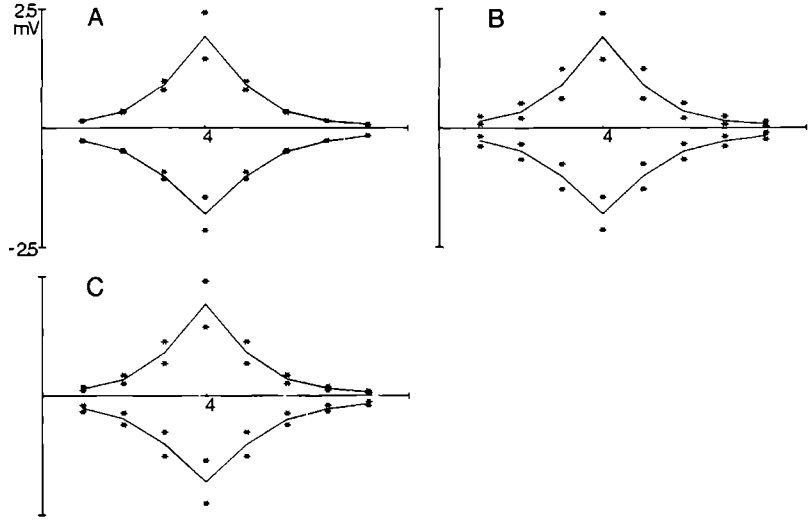

Figure VIII.9 : Positive and negative peak amplitudes as function of electrode number for model results of parameter variations which result in similar changes in the positive peak amplitude of electrode 4 but in different amplitude changes regarded over all electrodes. A) changes in distance, B) changes in anisotropy ratio, C) changes in scaling. The initial values and their changes are listed in table VIII.4.

the difficulties for the optimalisation procedure in finding a proper fit. From this finding, it can be concluded that one has to be aware of such mechanical distortions when studying multiple SFAP recordings obtained with scanning EMG.

VIII.4.2 Parameter results

The results in section VIII.3 show that, with the parameter estimation described in this chapter, very promising results have been achieved. For the parameters distance d, the height h, the anisotropy ratio a and the scaling s stable estimates are found. The parameter Θ, describing the rotation of the needle electrode around its longitudinal axis, appeared not to be very prominent.

The estimates for the parameter h are very stable. Although this parameter is essential in finding a proper fit to the measured data, it does of course not bring forward fundamental information on the volume conductor or the muscle fibre activity. That kind of information has to be derived from the estimates for the parameters d, a and s. Bearing in mind the complex intermingling of the influences of these three parameters on the SFAP recordings, the success of the estimations may on first sight seem surprising. A closer inspection, however, reveals that the use of multiple simultaneous recordings from the same SFAP brings forward enough information to separate the influences from these three parameters.

In fig. VIII.9, it is shown by model data how variations in the distance, the

anisotropy and the scaling are observed in a single SFAP recording, as well as in a multi-electrode recording. In fig. VIII.9A, VIII.9B and VIII.9C the solid lines connect peak amplitudes from a data-set obtained from the volume conductor model. The positive peak amplitude on electrode 4 is 2 mV. The parameters for this simulation are listed in the first data column of table VIII.4. The asterisks indicate the corresponding data points from simulations with adapted parameter sets.

Table VIII.4 Parameters fig. VIII.9

	default	el. 4 2.5 mV	el. 4 1.5 mV	fig. VIII.9
d (μm)	388	355	396	A
h (μm)	300			
a	5.0	3.2	8.2	B
s	1.0	1.25	0.75	C

In fig. VIII.9A, in one case the distance d is reduced such an amount that the positive peak amplitude on electrode 4 increases from 2.0 to 2.5 mV. The peak amplitudes on the other electrodes also increase, but much less than 0.5 mV. In the other case, the distance is increased such an amount that the amplitude on electrode 4 decreases to 1.5 mV. The corresponding distances are listed in table VIII.4. In fig. VIII.9B, the distance is maintained at the initial value as used in fig. VIII.9A but now the anisotropy ratio a is changed upward and downward (see table VIII.4) such that the same changes in the positive peak amplitude on electrode 4 are achieved. In fig. VIII.9C, it is shown how the amplitudes change when the scaling s is increased or decreased (table VIII.4) so that the same changes for electrode 4 are achieved. In the explanation of a change of plus or minus 0.5 mV in a single SFAP recording of only electrode 4 the influences of the distance, the anisotropy ratio or any other parameter cannot be separated from each other. When, however, the changes in the amplitudes of all 8 electrodes are viewed it becomes clear that the behaviour under a change in distance is quite different from that under a change in anisotropy or in the scaling.

Problems in the parameter estimation can arise when for some of the electrodes the SFAP cannot clearly be separated from the activity of the other muscle fibres within the same motor unit. This motor unit influence may take on different forms. One of these is shown in fig. VIII.7, where the amplitudes of the electrodes 4 to 8 do not show any decrease at all. In such a situation the SFAP waveform has disappeared in the MUAP waveform. The results listed in table VIII.2 show that, when an increasing number of SFAPs of which the amplitudes are almost equal are omitted from the parameter estimation, only minor changes are found in the values of the estimated parameters. The residual of the estimation reduces when the SFAPs with constant amplitude are omitted.

From these findings two conclusions can be drawn. The first one is that the size of the input data set (default 16 amplitude values) can be reduced to 12 or 8 without causing instabilities in the optimalisation procedure. The second one is that in multi-electrode recordings, where for the reason mentioned above or for any other reason, SFAPs are missing this stable behaviour of the optimalisation procedure is essential, ensuring that the parameter estimates obtained from such incomplete data sets are reliable. These two conclusion may seem to indicate

that for all multi-electrode recordings 4 SFAPs will contain sufficient information for a reliable parameter estimation There are, however, cases in which 4 SFAPs are insufficient to perform a stable estimation Examples of such cases are when all recording electrodes lie below or above the plane in which the muscle fibre is located

The combination of a multi-electrode SFAP recording and a sophisticated volume conductor model is capable of separating the influences of the recording distance, the anisotropy ratio of the muscle tissue and the general scaling which is a combination of the muscle tissue conductivity and the fibre diameter The unrealistic estimates for the distance, the anisotropy or the scaling that have often been found when a homogeneous model is used in the optimalisation procedure indicate that it is necessary to use a volume conductor model that incorporates a proper description of the recording electrode This description of the influence of the recording electrode appears to be more essential than a very detailed description of the muscle tissue A model which was concentrating on the latter aspect only [4,49] found a lesser degree of correspondence between recorded and simulated SFAPs [5] than has been found by the parameter estimation procedure described here

Adding the oedematous layer to the model has almost the same effect on the estimated parameters as the use of the homogeneous model The estimated distances decrease and the anisotropy ratio and the scaling show a considerably greater variation This observation, and the observation that adding the oedematous layer to the model is not resulting in lower residuals, suggests that during the recordings the influence of the oedematous layer has been marginal Therefore, no further attempts have been made to incorporate the width of the oedematous layer as an active parameter in the optimalisation procedure

VIII.4.3 Conclusions

The general conclusion on the procedure described in this chapter is that from a multi-electrode SFAP recording the essential parameters describing the volume conductor geometry of the recording can be estimated This is an essential condition which has to be fulfilled before the procedure may be extended to the estimation of parameters describing the source activity of the muscle fibre Adding an extra electrode, placed aside of the linear array of the other electrodes, to the multi-electrode [115] allows the estimation of the propagation velocity of the action potential From volume conduction theory, it is known that this parameter has a strong relation to the source strength of an active fibre [96] This aspect of muscle fibre activity should be incorporated in future research on parameter estimations on muscle fibre action potentials.

Chapter IX

Summary and Conclusions.

This thesis deals with the analysis of the electrical activity which can be recorded from human skeletal muscle during voluntary contraction. Physical and mathematical methods are used to develop models for the interpretation of single muscle fibre action potentials (SFAPs) and motor unit action potentials (MUAPs). The predictions of the models are compared with various experimental techniques used to obtain SFAP and MUAP recordings.

In Chapter I, the historical background and the present state of clinical and fundamental research concerning the interpretation of electromyographic signals, and the supporting volume conductor modelling are described. The main issues of investigation are indicated.

Chapters II to VI concern the four basic questions that were raised in Chapter I (General Introduction). In Chapter II, a new algorithm for single muscle fibre action potential simulations is presented in which the temporal and the spatial properties of the muscle fibre activity pattern and of the volume conduction weighting function are treated separately. By using a homogenised characterisation of the muscle tissue it is shown that the capacitive properties of the muscle fibre membrane need not be incorporated in the volume conductor description. The choice between a purely resistive description of the muscle tissue conductivity or a capacitive conductivity, which was raised by the first question, has thereby fallen to a resistive description. It has also been concluded in Chapter II that the phenomenon of current redistribution, described in the bi-domain models, needs not to be taken into account for muscle fibre SFAPs.

The second question raised in the introduction concerned the importance of the finite muscle fibre length. In Chapter II, it has been found that the effect of the action potential propagation stop at the muscle fibre end is important. It can mathematically be described by a non-moving dipole source, in contrast to the propagating action potential, which can be caracterised as a moving quadrupole source.

The potential fields of dipole sources differ quite substantially in finite and infinite volume conductor geometries. When the dimensions of a motor unit are

compared with those of the muscle in which the motor unit is located, or of the limb in which the muscle is located, it becomes clear that a proper MUAP model, including the effects of the propagation stop, may require a finite volume conductor description. This holds especially true for the simulation of surface EMG signals. To make such a description possible, a numerical method is developed in Chapter III which makes it possible to calculate potential fields in an inhomogeneous cylinder symmetrical volume conductor of finite dimensions. In this method, a re-formulation of the matrix equation describing the physical boundary conditions is combined with a logarithmic evaluation of the higher order modified Bessel functions. Owing to this combination, potential fields can be calculated without the numerical instabilities that would otherwise arise in calculations in which these modified Bessel functions are used.

With the aid of this new numerical tool the answer to the third question : whether or not a finite volume conductor description is essential, is given in Chapter IV. As was predicted in Chapter II, the finiteness of the volume conductor can have substantial influence on the SFAPs and MUAPs. The simulation results show that the stop effect described in Chapter II becomes very important for both SFAPs and MUAPs observed on the outer surface of the volume conductor. The simulated SFAP waveforms are clearly dominated by the stop effect. This is one aspect explaining why action potential propagation velocity estimates, obtained from surface EMG recordings, are often disturbed by peaks with equal latencies occurring on both simultaneous registrations. These peaks are most probably the end-effect peaks of motor units action potentials.

In the MUAP waveforms the stop effect is less prominent but still clearly present. In surface EMG, both SFAPs and MUAPs are attenuated by the fat layer surrounding the muscle tissue. It can be concluded from the MUAP simulations that the widening of the MUAP waveform due to the volume conduction is much greater than the widening due to the temporal dispersion factors : differences in pathlengths of motoneuron branches, synapse jitter and muscle fibre action potential propagation velocities, which are described in Chapter IV. The influence of the stop effect is mainly of interest for intramuscular observations when the SFAP or MUAP is recorded at some distance from the muscle fibre or motor unit. Simultaneous recordings of intramuscular and surface MUAPs support the findings of the model.

We have concluded from Chapters II and IV that a proper description of the volume conductor for MUAP simulations should have finite dimensions and should contain muscle fibres of finite length. Its conductivities can be characterised as being purely resistive. In this geometry, which should also contain the subcutaneous fat layer, the structural data of the organisation of a motor unit can then be incorporated to obtain simulated MUAP waveshapes. For surface EMG the finiteness of the muscle tissue and fat layer geometry is the most important factor. For intramuscular MUAPs the strucutral parameters describing the motor unit are the most important parameters.

A conclusion on how realistic the simulated waveshapes are, can only be reached when also the aspects that influence the recorded waveshapes and which are not directly related to the active sources or to the conducting medium, are understood. Probably the most important of these aspects is the disturbance by the needle

electrode on the potential field generated by the myo-electric activity. In Chapters V and VI, this aspect, which was formulated in the fourth question raised in the General Introduction, is studied. In Chapter V, an analytical model is described which incorporates the influence of the needle electrode shaft on SFAP waveforms recorded with a typical single fibre electrode. In order to be able to calculate the potential field in the presence of the electrode cannula, the model has to break with several traditions of "classical" SFAP modelling. The symmetry axis for the cylinder symmetrical potential field problem is chosen parallel to the needle cannula and not, as usual, parallel to the muscle fibre. The theoretical validations of this choice and other necessary assumptions are also derived in this chapter. The main implications of this model for the experimental, clinical recording set-up are elaborated in Chapter VI.

The results indicate that the presence of an electrical double layer between the metal surface of the cannula and the surrounding tissue has a great influence on the amplitudes of the simulated SFAPs. An amplification of 70 % is found for a muscle fibre located at the same side of the electrode shaft as the leading-off point, at a short distance from the electrode surface. This amplification is caused by the very high impedance of the electrical double layer surrounding the metal electrode shaft owing to electrochemical reactions between the shaft metal and the tissue fluid. The high impedance of the electrical double layer completely shields off the high metal conductivity. When the distance between electrode and muscle fibre increases, the amplification gradually decreases. A "shadow" phenomenon is found for muscle fibres located at the back of the electrode. For SFAPs of these muscle fibres, a maximal attenuation of 50 % occurs. Only in SFAPs recorded from muscle fibres located at a short distance from the rear of the electrode have waveshape alterations been found. These waveshape changes are not of practical importance.

When the muscle tissue gets irritated or when muscle fibres are damaged an oedematous layer may form between the needle electrode and the surrounding muscle tissue. This oedematous layer counteracts the effects caused by the electrical double layer. The amount of counteraction depends on the thickness and the conductivity of the oedematous layer.

The simulation results obtained from the models described above are complemented with the SFAPs and MUAPs registered with two experimental techniques: scanning EMG and multi-electrode EMG. Although both techniques have been known for some time they did not develop into standard clinical techniques. However, these two techniques are expected to provide information on several of the major topics already studied in the simulation models.

In Chapter VII, the technique of scanning EMG is used to obtain information on the volume conduction behaviour of the activity of an entire motor unit and on the influence of the concentric needle electrode with which this activity is usually recorded. By means of this motor unit activity, the structure of motor units of the human quadriceps muscle is studied on a group of healthy volunteers and on two groups of patients with proven a neurogenic or myogenic neuromuscular disorder. In total, 86 scans have been recorded. The obtained scanning EMG data are characterised by two parameters : 1) the extension of the motor unit territory and 2) the temporal dispersion within the motor unit. These two parameters have, in

this form, previously not been used as "diagnostic" parameters. The motor unit territory is capable of separating the two patient groups. The vast majority of myogenic patients shows motor unit territories of less than 4 mm where a clear majority of the neurogenic patients shows motor unit territories greater then 4 mm. The time dispersion for both patient groups ranges from 2 to 12 ms while, for the volunteers, it ranges from 1 to 4 ms.

In a special, monopolar set-up of scanning EMG, separate recordings are obtained simultaneously from the leading-off surface and from the shaft of a typical concentric needle electrode. Although this electrode is commonly used in clinical EMG examinations, no complete description of its influence on the recorded potentials is available. The monopolar recordings indicate that the influence of this electrode type on the two parameters used to analyse the scanning EMG data is negligible.

As the first step to an "inverse model" approach, multi-electrode SFAP recordings, and multiple SFAP recordings extracted from scanning EMG data, have been used in a parameter estimation procedure on single fibre action potentials. The volume conductor model describing the influence of the presence of a metal needle electrode on the SFAP recordings (Chapter V) has been included as implied forward procedure.

In spite of the complicated relation between the electrode-to-muscle-fibre distance and the anisotropy ratio of the muscle tissue conductivities, stable estimates are found for these two parameters. A scaling parameter, which is proportional to the muscle fibre diameter and inverse-proportional to the muscle tissue conductivity, is also estimated. It has been estimated that the average recording distance is 165 μm, the average anisotropy ratio 5.0 and the average muscle fibre diameter 58 μm. The method uses the extra information that can be obtained from multiple SFAP recordings, and it can derive parameters from measured data that could not previously be obtained from SFAP recordings.

In general, we can conclude that the two EMG registration techniques, which have been used, are capable of providing much information on various aspects of the state of human skeletal muscle. The advantages of the two techniques have become clear, although the scanning EMG technique and the multi-electrode recordings are more complicated than standard clinical EMG methods. Aspects, which could previously not be assessed by clinical EMG examination, appear to come into the reach of clinical applications now. The various biophysical models, which have been described in this thesis, have given a substantial contribution to the understanding of the obtained experimental results. In the last chapter, the biophysical model has even been of decisive importance in the correct interpretation of the electrical activity in human skeletal muscle.

Chapter X

Samenvatting en Conclusies.

In de diagnose van spier- en zenuwaandoeningen speelt het electromyografisch onderzoek een belangrijke rol. Een klinisch EMG onderzoek omvat, naast het meten van geleidingssnelheden van zenuwen en het onderzoeken van reflexen, ook het zogenaamde spierbeeld-onderzoek. Bij dit laatste onderzoek wordt met behulp van naaldelectrodes, die in de spier ingebracht worden, de electrische activiteit in de spier op verschillende wijzen bekeken. De aandacht gaat hierbij vooral uit naar de electrische activiteit van de zogenaamde *motor units* zoals die tijdens vrijwillige aanspanning wordt geregistreerd.

Een dergelijke motor unit bestaat uit 1) een motorische zenuwcel, gelegen in het ruggemerg, 2) het lange axon van deze cel dat ononderbroken doorloopt tot in de spier, 3) de vertakkingen van dit axon naar de individuele spiervezels, 4) de motorische eindplaatjes (de uiteinden van de axon-vertakkingen waar de electrische prikkel van zenuwvezel op spiervezel wordt overgedragen) en 5) de spiervezels. Wanneer de motorsturingscentra in de hersenen een bepaalde motor unit in een bepaalde spier wensen te activeren, zal via zenuwbanen in het ruggemerg het gewenste motorneuron geactiveerd worden. Dientengevolge zal zich langs het axon van het motorneuron een actiepotentiaal voortplanten met een snelheid in de orde van 50 m/s. Bij de spier aangekomen zal deze actiepotentiaal zich opsplitsen over alle vertakkingen van het axon en uiteindelijk zullen alle motorische eindplaatjes geactiveerd worden. Na de impulsoverdracht op de spiervezels zullen zich langs elke spiervezel, vanaf de plaats van het eindplaatje ergens in het midden van de spiervezel, twee actiepotentialen voortplanten in tegenovergestelde richting. De gesommeerde activiteit van de actiepotentialen van alle individuele spiervezels (*single fiber actiepotentialen*, SFAP's) die tot een motor unit horen is de *motor unit actiepotentiaal* (MUAP).

Omdat de motor units de functionele eenheden zijn in skeletspieren is het registreren en beoordelen van MUAP's tijdens een klinisch EMG onderzoek van groot belang. Vrijwel alle veranderingen die in de spier optreden, al dan niet het gevolg van een ziekteproces, zullen in meerdere of mindere mate veranderingen teweeg brengen in de MUAP's. Dit is het gevolg van de vele factoren die samen de vorm

van een MUAP bepalen. Behalve de eigenschappen van de spiervezels als de eigenlijke electrische bronnen in de spier, en de eigenschappen van het spierweefsel dat als medium dient waarin tengevolge van de aanwezige bronnen een potentiaalveld ontstaat, speelt ook de geometrie van de motor unit een belangrijke rol. Onder deze geometrie vallen parameters als de ligging van de motorische eindplaatjes, de vorm van het motor unit territorium (= dwarsdoorsnede door het gebied van een motor unit) en de ligging van de spiervezels in het motor unit territorium.

Om een inzicht te krijgen in de factoren die de vorm van een MUAP bepalen en om de veranderingen die in MUAP's kunnen optreden onder invloed van ziekteprocessen te verklaren maakt men al meer dan tien jaar gebruik van motor unit modellen die MUAP's zo realistisch mogelijk trachten na te bootsen (de zgn. *voorwaartse simulatie modellen*). Een motor unit model bestaat uit twee delen. Het eerste deel van het motor unit model geeft een beschrijving van de geometrie van de motor unit binnen de spier. Het tweede deel berekent individuele SFAP's. Dit deel van het MUAP model is gebaseerd op de volumegeleidings theorie, d.w.z. dat deel van de electriciteitsleer dat in een drie-dimensionale ruimte potentiaalvelden en stroomlijnen beschrijft die het gevolg zijn van electrische bronnen. In het geval van EMG zijn de actieve spiervezels te beschouwen als stroombronnen en is de spier de omringende volumegeleider. Voor de SFAP modellering zijn de bronbeschrijving van de spiervezel en de eigenschappen van het omringende spierweefsel de belangrijkste aspecten. Uit het eerste deel van het motor unit model worden de gegevens genomen die nodig zijn om de individuele SFAP's te berekenen waarna de MUAP verkregen wordt als de som van de SFAP's.

Ondanks het feit dat tal van aspecten van pathologische MUAP's qualitatief goed beschreven kunnen worden met behulp van veranderingen in de parameters van de motor unit modellen is een quantitatieve vergelijking tot op heden moeizaam gebleven.

Het doel van het onderzoek waar dit proefschrift een deel van beschrijft, is het zoeken van een biofysische basis voor SFAP en MUAP modellering die een betere kwantitatieve, diagnostisch bruikbare analyse van MUAP's kan opleveren.

De hoofdstukken II, III en IV houden zich bezig met het modelleren van SFAP's en in het bijzonder met het onderzoeken van welke aspecten van SFAP modellering die in huidige MUAP modellen ontbreken toch meegenomen moeten worden in een motor unit model. In hoofdstuk II wordt geconcludeerd dat de beschrijving van spierweefsel met een electrische geleidbaarheid die zuiver resistief van aard is een voldoende correcte beschrijving is. Het toevoegen van de capacitieve effecten die veroorzaakt worden door de aanwezigheid spiervezelmembranen geeft veranderingen van minder dan 1% (fig. II.9, pagina 28).

Omwille van rekentechnische eenvoud is in de literatuur van de SFAP modellering tot nu toe steeds een oneindige vezellengte aangenomen. Voor SFAP observaties dicht bij de spiervezel en op enige afstand van het eindplaatje of het einde van de spiervezel is deze aanname redelijk. Bij MUAP registraties zal echter niet altijd aan deze voorwaarden voldaan zijn. Een tweede, belangrijke conclusie van hoofdstuk II is dat het incorporeren van de eindige lengte van de spiervezels in de SFAP berekeningen en het opstarten en weer stoppen van de twee actiepotentialen een grote invloed kan hebben op de SFAP golfvormen (fig. II.7 en II.8, pagina 26 en 27).

Om in de MUAP simulaties ook de invloed van de eindige afmetingen van de spier in rekening te brengen is een aanpassing nodig van het volumegeleidings model dat de SFAP's berekent. De tot nog toe gebruikelijke methode om potentiaalvelden te bereken in een eindige volumegeleider is echter niet onder alle omstandigheden stabiel. In hoofdstuk III wordt een oplossing beschreven voor dit numerieke probleem.

Met de nieuwe stabiele rekenmethode worden in hoofdstuk IV potentiaalvelden berekend in een spier van eindige afmetingen, omgeven door een laag vetweefsel. De resultaten van SFAP en MUAP berekeningen voor observatie plaatsen aan het (huid)oppervlak laten duidelijk zien hoe belangrijk de eindige lengte van de spiervezels is. De SFAP veranderingen ten gevolge van het stoppen van de actiepotentialen aan de vezeleinden worden in het eindige volumegeleidingsmodel aanmerkelijk versterkt (fig. IV.5, pagina 51). Voor intramusculaire MUAP registraties blijkt dit geen grote gevolgen te hebben (fig. IV.6, pagina 52). MUAP's geregistreerd met oppervlakte electrodes blijken wel sterk beïnvloed te worden. Deze beïnvloeding uit zich onder andere in de verkeerde schattingen uit oppervlakte EMG registraties van de voortplantingssnelheid van de spiervezel-actiepotentialen, die in de literatuur beschreven zijn.

De hoofdstukken II t/m IV leiden tezamen tot de conclusie dat in de simulatie van intramusculair geregistreerde MUAP's de eindige lengte van de spiervezel verdisconteerd moet worden en dat het spierweefsel als zuiver resistief beschreven kan worden. Voor de simulatie van oppervlakte registraties van MUAP's is een volumegeleidingsbeschrijving van eindige dimensies, met daarin opgenomen een onderhuidse vetlaag, noodzakelijk i.v.m. de grote veranderingen in de SFAP's die hierdoor optreden.

De meeste EMG registraties worden gemaakt met behulp van metalen naaldelectrodes. Het ligt voor de hand dat deze electrodes een verstoring zullen veroorzaken in de potentiaalvelden zoals die door de actieve spiervezels worden opgewekt. Een precieze beschrijving van deze verstoring was tot op heden nog niet voorhanden. De enkele malen dat een poging tot beschrijven van de naaldinvloed werd ondernomen gebeurde dat op basis van intuïtieve argumenten. In de hoofdstukken V en VI van dit proefschrift wordt een model voor een zogenaamde *single fiber electrode* beschreven. Hoofdstuk V geeft de mathematische beschrijving van het model terwijl in hoofdstuk VI de verkregen resultaten worden geëvalueerd. Het belangrijkste aspect van dit model blijkt de electrische dubbellaag te zijn die tengevolge van electro-chemische reacties tussen de metalen naaldschacht en de ionen in het weefselvocht ontstaat. Deze laag heeft een zeer hoge impedantie. Hierdoor wordt de lage weerstand van de metalen naaldschacht afgeschermd (fig. V.6, pagina 69). Men kan zelfs stellen dat zonder een electrische dubbellaag metalen naaldelectrodes onbruikbaar zouden zijn. Tevens treden er aanmerkelijke veranderingen op in de amplitudes van de SFAP's. De SFAP's tengevolge van spiervezels, die aan dezelfde zijde van de electrode gelegen zijn als het kleine afleidoppervlak van de single fiber electrode, worden versterkt met maximaal 70 %. Dit percentage geldt voor de vezels die het dichtst bij de naaldelectrode gelegen zijn (fig. VI.3C, pagina 81). SFAP's van spiervezels die aan de achterzijde van de electrode liggen worden met maximaal 50 % verzwakt (fig. VI.3F).

In de hoofdstukken VII en VIII worden de resultaten van de modellen uit de eerdere hoofdstukken aangevuld met experimentele gegevens. Hiertoe zijn twee EMG technieken die al eerder in de literatuur beschreven zijn, maar die niet tot de klinische routine zijn doorgedrongen, tot nieuw leven gewekt.

In hoofdstuk VII wordt de scanning EMG methode gebruikt, die ontwikkeld is om een inzicht te krijgen in de ruimtelijke structuur van motor units. Het doel is het onderzoeken van de bruikbaarheid van scanning EMG als diagnostische techniek. Hiertoe zijn bij een groep gezonde proefpersonen en twee duidelijk verschillende patiëntengroepen scanning EMG registraties gemaakt. Het blijkt dat de grootte van het motor unit territorium, zoals die in hoofdstuk VII gedefinieerd is, goed in staat is de groep neurogene patiënten te scheiden van de groep myogene patiënten. Vrijwel alle myogene patiënten tonen territoria van minder dan 4 mm doorsnede terwijl de grote meerderheid van neurogene patiënten territoria van meer dan 4 mm vertoont (fig. VII.6, pagina 101). Zowel deze parameter als een parameter die de temporele structuur van de hele motor unit quantificeert blijken niet merkbaar verstoord te worden door de invloed van de concentrische naaldelectrode. Het gemak waarmee een eenvoudige parameter de twee patiëntengroepen kan scheiden duidt op een duidelijk perspectief voor een genuanceerder onderscheid aan de hand van een gedetailleerder quantificering van de scanning EMG gegevens. Tevens is aangetoond dat de veranderingen in de bepaalde parameters, door het gebruik van zogenaamde concentrische naaldelectrodes voor het registreren van de scanning signalen, gering zijn.

In hoofdstuk VIII is een 8 kanaals multi-electrode gebruikt om 8 simultane SFAP registraties te maken van een enkele spiervezel, met behulp van de rij op gelijke onderlinge afstanden gelegen afleidoppervlakken die in de naaldschacht zijn gemonteerd zijn. Tezamen met het naaldelectrode model ontwikkeld in hoofdstuk V, is een parameter schattings procedure ontwikkeld. In deze procedure worden aan de hand van de 8 SFAP's de waarden van een aantal parameters geschat die de geometrie van electrode en spiervezel tijdens de registratie, en enkele eigenschappen van het spierweefsel en de spiervezel, beschrijven. Het is vanuit het onderzoek aan volumegeleidings modellen al lang bekend dat twee van de geschatte parameters, 1) de afstand tussen de electrode en de vezel en 2) de anisotropie-verhouding van de geleidbaarheden van het spierweefsel, op een complexe manier de amplitude van SFAP's mee bepalen. Desondanks slaagt de procedure erin stabiele en betrouwbare schattingen van deze parameters te maken (tabel VIII.1, pagina 115). Dit resultaat werd tot op heden binnen de electrofysiologische modelvormings literatuur voor onmogelijk gehouden.

Samenvattend kan men zeggen dat de twee beschreven registratiemethoden, alhoewel ze complexer zijn dan de huidige methoden uit het klinische EMG onderzoek, in staat zijn veel informatie te leveren over diverse aspecten van de toestand van een skeltspier. Aspecten die tot nu toe niet beoordeeld konden worden in klinisch EMG onderzoek en die binnen afzienbare tijd in het bereik van een klinische toepassing zullen komen. De diverse biofysische modellen die beschreven zijn, hebben duidelijk bijgedragen aan het begrip van de verkregen resultaten en zijn in het laatste hoofdstuk zelfs van doorslaggevend belang gebleken bij het correct analyseren van de electrische activiteit in menselijke skeletspieren.

Bibliography

[1] ABRAMOWITZ M AND IA STEGUN. *Handbook of Mathematical Functions.* Dover Publication Inc., New York, 1972.

[2] ADRIAN ED AND DW BRONK. The discharge of impulses in motor nerve fibers. The frequency of discharges in reflex and voluntary contractions. *J. Physiol* **67**:119-151, 1929.

[3] ALBERS BA, RUTTEN WLC, WALLINGA-DE JONGE W AND HBK BOOM. A model study on the influence of structure and membrane capacitance on volume conduction in skeletal muscle tissue. *IEEE Trans. Biomed. Eng.* **33**:681-689, 1986.

[4] ALBERS BA. *Microscopic Volume Conduction of Myo-electrical Activity.* Ph.D. Thesis, University of Twente, The Netherlands, 1987.

[5] ALBERS BA, PUT JHM, WALLINGA W AND P WIRTZ. Quantitative analysis of single muscle fiber action potentials recorded at known distances. *Muscle & Nerve* **73**:245-2543, 1989.

[6] ANDREASSEN S AND A ROSENFALCK. Relationship of intrcellular and extracellular action potentials of skeletal muscle fibers. *CRC Crit. Rev. in Bioeng* **6**:267-306, 1981.

[7] ANDREASSEN S AND N JÖRGENSEN. A model for the motor unit potential. *Electroenceph. Clin. Neurophysiol.* **52**:1163, 1981.

[8] ANTONI L, STÅLBERG E AND P HILTON-BROWN. Acquisition and analysis of scanning EMG. *Personal communication*, 1984.

[9] AQUELONIUS S, ASKMARK H, GILLBERG P, NANDEDKAR S AND Y ALSSON. Topographical localization of motor endplates in cryosections of whole human muscles. *Muscle & Nerve* **7**:287-293, 1984.

[10] BARACH JP AND JP WIKSWO. Computer simulation of action potential propagation in septated nerve fibers. *Biophys. J.* **51**:177-183, 1987.

[11] BERGMANS J. Computer assisted on-line measurement of motor unit potential parameters in human electromyography. *Electromyography* **11**:161-181, 1971.

[12] BIRO G AND CD PARTRIDGE. Analysis of multi-units spike records. *J. App. Physiol.* **30**:521-526, 1976.

[13] DE BOER RW AND A VAN OOSTEROM. Electrical properties of platinum electrodes: impedance measurements and time-domain analysis. *Med. & Biol. Eng. & Comp.* **1**:1-10, 1978.

[14] BOYD DC, LAWRENCE PD AND PJ BRATTY. On modelling the single motor unit action potential. *IEEE Trans. Biomed. Eng.* **25**:236-243, 1978.

[15] BRANDSTATER ME AND EH LAMBERT. Motor unit anatomy. Type and spatial arrangement of muscle fibres. In : DESMEDT JE (ed.) *New Developments in Electromyography and Clinical Neurophysiology.* **1**:14-22. Karger, Basel, 1973.

[16] BROMAN H, BILOTTO G, AND CJ DELUCA. A note on the noninvasive estimation of muscle fiber conduction velocity. *IEEE Trans. Biomed. Eng.* **32**:341-343, 1985.

[17] BUCHTHAL F, GULD C AND P ROSENFALCK. Multielectrode study of the territory of motor unit. *Acta Physiol. Scand.* **39**:83-104, 1957.

[18] BUCHTHAL F, ERMINIO F AND P ROSENFALCK. Motor unit territory in different human muscles. *Acta Physiol. Scand.* **45**:72-87, 1959.

[19] BUCHTHAL F. The general concept of motor unit. *Neuromusc. Disorders* **38**:3-30, 1961.

[20] BUCHTHAL F. On the Structures of Motor Units. In: DESMEDT JE *New Developments in EMG and Clinical Neurophysiology.* Karger, Basel, 1973.

[21] BUCHTHAL F. The diagnostic yield of quantified electromyography and quantified muscle biopsy in neuromuscular disorders. *Muscle & Nerve* **5**:265-280, 1982.

[22] BURGER CH AND R VAN DONGEN. Specific electric resistance of body tissues. *Phys. in Med. Biol.* **5**:431-447, 1961.

[23] CHRISTENSEN E. Topography of terminal motor innervation in striated muscles from still born infants. *Amer. J. Phys. Med.* **38**:65-78, 1959.

[24] CLARK J AND R PLONSEY. The extracellular potential field of the single active nerve fiber. *Biophys. J.* **8**:842-864, 1968.

[25] CÖERS C AND WOOLF AL. Normal histology of the intramuscular nerves and nerve endings. In : *The innervation of muscle* Blackwell Scient. Publ., Oxford, 1957.

[26] COËRS C AND AL WOLF. *The Innervation of Muscle.* Blackwell, Oxford, 1959.

[27] CORNELIS JPH AND EHG NYSSEN. Potentials produced by arbitrary current sources in an infinite- and finite-length circular conducting cylinder. *IEEE Trans. Biomed. Eng.* **BME-32**:993-1001, (1985).

[28] DIMITROV G AND N DIMITROVA. Extracellular potential field of a single striated muscle fiber immersed in an anisotropic volume conductor. *Electromyogr. Clin. Neurophysiol.* **14**:423-436, 1974.

[29] DIMITROV GV, LATEVA ZC AND NA DIMITROVA. Effects of changes in asymmetry, duration and propagation velocity of the intracellular potential on the power spectrum of extracellular potentials produced by an excitable fiber. *Electromyogr.Clin.Neurophysiol.* **28**:93-100, 1988.

[30] DIMITROVA N. Model of the extracellular potential field of a single striated muscle fiber. *Electromyogr. Clin. Neurophysiol.* **14**:53-66, 1974.

[31] DORFMAN LJ, HOWARD JE AND KC MCGILL. Motor unit firing rates and firing rate variability in the detection of neuromuscular disorders. *Muscle & Nerve* **73**:215-224, 1989.

[32] DUBOWITZ V AND M BROOKE. *Muscle biopsy ; a modern approach.* P.A. Saunders, Philadelphia, 1973.

[33] EKSTEDT J. Human single muscle fiber action potentials. *Acta Physiol. Scand.* **61**, Suppl. 226:1-96, 1964.

[34] EKSTEDT J AND EV STÅLBERG. How the size of the needle electrode leading-off surface influences the shape of the single muscle fibre action potential in electromyography. *Comp. Prog. Biomed.* **3**:204-212, 1973.

[35] ERMINIO F, BUCHTHAL F AND P ROSENFALCK. Motor unit territory and muscle fiber concentration in paresis due to peripheral nerve injury and anterior horn cell involvement. *Neurology* **9**:657-671, 1959.

[36] FALCK B. *Automatic Analysis of Individual Motor Unit Potentials Recorded with a Special Two Channel Electrode.* Ph.D. Thesis, Turku, Finland, 1983.

[37] FEINSTEIN B, LINDEGARD B, NYMAN E AND G WOHLFART. Morphological studies of motor units in normal human muscles. *Acta Anat.* **23**:127-142, 1955.

[38] FLEISHER SM, STUDER M AND GS MOSCHYTZ. Mathematical model of the single-fiber action potential. *Med. Biol. Eng. Comp.* **22**:433-439, 1984.

[39] FORSYTHE GE, MALCOLM MA AND CB MOLER. *Computer Methods for Mathematical Computations.* Prentice Hall, Englewood Cliffs, New Yersey, 1977.

[40] FRANK E, JANSEN JKS, LOMO T AND R WESTGAARD. The interaction between foreign and original motor nerves innervating the soleus muscle of rats. *J. Physiol.* **247**:725-743, 1975.

[41] FRICKE H. The theory of electrolytic polarization. *Phil. Mag.* **14**:310-318, 1932.

[42] GANAPATHY N , CLARCK JW AND OB WILSON. Extracellular potentials from skeletal muscle *Mathem. Biosc.* **83**:61-96, 1987.

[43] GASSER HS AND H GRUNDFEST. Axon diameters in relation to the spike dimensions and the conduction velocity in mammalian A fibers. *Amer. J. Physiol* **127**:393-414, 1939.

[44] GATH I AND R SHENHAV. Probabilistic model of the spatial distribution of muscle fibres in human muscles. *Biol. Cybern.* **53**:73-78, 1985.

[45] GEDDES LA AND LE BAKER. The specific resistance of biological material: A compendium of data for the biomedical engineer and physiologist *Med. Biol. Eng.* **5**:271-293, 1967.

[46] GEDDES LA, BAKER LE AND M MCGOODWIN. The relationship between electrode area and amplifier input impedance in recording muscle action potentials. *Med. Biol. Eng.* **5**:561-569, 1967.

[47] GEDDES LA, DA COSTA CP AND G WISE. The impedance of stainless-steel electrodes. *Med. Biol. Eng.* **9**:511-521, 1971.

[48] GIELEN FLH. *Electrical Conductivity and Histological Structure of Skeletal Muscle.* Ph.D. Thesis, University of Twente, The Netherlands, 1983.

[49] GIELEN FLH, CRUTS HE, ALBERS BA, BOON KL, WALLINGA-DE JONGE W AND HBK BOOM. Model of electrical conductivity of skeletal muscle based on tissue structure. *Med. Biol. Eng. Comp.* **24**:34-40, 1986.

[50] GOOTZEN THJM, STEGEMAN DF, VAN OOSTEROM A AND HJM VINGERHOETS. A comprehensive model description for motor unit action potentials. *Electroencceph. Clin. Neurophysiol.* **66**:S40, 1987.

[51] GOOTZEN THJM, VINGERHOETS HJM AND DF STEGEMAN. Volume conductor modelling of motor unit action potentials in the surface electromyogram. In : *Electro-physiological Kinesiology.* (edited by W Wallinga-de Jonge) Excerpta Medica International Congress Series 804, pp.227-230, Elsevier, Amsterdam, 1988.

[52] GOOTZEN THJM, THEEUWEN MHJM AND DF STEGEMAN. The calculated influence of a metal electrode shaft in needle EMG recordings. In : YONGMIN KIM (ed.) *Images of the Twenty-First Century.* Proc. Ann. Conf. of the IEEE Eng. in Med. and Biol. Soc. **3**:992-993, 1989.

[53] GOOTZEN THJM, STEGEMAN DF AND A VAN OOSTEROM. A general approach to modelling action potentials of finite length muscle fibers. *Submitted to IEEE Trans. Biomed. Eng.* Chapter II of this thesis.

[54] GOOTZEN THJM, STEGEMAN DF AND A HERINGA. On numercial problems in analytical calculations of extracellular fields in bounded cylindrical volume conductors. *J. App. Physics* **66**:4504-4508, 1989. Chapter III of this thesis.

[55] GOOTZEN THJM, DF STEGEMAN AND A VAN OOSTEROM. Finite limb dimensions and finite muscle length in a model for the generation of electromyographic signals. *Accepted by to Electroenceph. Clin. Neurphysiol.* Chapter IV of this thesis.

[56] GOOTZEN THJM, THEEUWEN MMHJ AND DF STEGEMAN. Intramuscular potential changes caused by the presence of the recording EMG needle electrode. Part I : Mathematical formulation and basic results. *Submitted in adapted form to IEEE Trans. Biomed. Eng. Comp.* Chapter V of this thesis.

[57] GOOTZEN THJM, STEGEMAN DF AND HJM VINGERHOETS. Intramuscular potential changes caused by the presence of the recording EMG needle electrode. Part II : Evaluation and practical consequences. *Submitted in adapted form to Electroenceph Clin. Neurophysiol.* Chapter VI of this thesis.

[58] GOOTZEN THJM, HJM VINGERHOETS AND DF STEGEMAN Electrophysiological investigation of motor unit structure by means of scanning EMG. *Submitted in adapted form to Muscle & Nerve.* Chapter VII of this thesis.

[59] GOOTZEN THJM, STEGEMAN DF AND A VAN OOSTEROM. Parameter estimation on muscle fiber action potential sources. *Submitted to IEEE Trans. Biomed. Eng.* Chapter VIII of this thesis.

[60] GRAY A AND GB MATHEWS. *A treatise on Bessel functions and their application to physics* Dover Publications Inc., New York, 1966.

[61] GREATBATCH W. Metal electrodes in bioengineering. *CRC Crit.Rev. in Bioeng.* **5**:1-36, 1981.

[62] GRIEP PAM, BOON KL AND DF STEGEMAN. A study of the motor unit action potential by means of computer simulation. *Biol. Cybern.* **30**:221-230, 1978.

[63] GRIEP PAM. *The Motor Unit Action Potential.* Ph.D. Thesis, University of Twente, The Netherlands, 1979.

[64] GRIEP PAM, GIELEN, FLH, BOOM HBK, BOON KL, HOOGSTRATEN LLW, POOL CW AND W WALLINGA-DE JONGE. Calculation and registration of the same motor unit action potential. *Electroenceph. Clin. Neurphysiol.* **53**:388-404, 1982.

[65] GYDIKOV A, GERILOVSKY L, RADICHEVA N AND N TRAYANOVA. Influence of the muscle fiber end geometry on the extracellular potentials. *Biol. Cybern.* **54**:1-8, 1986.

[66] GYDIKOV A AND N TRAYANOVA. Extracellular potentials of single active muscle fibers : effects of finite fiber length. *Biol. Cybern.* **53**:363-372, 1986.

[67] HARY D, BEKEY GA AND DJ ANTONELLI. Circuit models and simulation analysis of electromyographic signal sources I : The impedance of EMG electrodes. *IEEE Trans. Biomed. Eng.* **34**:91-97, 1987.

[68] HERINGA A, STEGEMAN DF, UIJEN GHJ AND JPC DE WEERD. Solution methods of electrical field problems in physiology. *IEEE Trans. Biomed. Eng.* **29**.34-42, 1982.

[69] HILTON-BROWN P AND E STÅLBERG. The motor unit in muscular dystrophy, a single fiber EMG and scanning EMG study. *J. Neurol. Neurosurg. Phychiat.* **46**:981-995, 1983.

[70] HILTON-BROWN P AND E STÅLBERG. Motor unit size in muscular dystrophy, a macro EMG and scanning EMG study. *J. Neurol. Neurosurg. Psychiat.* **46**.996-1005, 1983.

[71] HODGKIN, AL AND AF HUXLEY. A quantitative description of membrane current and its application to conduction and excitation in nerve. *J. Physiol.* **117**.500-544. 1952.

[72] JACKSON JD. *Classical Electrodynamics* John Wiley & Sons, New York, 1975.

[73] KATZ B AND R MILEDI. Propagation of electric activity in motor nerve terminals. *Proc. Roy. Soc.* **161**:453-482, 1965.

[74] KLEINPENNING PH, GOOTZEN THJM, STEGEMAN DF AND A VAN OOSTEROM. The equivalent source description representing the extinction of propagation at a muscle fibre ending. *Mathem. Biosc., in press.*

[75] KOPEC J AND I HAUSMANOWA-PETRUSEWICZ. On-line computer application in clinical quantitative electromyography. *Electromyogr. Clin. Neurophysiol.* **16**:49-64, 1976.

[76] KOSAROV D AND A GYDIKOV. The influence of the volume conduction on the shape of the action potentials recorded by various types of needle electrodes in normal human muscle. *Electromyogr. Clin. Neurophysiol.* **15**:319-335, 1975.

[77] KUGELBERG E AND L EDSTROM. Differential histochemical effects of muscle contraction on phosphorylase and glycogen in various types of fibres: relation to fatigue. *J. Neurol. Neurosurg. Psychiat.* **31**:415-423, 1968.

[78] LATEVA ZC. Dependence of quantitative parameters of the extracellular potential power spectrum on propagation velocity, duration and asymmetry of action potentials. *Electromyogr.Clin.Neurophysiol.* **28**:191-203, 1988.

[79] LEFEVER RS AND CJ DELUCA. A procedure for decomposing the myoelectric signal into its constituent action potentials. Part I : Technique, theory and implementation. *IEEE Trans. Biomed. Eng.* **29**:149-157, 1982.

[80] LIU SH. Fractal model for the AC response of a rough interface. *Phys. Rev. Lett.* **55**:529-532, 1985.

[81] LUDIN HP. Microelectrode studies of normal and dystrophic human muscle. *Electroenceph. Clin. Neurophsyiol.* **25**:411, 1968.

[82] LUDIN HP. *Praktische Elektromyographie.* Ferdinand Enke Verlag, Stuttgart, 1976.

[83] LORENTE DE NÓ R. *A study of nerve physiology.* Studies of the Rockefeller Institute for Medical Research, 1947.

[84] MARQUARD DW. A algorithm for least-squares estimation of non-linear parameters. *J. Soc. Indust. Appl. Math.* **2**:431-441, 1963.

[85] MCGILL KC, CUMMINS KL AND LJ DORFMAN. Automatic decomposition of the clinical electromyogram. *IEEE Trans. Biomed. Eng.* **32**:470-477, 1985.

[86] NANDEDKAR SD AND EV STÅLBERG. Simulation of single muscle fiber action potentials. *Med. Biol. Eng. Comp.* **21**:158-165, 1983.

[87] NANDEDKAR SD, STÅLBERG EV AND DB SANDERS. Simulation techniques in electromyography. *IEEE Trans. Biomed. Eng.* **32**:775-785, 1985.

[88] NANDEDKAR SD, SANDERS DB AND EV STÅLBERG. Simulation of concentric needle EMG motor unit action potentials. *Muscle and Nerve* **11**:151-159, 1988.

[89] NANDEDKAR SD, SANDERS DB AND EV STÅLBERG. EMG of reinnervated motor units : a simulation study. *Electroenceph. Clin. Neurophysiol.* **70**:177-184, 1988.

[90] NANDEDKAR SD AND DB SANDERS. Simulation of myopathic motor unit action potentials. *Muscle & Nerve* **1**:197-202, 1989.

[91] NEUMAN MR. Biopotential electrodes. In : WEBSTER JG (editor) : *Medical Instrumentation, Application and Design.* Houghton Mifflin Company, Boston, 1978.

[92] OOSTENDORP TF AND A VAN OOSTEROM. Source parameter estimation in inhomogeneous volume conductors of arbitrary shape. *IEEE Trans. Biomed. Eng.* **36**:382-391, 1989.

[93] PAAKKARI IM AND M MUMENTHALER. Needle myopathy - an experimental study. *J. Neurol.* **208**:133, 1974.

[94] PLONSEY R AND DB HEPPNER. Considerations of quasi-stationarity in electrophysiological systems. *Bull. Math. Bioph.* **29**:657-664. 1967.

[95] PLONSEY R. *Bioelectric Phenomena* McGraw Hill, New York, 1969.

[96] PLONSEY R. The active fiber in a volume conductor. *IEEE Trans. Biomed. Eng.* **21**:371-381, 1974.

[97] PLONSEY R. Action potential sources and their volume conductor fields. *Proc.IEEE* **65**:601-611, 1977.

[98] PLONSEY R AND RC BARR. A critique of impedance measurements in cardiac tissue. *Ann. Biomed. Eng.* **14**:307-322, 1986.

[99] POLLAK V. The waveshape of action potentials recorded with different types of electromyographic needles. *Med.Biol.Eng.* **9**:657-664. 1971.

[100] POLLAK V. Computation of the impedance characteristics of metal electrodes for biological investigations. *Med. Biol. Eng.* **12**:460-464, 1974.

[101] POLLAK V. Impedance measurements on metal needle electrodes. *Med. Biol. Eng.* **12**:606-612, 1974.

[102] PRESS WH, FLANNERY BP, TEUKOLSKY SA AND WT VETTERLING. *Numerical recipes : the art of scientific computing.* Cambridge University Press, Cambridge, 1986.

[103] ROSENFALCK P. Intra- and extracellular potential fields of active nerve and muscle fibers. A physico-mathematical analysis of different models. *Acta Physiol. Scand.* **Suppl. 321**, 1969.

[104] ROSENFALCK P AND F BUCHTHAL. On the concept of the motor subunit. *Int. J. Neurosci.* **1**:27-37, 1970.

[105] ROTH BJ AND JP WIKSWO. The electrical potential and magnetic field of an axon in a nerve bundle. *Mathem. Biosc.* **76**:37-57, 1985.

[106] ROTH BJ AND FLH GIELEN. A comparison of two models for calculating the electrical potential in skeletal muscle. *Ann. Biomed. Eng.* **15**:591-602, 1987.

[107] ROTH BJ, GIELEN FLH AND JP WIKSWO. Spatial and temporal frequency-dependent conductivities in volume conduction calculations of skeletal muscle. *Mathem. Biosc.* **88**:159-189, 1988.

[108] RUSH S. Methods of measuring the resitivities of anisotropic conducting media in situ. *J. of Research of the National Bureau of Standards, section C Engineering and Instrumentation* **66C**:217-222, 1962.

[109] RUSH S, ABILDSKOV JA AND R MCFEE. Resitivity of body tissues at low frequencies. *Circ. Res.* **12**:40-50, 1963.

[110] SCHOONHOVEN R, STEGEMAN DF, VAN OOSTEROM A AND GFM DAUTZENBERG. The inverse problem in electroneurography I. Conceptual basis and mathematical formulation. *IEEE Trans. Biomed. En.* **35**:769-777, 1988.

[111] SCHWAN HP. Electrode polarization impedance and measurements in biological materials. *Ann. N.Y. Acad. Sci.* **148**:191-209, 1968.

[112] SCHWAN HP AND B ONARAL. Linear and nonlinear properties of platinum electrode polarisation III : equivalence of frequency- and time-domain behaviour. *Med. Biol. Eng. Comp.* **23**:28-32, 1985.

[113] SHERRINGTON C. Some functional problems attaching to convergence. *Proc. Roy.Soc. B* **105**:332-362,1925.

[114] STÅLBERG EV, SCHWARTZ MS, THIELE B AND HH SCHILLER. The normal motor unit in man. *J. Neurol. Sci.* **27**:291-301, 1976.

[115] STÅLBERG EV AND J TRONTELJ. *Single fibre electromyography.* The Mirvalle Press, Old Woking (UK), 1979.

[116] STÅLBERG EV AND I GATH. Measurements of the uptake area of small-size electromyographic electrodes. *IEEE Trans. Biomed. Eng.* **BME 26**:371-376, 1979.

[117] STÅLBERG EV AND L ANTONI. The elctrophysiological cross section of a motor unit. *J. Neurol. Neurosurg. Psychiat.* **43**:409-474, 1980.

[118] STÅLBERG EV, ANDREASSEN A, FALCK B, LANG H, ROSENFALCK A AND TROJABORG W. Quantitative analysis of individual motor unit potentials : a proposition for standardized terminology and criteria for measurement. *J. Clin. Neurophysiol.* **3**:313-348, 1986.

[119] STÅLBERG EV. Single fiber EMG, macro EMG and scanning EMG. New ways of looking at the motor unit. *CRC Crit. Rev. Clin. Neurobiol.* **2**:125-167, 1986.

[120] STÅLBERG EV AND PO ERIKSSON. A scanning electromyographic study of the topography of human masseter single motor units. *Arch. Oral Biol.* **32**:793-797, 1987.

[121] STEGEMAN DF , DE WEERD JPC AND EGJ EIJKMAN. A volume conductor study of compound action potentials of nerves in situ : The forward problem. *Biol.Cybernetics.* **33**:97-111, 1979.

[122] STEGEMAN DF, VAN OOSTEROM A AND THJM GOOTZEN. Mechanisms behind far-field electric activity induced by a moving generator. In : *Proc. 9th Ann. Conf. IEEE Med. & Biol. Soc.*, pp. 1410-1411, Boston, USA, 1987.

[123] STEGEMAN DF, SCHOONHOVEN R, DAUTZENBERG G AND J MOLEMAN. The inverse problem in electroneurography II. Computational aspects and evaluation using simulated data. *IEEE Trans. Biomed. Eng.* **35**:778-788, 1988.

[124] STEGEMAN DF, GOOTZEN, THJM AND HJM VINGERHOETS. The dominating role of finite muscle and limb dimensions in surface electromyography. In : YONGMIN KIM (ed.) *Images of the Twenty-First Century.* Proc. Ann. Conf. of the IEEE Eng. in Med. and Biol. Soc. **3**:992-993, 1989.

[125] SUN HH, WANG X AND B ONARAL. Onset of nonlinearity in fractal dimension systems : an application to polarized bioelectrode interfaces. *Ann. Biomed. Eng.* **16**:111-121, 1988.

[126] THEEUWEN MMHJ, GOOTZEN THJM AND DF STEGEMAN. The effect of needle electrodes on recorded action potentials revealed by an analytical model. *Submitted to IEEE Trans. Biomed. Eng.*

[127] VAN OOSTEROM A AND GJ HUISKAMP. The effect of torso inhomogeneities on body surface potentials quantified using "tailored" geometry. *J. of Electrocard.* **22**:53-72, 1989.

[128] WALLINGA-DE JONGE W, GIELEN FLH, WIRTZ P, DE JONG P AND J BROENINK. The different intracellular action potentials of fast and slow muscle fibers. *Electroenceph. Clin. Neurophsyiol.* **60**.539-547, 1985.

[129] WANI AM AND GUHA SK. Synthesising of a motor unit potential based on the sequential firing of muscle fibres. *Med. Biol. Eng. Comp.* **18**:719-726, 1980.

[130] WEAST RC (editor). *CRC Handbook of Chemistry and Physics.* 56th edition, CRC Press, Cleveland, 1976.

[131] WILLISON RG. Analysis of electrical activity in healthy and dystrophic muscle in man. *J. Neurol. Neurosurg. Psychiat.* **27**:386-394, 1964.

Dankwoord

Allereerst wil ik hier diegenen noemen aan wie ik grote dank verschuldigd ben voor de wijze waarop ze aan de totstandkoming van dit proefschrift hebben bijgedragen:

- Dick Stegeman, wiens toewijding en inzicht van onschatbare waarde zijn geweest,
- Dick Vingerhoets, mijn vaste rechterhand, die bij scanning EMG eigenlijk geen stappenmotor nodig had,
- Jan Moleman, die op de bijna prehistorische PDP's het onmogelijke toch mogelijk maakte,
- Marc Theeuwen, wiens theoretische vaardigheid uitmonde in het zo belangrijke naald-model,
- Pax Janssen, Ad van Rossum, Marc Massa en Geert vd. Voorst die de 10-kanaals versterker en de scanning EMG opstelling hebben gebouwd in een tijd waarin de Instrumentele Dienst onder zware bezuinigingsdruk stond,
- de patiënten en proefpersonen die ons geheel belangeloos hun bovenbeenspieren hebben laten prikken,
- Guido Dautzenberg, Mieke Merks, Cees van Perlo en Guiseppe Patane, die tal van software en hardware klussen voor mij klaarden,
- Mevr. O. Viejou, voor haar hulp bij het corrigeren van het manuscript.

Daarnaast zijn er velen die gezorgd hebben voor een omgeving waarin het prettig was om te werken: alle collega's van het laboratorium voor Medische Fysica & Biofysica en de afdeling Klinische Neurofysiologie.
Tot slot wil ik mijn naaste familie bedanken voor de niet aflatende morele ondersteuning:

- Mijn ouders, die mij geleerd hebben door te zetten maar tegelijkertijd ook te blijven relativeren en opgewekt verder te leven,
- Marie-Christine, die liefdevol begrip toonde voor alle perikelen die een promoverende echtgenoot met zich meebrengt,
- Eveline, wiens eerste zinnetje luidde "pappa boven", maar die ook voor veel leuke en ontspannende momenten wist te zorgen.

Curriculum Vitae

De ouverture van het leven van de auteur van dit proefschrift begint op 22 september 1962 in het dorpje Hegelsom, gelegen aan de rand van de Peel. Als het eerste dozijn levensjaren gevuld is, worden de bakens verzet naar Venray waar zich de eerste akte afspeelt. Hier wordt op het Boschveldcollege, waar de geest der Franciscanen nog voelbaar is en waar het "Io Vivat" vaak weerklinkt, het Gymnasium doorlopen. In mei 1980 wordt de middelbare schoolopleiding afgesloten met een Gym-β diploma.

De volgende akte speelt zich af in Nijmegen, waar in de loop van een tiental jaren een wetenschappelijke "Gradus ad Parnassum" zichtbaar wordt. Vanaf september 1980 leiden de fysische etudes in allegro via het kandidaatsexamen N2 in november 1983 naar het doctoraal examen in januari 1986. De laatste anderhalf jaar van de doctoraalstudie worden onder de inspirerende leiding van Pieter Wijn besteed aan het bestuderen van Doppler spectra gemeten aan perifere vaten. Hier blijkt hoe uitdagend het kan zijn om als fysicus in een klinische sfeer te werken. Als dan ook gekozen kan worden voor een promotieonderzoek dat deze lijn vervolgt is daar geen lange beraadslaging voor nodig.

De derde akte speelt zich eveneens in Nijmegen af. Vanaf januari 1986 ontspint er zich een innig duet tussen het fundmentele werk in de pre-kliniek en de toepassingen in de kliniek. Dit geheel onder leiding van de fysicus Prof. van Oosterom en de klinicus Prof. Notermans. Meer op de voorgrond dragen de fysische Dick (Stegeman) en de klinische Dick (Vingerhoets) op harmonieuze en waardevolle wijze bij aan een voorspoedig verloop van deze akte waarvan U de partituur nu in handen heeft.

Van de vierde akte is het libretto op dit moment nog volop in bewerking. Het hoofdthema zal zondermeer in het teken staan van de brede blik die de toegepast fysicus dient te kenmerken.

Stellingen

behorende bij het proefschrift

Muscle Fibre and Motor Unit Action Potentials

A biophysical basis for clinical electromyography.

in het openbaar te verdedigen op maandag 14 mei 1990,
des namiddags te 3.30 uur,

door

Theodorus Hubertus Johannes Maria Gootzen

1. Het toevoegen van capacitieve membraaneigenschappen en van stroomredistributie door de vezelmembranen aan simulatiemodellen voor spiervezel actiepotentialen heeft geleid tot een onnodige complexiteit van de modellen die niet in een effectief betere beschrijving heeft geresulteerd.

   B Roth, F Gielen en J Wikswo, *Mathem. Biosc.* **88**:159-189, 1988,

   Hoofdstuk II

2. Temporele dispersies, zoals die veroorzaakt worden door variaties in de spiervezel diameter van de individuele vezels in de motor unit, kunnen het beste afgeschat worden uit de eind-effect pieken van aan het huidoppervlak geregistreerde motor unit potentialen .

   Hoofdstuk IV

3. Electrofysiologische metingen met behulp van metalen naaldelectrodes blijken slechts mogelijk te zijn dank zij de isolerende werking van de electrolytische dubbellaag. Er zijn derhalve geen theoretische belemmeringen voor het gebruik van metalen naaldelectrodes.

   Hoofdstukken V en VI

4. Geavanceerde EMG meettechnieken zoals scanning EMG en multi-electrode EMG zijn in staat zeer waardevolle informatie over de toestand van skeletspieren te verschaffen. Een ondubbelzinnige interpretatie van de meetgegevens vereist een gedegen onderbouwing met biofysische modellen.

   Hoofdstukken VII en VIII

5. Bij Doppler-ultrageluid snelheidsmetingen aan bloedvaten dient het correct aanstralen van het bloedvat en de keuze van een optimale bundelbreedte meer aandacht te krijgen dan het ontwerpen van filters die een niet-correct aanstralen verdoezelen.

   P Wijn, P van der Sar, T Gootzen, M Tilmans en S Skotnicki,

   Med. Biol. Eng. Comp. **25**:377-385, 1987.

6. De Katholieke Universiteit zou in haar functioneren als maatschappelijke instelling een grotere betrokkenheid dienen na te streven bij het conciliair proces.

7. In een avant-gardistische stroming als de Musique Concrète zouden hoorbaar gemaakte EMG signalen een belangrijke menselijke inbreng in de composities kunnen hebben.

8. Het niet langer verplicht stellen van stellingen zal stellig leiden tot een verarming van de promotie-traditie.

Nijmegen, mei 1990.